



universität  
wien

# DISSERTATION

Titel der Dissertation

The glass transition in nanoscaled confinement  
probed by dynamic mechanical spectroscopy

angestrebter akademischer Grad

Doktor der Naturwissenschaften (Dr. rer.nat.)

Verfasserin / Verfasser:	Johannes Koppensteiner
Matrikel-Nummer:	9903099
Dissertationsgebiet:	Physik
Betreuerin / Betreuer:	Ao. Prof. Dr. Wilfried Schranz

Wien, am 14. Dezember 2009





## **Assertion**

This script contains three articles, one of them is published in European Physical Letters, two in Physical Review B. Major parts of these publications were contributed by Mag. Johannes Koppensteiner.

---

Ao. Prof. Dr. Wilfried Schranz

---

Mag. Johannes Koppensteiner

## Abstract

A glass transition in a liquid is characterized by a massive change in some of its physical properties as viscosity  $\eta$  and molecular relaxation time  $\tau$ , whereas no change in structure or long range order can be detected. Up to now an overall theory explaining the very nature of the glass transition and therewith all experimental findings is not available.

Today's common approach, reaching back to Adams and Gibbs in 1963, is based on a cooperative rearrangement of molecules in groups whose size increases, when the glass transition is approached. In this picture a typical number of correlated molecules  $N_{corr,T}$  form a compact cluster of a typical size  $\xi$ , predicted to be in the nm-range at  $T_g$ . If this is true, nanoscaled confinement of a glass forming liquid should considerably influence this transition. In a pioneer work of 1991 Jackson and McKenna found a downshift  $\Delta T_g \propto 1/d$  in nm-sized pores of diameter  $d$ . This paper started a new field of physics, the glass transition in confinement being investigated in experiment, simulation and theory. 20 years of research created partly contradictory results pointing to a large influence of side effects in confinement, opponent in their impact on  $T_g$ . Both  $T_g$  upshifts and downshifts were found in 2D and 3D confining geometries showing that spatially hindered molecular rearrangement is blurred by surface interactions and a negative pressure effect. An accurate investigation of side effects therefore is essential.

The present thesis contributes to this rich field and aims to help bridging the often cited gap between theory and experiments. For the first time a *mechanical* approach is chosen and the *dynamic elastic response* of a mesoporous host matrix filled with a glass forming liquid is used to model the liquids behaviour across the glass transition. Low frequency dynamic mechanical measurements are proven to be very sensitive of the vitrification of the filling liquid. DMA turned out as a highly efficient and versatile tool, able to join the row of successfully used experimental methods as NMR, light scattering, dielectric and calorimetric spectroscopy.

A main point of investigation was inhomogeneous relaxation within a nm-sized pore geometry. An increase of  $\tau$  when approaching the rough (untreated) pore surface as recently proposed by computer simulations nicely reproduces the data at hand, yielding a downshift of  $T_g \propto 1/d$  in perfect agreement with literature data. Interaction with the pore walls to a large extend was removed by silanation. Homogeneous relaxation is found within silanated pores following a Vogel-Fulcher-Tammann relation. This lubrication effect leads to a stronger downshift of  $T_g$  with decreasing pore size. Further, high resolution thermal expansion measurements of silanated and untreated porous silica samples, both unfilled and filled, revealed the intensely discussed contribution of negative pressure.

These findings allow to separate competing side effects from the pure confinement induced acceleration of molecular dynamics. Thereon, the dynamic elastic susceptibility data for the first time were analyzed in terms of a recently proposed procedure [C. Dalle-Ferrier et al., Phys. Rev. E **76**, 041510 (2007)], relating the number  $N_{corr,T}$  of molecules, whose dynamics is correlated to a local enthalpy fluctuation, to the three-point dynamic susceptibility  $\chi_T$ . The observed increase of  $N_{corr,T}$  with decreasing temperature strongly indicates that the size  $\xi$  of dynamic heterogeneities increases when approaching  $T_g$  to  $\xi \approx 3$  nm. The calculation of  $N_{corr,T}$  and estimation of  $\xi(T_g)$ , both of nanoscopic nature, from a macroscopic probe experiment are major results of this thesis.

## Zusammenfassung

Der Glasübergang einer Flüssigkeit ist charakterisiert durch die massive Änderung einiger ihrer physikalischen Eigenschaften wie Viskosität  $\eta$  oder molekulare Relaxationszeit  $\tau$ , während gleichzeitig keine Änderung in Struktur und keine langreichweitige Ordnung stattfindet. Bis dato existiert keine allumfassende Theorie, die die Natur des Glasübergangs, und somit alle experimentellen Befunde kohärent beschreibt.

Der heute gängigste Ansatz (Adam und Gibbs, 1963) ist ein kooperatives Neuordnen von Molekülen in Gruppen, deren Grösse bei Annäherung an den Glasübergang anwächst. Dabei bildet eine typische Anzahl  $N_{corr,T}$  korrelierter Moleküle einen kompakten Cluster der Grösse  $\xi$ , die bei  $T_g$  im nm-Bereich vorhergesagt wurde. Trifft dies zu, müsste eine lokale Einschränkung im nm-Bereich empfindlichen Einfluss auf  $T_g$  haben. In einer Pionierarbeit von 1991 haben Jackson und McKenna eine Verschiebung von  $\Delta T_g \propto 1/d$  in nm grossen Poren des Durchmessers  $d$  nachgewiesen. Der Glasübergang in eingeschränkten Geometrien wird seither experimentell, theoretisch und mittels Simulationen untersucht. 20 Jahre Forschung führten zu teils widersprüchlichen Ergebnissen, die auf einen grossen Einfluss von Nebeneffekten im Confinement hinweisen, gegenläufig in ihrer Wirkung auf  $T_g$ . Sowohl positive als auch negative Verschiebungen wurden in 2D oder 3D einschränkenden Geometrien gefunden, was zeigt, dass die lokale Behinderung der molekularen Neuordnung überlagert wird von Oberflächen-Interaktion und negativem Druck in den Poren. Eine akurate Untersuchung dieser Nebeneffekte ist daher unumgänglich.

Diese Dissertation trägt zu diesem reichhaltigen Gebiet bei und soll helfen, die oft zitierte Lücke zwischen Experiment und Theorie zu füllen. Zum ersten Mal wurde ein *mechanischer* Zugang gewählt und der *dynamisch elastische Response* einer mesoporösen Gastmatrix, gefüllt mit einer Glas bildenden Flüssigkeit wird benutzt, um das Verhalten der Flüssigkeit über den Glasübergang hinweg zu modellieren. Niederfrequente dynamisch mechanische Messungen erwiesen sich als überaus sensitiv für die Messung der Verglasung der Füll-Flüssigkeit. DMA zeigte sich als hocheffizientes und vielseitiges Werkzeug, das sich nun einreicht zu anderen erfolgreich angewandten Methoden wie NMR, Lichtstreuung, dielektrische und kalorimetrische Spektroskopie, bzw. in einigen Punkten diesen Methoden sogar überlegen ist.

Ein Hauptpunkt der Untersuchungen war inhomogene Relaxation in nm großer Porengeometrie. Ein Anstieg von  $\tau$  nahe der rauhen (unbehandelten) Porenwand, wie kürzlich von Simulationen vorgeschlagen, reproduziert die vorliegenden Daten hervorragend und führt zu einem negativen Verschiebung  $\Delta T_g \propto 1/d$  in perfekter Übereinkunft mit Literaturdaten. Interaktion mit den Porenwänden wurde zum grössten Teil entfernt durch Silanisation. Homogene Relaxationsdynamik zeigte sich in silanisierten Poren, die einer Vogel-Fulcher-Tammann Relation folgt. Dieser Schmiereffekt der Porenwände führt zu einem stärkeren Verschiebung von  $T_g$  mit abnehmender Porengrösse. Weiters zeigten hochauflösende Messungen der thermischen Ausdehnung unbehandelter und silanisierter Proben, jeweils befüllt und unbefüllt, den intensiv diskutierten Beitrag von negativem Druck in den Poren.

Nun war es möglich, Nebeneffekte vom reinen Effekt des Confinements, der Beschleunigung der molekularen Dynamik mit abnehmender Porengrösse, zu trennen. Daraufhin konnten die Daten der dynamisch elastischen Suszeptibilität zum ersten Mal im Sinne einer kürzlich veröffentlichten Prozedur [C. Dalle-Ferrier et al., Phys. Rev. E **76**, 041510 (2007)] analysiert werden, die die Anzahl dynamisch mit Enthalpiefluktuationen korrelierter Moleküle  $N_{corr,T}$ , mit der dynamischen drei-Punkt-Suszeptibilität  $\chi_T$  in Beziehung setzt. Der beobachtete Anstieg von  $N_{corr,T}$  mit abnehmender Temperatur indiziert ein starkes Anwachsen der Grösse  $\xi$  der dynamischen Heterogenitäten bei Annäherung an  $T_g$  und  $\xi(T_g) \approx 3$  nm. Diese nanoskopischen Aussagen, gewonnen aus einem makroskopischen Experiment bilden die zentralen Ergebnisse dieser Arbeit.

# Abbreviations and Symbols

RT	....	room temperature
LT	....	low temperature
DMA	....	dynamic mechanical analysis
TMA	....	thermomechanical analysis
DSC	....	differential scanning calorimetry
LVDT	....	linear variable differential transformer
HMDS	....	hexamethyldisilazane, $\text{C}_6\text{H}_{19}\text{NSi}_2$
PSD	....	pore size distribution
BJH	....	Barrett, Joyner, and Halend
BET	....	Brunauer, Emmet and Teller
CRR	....	cooperative rearranging region
FWHM	....	full width at half maximum
$\rho$	....	density ( $\text{kg/m}^3$ )
$\Phi$	....	porosity
$G$	....	shear modulus (GPa)
$Y$	....	Young's modulus (GPa)
$K$	....	bulk modulus (GPa)
$\nu$	....	Poisson's ratio
$\nu$	....	frequency (Hz)
$\omega = 2 \cdot \pi \cdot \nu$	....	circular frequency (Hz)
$f$	....	filling fraction
$T$	....	temperature (K)
$T_m$	....	melting temperature (K)
$T_g$	....	glass transition temperature (K)
$\xi$	....	size of dynamically correlated regions (nm)
$\tau$	....	relaxation time (s)
$k_B$	....	Boltzmann's constant (J/K)
$d$	....	pore diameter (nm)
$R = d/2$	....	pore radius (nm)
$V$	....	volume ( $\text{nm}^3$ )

# Content

<b>1</b>	<b>Introduction</b>	<b>1</b>
1.1	Thesis Introduction . . . . .	1
1.2	Project Definition and Aims . . . . .	4
<b>2</b>	<b>Samples and preparation</b>	<b>7</b>
2.1	Porous Host Matrices . . . . .	7
2.1.1	Vycor 7930 . . . . .	8
2.1.2	Gelsil . . . . .	8
2.2	Cutting, Sanding, Cleaning and Storage . . . . .	11
2.3	N <sub>2</sub> -Sorption characterization . . . . .	12
2.4	Silanation Process . . . . .	16
2.5	Filling procedure . . . . .	17
<b>3</b>	<b>Laboratory equipment and details</b>	<b>19</b>
3.1	Method . . . . .	19
3.2	Perkin Elmer DMA series 7 . . . . .	22
3.2.1	Temperature control . . . . .	22
3.2.2	Calibration . . . . .	23
3.2.3	Measurement procedure . . . . .	24
3.3	Perkin Elmer Diamond DMA . . . . .	26
3.3.1	Calibrations . . . . .	27
3.3.2	Measurement procedure for 3PB . . . . .	29
3.3.3	Optimizing sample dimension . . . . .	30
3.3.4	3PB measuring cell for small samples . . . . .	33
<b>4</b>	<b>Heterogeneous relaxation dynamics of nano-confined salol probed by DMA, EPL 79, 36006 (2007)</b>	<b>35</b>
4.1	Introduction . . . . .	37
4.2	Experimental results . . . . .	38

4.3	Interpretation and comparison with experiment . . . . .	41
4.4	Conclusion . . . . .	46
<b>5</b>	<b>Confinement effects on glass forming liquids probed by dynamic mechanical analysis, PRB 78, 054203 (2008)</b>	<b>47</b>
5.1	Introduction . . . . .	49
5.2	Experimental . . . . .	51
5.2.1	Sample preparation . . . . .	51
5.2.2	Dynamic mechanical analysis (DMA) . . . . .	51
5.3	Results and Discussion . . . . .	52
5.3.1	Dynamic elastic response . . . . .	52
5.3.2	Filling process and accompanying effects . . . . .	61
5.3.3	Negative pressure effect . . . . .	63
5.4	Conclusions . . . . .	65
<b>6</b>	<b>Revealing the pure confinement effect in glass forming liquids by dynamic mechanical analysis, accepted by PRB (2009)</b>	<b>69</b>
6.1	Introduction . . . . .	71
6.2	Experimental . . . . .	73
6.2.1	Sample preparation . . . . .	73
6.2.2	Dynamic mechanical analysis . . . . .	74
6.2.3	Resonant ultrasound spectroscopy . . . . .	74
6.3	Results and Discussion . . . . .	75
6.4	Conclusions . . . . .	84
<b>7</b>	<b>Unpublished Results</b>	<b>87</b>
7.1	Overview . . . . .	87
7.2	Stress-strain relation in mesoporous silica in 3PB . . . . .	88
7.3	Toluene in confinement . . . . .	91
7.4	Orthoterphenyl in confinement . . . . .	94
<b>8</b>	<b>RUS Results</b>	<b>99</b>
8.1	Method and Theory . . . . .	99
8.2	Room temperature elastic constants of mesoporous silica . . . . .	101
8.3	Low temperature scans . . . . .	105
8.3.1	Vycor clean . . . . .	106
8.3.2	Vycor filled with glass forming liquids . . . . .	108
<b>9</b>	<b>Conclusions</b>	<b>113</b>

9.1	Spatial Confinement and the Glass Transition . . . . .	113
9.2	Resonant ultrasonic spectroscopy . . . . .	117
<b>10</b>	<b>Workshop drawings</b>	<b>119</b>
<b>11</b>	<b>List of Figures and Tables</b>	<b>121</b>
11.1	List of Figures . . . . .	121
11.2	List of Tables . . . . .	127
<b>12</b>	<b>Literature</b>	<b>128</b>
<b>13</b>	<b>Ad Persona</b>	<b>139</b>
10.1	Curriculum Vitae . . . . .	139
10.2	Publications . . . . .	140
10.3	Conference contributions . . . . .	141
10.4	Honouring . . . . .	141
10.5	Cooperations within IK "Nanostructured Materials" . . . . .	141
10.6	National and international cooperations . . . . .	142
10.7	Acknowledgements . . . . .	143





# Chapter 1

## Introduction

### 1.1 Thesis Introduction

Glass-forming materials have been produced by mankind since more than 6000 years. Despite several decades of intense research the transition of a liquid into its glassy state is still lacking a universal theory explaining both the increase of viscosity  $\eta$  and molecular relaxation rates by 14 orders of magnitude [1, 2] without creating any long range order. A widely used explanation going back to Adam and Gibbs [3] is based on the assumption of cooperative rearrangement of molecules ("cooperative rearranging regions, CRR"), forming compact clusters of a typical size  $\xi$  and increasing relaxation times  $\tau$  as  $T_g$  is approached [4]. Such a subsystem of molecules can rearrange into another configuration independently of its environment.

The size of these groups of molecules is considered to grow to some nm as  $T_g$  is approached [5]. E.g. random first order transition theory of glasses [6, 7] predicts  $\xi = r_0 0.51 (\ln \frac{\tau}{\tau_0})^{\frac{2}{3}}$ . At  $T_g$  where  $\tau \approx 100$  s one obtains for typical values of  $\tau_0 \approx 10^{-12}$  s and  $r_0 \approx 1$  nm,  $\xi(T_g) \approx 5$  nm. Measuring the size of such dynamic heterogeneities is one of the most important but at the same time difficult issues in the field of glass formation. Experimental setups like specific heat spectroscopy [5, 8], multidimensional NMR [9, 10, 11] and dielectric spectroscopy [12], etc. have been used to determine a possible growing length scale accompanying the glass transition. All these results agree in the fact, that the obtained cooperative regions are of the order of several nm near  $T_g$ , and are displaying a weak temperature dependence [13]. The idea of a rather modest growth of the dynamically correlated regions when approaching the glass transition is strongly supported by recent computer simulations [14, 15, 16], although not strictly proven, since computer simulations cannot treat the time range of the  $\alpha$ -process near the glass transition.

Very recently in a groundbreaking work Biroli et al. [17] found direct evidence for a gro-

wing dynamical length scale in supercooled liquids by applying inhomogeneous mode-coupling theory. The authors obtained a rather modest growth of the dynamical length scale  $\xi$  with decreasing temperature, which is in very good agreement with computer simulations [16] and experimental results [5, 8, 9, 10, 11]. Based hereon the authors recently developed a method to quantify the size of the correlated regions [12] by analyzing three-point dynamic susceptibilities. For a large number of supercooled liquids they could indeed confirm growing of the correlated regions when approaching the glass transition [18].

An alternative experimental approach to get a reference to a possibly existing cooperation length  $\xi$  which increases when  $T \rightarrow T_g$  is by spatial limitation of a glass forming liquid. Spatially confining geometries as ultrathin films, mesoporous silica or zeolites have already been used to study phase transitions of water [19], hydrocarbons [20], noble gases [21, 22], liquid crystals [23] or alkenes [24]. This concept also illuminated the old and still open question on the very nature of the glass transition and its dynamics [25]: In a pioneering work Jackson and McKenna [26] studied the glass transition of organic liquids in controlled pore glasses (CPG) for pore sizes  $4 \text{ nm} < d < 73 \text{ nm}$ . They found a reduction of the glass transition temperature  $T_g$  for liquids in confinement as compared to the bulk material. The downshift of  $T_g$  was larger for smaller pore sizes, i.e.  $\Delta T_g \propto 1/d$ . This effect is similar to - but not as strong as - the suppression known for the melting temperature  $T_m$  in confinement [27]. During the following two decades this effect was studied via calorimetry [28, 29], dielectric spectroscopy [30], neutron scattering [31], light scattering [32] and molecular dynamics [33]. It was shown that in many cases confinement below a characteristic length impedes [29] the transition, implying that molecules within a region of the size  $\xi_g$  (approaching  $T_g$  typically some nm [34, 35]) have to cooperate and rearrange in order to create the glassy state. Hindering this cooperation first leads to a downshift of  $T_g$  if  $d \sim \xi_g$  and finally to a suppression of the transition if  $d < \xi_g$  [29].

As presented in Ref. [36] (see chapter 4), in 2007 the glass-forming liquid salol was studied for the first time via dynamic mechanical analysis measurements (DMA) in Vycor with  $d = 7 \text{ nm}$  pore size. It turned out that the dynamic elastic response is very sensitive to the glass transition of liquids confined to mesoporous samples. Based on the results of computer simulations [33, 37] acceleration effects due to confinement could be disentangled from slowing down of molecular motion due to interaction of the molecules with the rough pore surface. It was even possible to predict the pore size dependence of the dynamic elastic response (see Fig. 4.4 of chapter 4, Fig. 4 of Ref. [36]). In order to test these predictions and to study the glass transition of salol for different pore sizes, further measurements have been performed. Ref. [38] (chapter 5) displays novel experimental results of the temperature and frequency

dependence of the complex dynamic elastic susceptibility of salol confined in mesoporous matrices of  $d = 7.5$  nm, 5.0 nm and 2.6 nm.

However, the abundance and diversity of experimental findings in literature shows that an accurate discussion of the following side effects is essential when interpreting experimental findings on glass forming liquids in confinement:

a) Negative pressure due to mismatching thermal expansion coefficients of liquid and confining matrix is such a side effect. It was discussed by various authors [32, 39] and sometimes even made responsible for the whole downshift of  $T_g$  in confinement [32]. Being true, it would disprove the idea of a growing length scale of cooperativity. Within this thesis negative pressure effects for salol in natural uncoated pores of size 7.5 to 2.6 nm were determined from high resolution thermal expansion measurements. An upper bound for the contribution of negative pressure to the total downshift of  $T_g$  of  $\approx 30\%$  was found. (chapter 5, Ref. [38])

b) A second, and much larger effect on the glass transition of liquids in confinement arises from the interaction of the molecules with the huge inner surface of confining host matrices which can take values up to 600 m<sup>2</sup>/g (see Tab. 2.1). Confined liquids tend to form H-bonds with the hydrophilic pore surface, which leads to an immobile surface layer of molecules and a retarded relaxation behavior when approaching the glass transition. A competition appears between slowing down of molecular motions due to pinning of molecules near the pore walls and acceleration of the dynamics due to decreasing size of the pores. Within the present work, extinction of this surface interaction could be largely achieved by silanation of inner pore walls, revealing the pure confinement effect (Ref. [40], chapter 6). Silanation leads to an enhancement of the molecular dynamics in the pores, resulting in a stronger downshift of  $T_g$  as compared to the uncoated pores. These findings allow to separate the surface effect from confinement induced acceleration of the dynamics, and a simultaneous quantitative statement about negative pressure (no change due to silanation) within one and the same measurement technique and confinement geometry.

Having revealed the pure confinement effect and using the recently proposed method of Berthier et al. [12] the number  $N_{corr,T}$  of dynamically correlated molecules was determined for the first time directly from elastic susceptibility data as a function of temperature and pore size (chapter 6, Ref. [40]).

The present thesis is organized as follows: Chapter 2 gives details on preparation, characterization, silanation and filling of mesoporous silica samples. It is followed by chapter

3 explaining technical details on the DMA method and analyzers in use. Chapters 4-6 are manuscripts of three published articles whose scientific content forms the main body of this thesis. Chapters 7 and 8 present unpublished results from DMA and RUS measurements. A conclusion summarizing both published and unpublished results is given in chapter 9. Chapter 10 displays technical drawings and chapter 11 comprises personal details of the author.

## 1.2 Project Definition and Aims

This work has been done within the frame of the Initiativkolleg "Experimental Materials Science - Nanostructured Materials" (I022-N) founded by the University of Vienna and was scheduled from Sept. 2006 to Sept. 2009. Prof. Andrej Kityk inspired the use of dynamic mechanical analysis to study phase transitions in confining host matrices by preliminary measurements on water in Vycor in 2005 (unpublished). In September 2006 preliminary measurements on the glass forming liquid salol in 7 nm pores of mesoporous Vycor glass have already been successfully performed by Dr. Madalina Puica. The publication Ref. [36] (chapter 4) at that time was in preparation by Prof. Wilfried Schranz. All of this thesis' aims concern a continuation of the started efforts, targeting a complete dynamic mechanic analysis and further insight into this manifold topic.

Further exploration on glass forming liquids in mesoporous confinements was intended to be achieved by

- the search for new confining host matrices proper for mechanical test enlarging the range of pore diameters in use to 2-20nm
- advancement of sample preparation methods
- use of different pore filling liquids
- exhausting the force and frequency range of the Perkin Elmer DMA 7
- installation, calibration and use of a new Perkin Elmer Diamond DMA, promising enhanced temperature control and resolution
- use of resonant ultrasonic spectroscopy (RUS) i.o. to extend the test frequency range to the MHz region
- development and application of molecular relaxation models, embedding results from computer simulations
- estimation of the size of dynamically correlated regions  $\xi$  approaching the glass transition

- establishing contact to the glass physics and nano-physics community and publication of the achieved findings

The most challenging aspect was that dynamic mechanical analysis was practically not used as an experimental method for research on glass transitions in confinement. At the same time a strong expertise on dynamical mechanical analysis exists at the Faculty of Physics and results of great impact have been achieved within the last 10 years [41, 42, 43, 44, 45].



## Chapter 2

# Samples and preparation

### 2.1 Porous Host Matrices

The influence of spatial confinement on a broad spectrum of physical phenomena has been a topic of experimental and theoretical investigation for nearly three decades. Confinement effects on viscous flow [46], diffusion [47], molecular bondings [48] and quantum fluctuations in  $^4\text{He}$  [49] are only a few examples. Also structural phase transitions [23, 50], as well as crystallization and melting [51] have been found to be crucially modified in nm-scaled spatial limitation. In 1991 the working field of confinement effects on the glass transition has been initialized by a pioneer work of Jackson and McKenna [26] by showing a downshift of  $T_g \propto 1/d$ . Comprehensive reviews of this topic are given in Refs. [34] and [52].

One can think of different arrangements for spatial limitation of liquids, i.e. a pure 1-dimensional confinement between parallel plates, a 2-dimensional confinement in narrow cylinders, or a 3-dimensional confinement within spherical voids. Confinement effects crucially depend on this dimensionality, since it strongly influences the surface-to-volume ratio. However, for laboratory application and due to chemical and mechanical stability, optical properties and availability, the first choice for investigators is to use mesoporous silica as host matrix.

Controlled pore glass (CPG) was invented by Dr. Wolfgang Haller in the 1970s. CPG still is widely used in chemistry [53, 54] and physics [55, 56], but is only available as powder, and though not appropriate for mechanical tests. Compact samples of "Vycor 7930" are manufactured in disc-like shape by Corning Inc., NY. Both CPG and Vycor originate from spinoidal decomposition, resulting in a skeleton of nearly pure  $\text{SiO}_2$  containing a network of interconnected nm-sized pores of narrow PSD, random in length and direction [57]. The confinement dimensionality can be considered between 2D and 3D [52]. Production of "Gelsil" glasses involves a sol-gel process resulting in a different structure. (see Secs. 2.1.1 and 2.1.2).

Gelsil is also available in rigid, monolithic shape, showing a rather broad PSD in the nm-range, and large inner surfaces up to 600 m<sup>2</sup>/g.

Other host matrices in use are regular porous silica such as MCM-41 and SBA-15 [58] or low density silica monoliths [59, 60]. MCM-41 and SBA-15 is a powder that consists of hexagonally arranged cylindrical, not interconnected pores which penetrate the grains of the powder, though realizing a perfect 2D confinement, but those media are not commercially available. Highly porous, low dense silica monoliths, showing a hierarchical system of mesopores and micropores were provided to us by Dr. Sarah Hartmann, University of Ulm, but turned out to be more chalk-like and far too fragile to do mechanical tests or sample preparation.

### 2.1.1 Vycor 7930

The porous glass sold under the brand name "Vycor 7930" by Corning Inc., NY arises from a temperature induced phase separation within a Na<sub>2</sub>O-B<sub>2</sub>O<sub>3</sub>-SiO<sub>2</sub> melt. After cooling the Ba<sub>2</sub>O<sub>3</sub>-rich phase is leached out with an acidic solution, which leaves a 96% pure SiO<sub>2</sub> skeleton [61]. Pores are cylindrical and randomly distributed in length, density and angle (see scheme Fig. 2.1). The leaching process ensures that all pores are open, but not fully interconnected as pockets show up in TEM pictures [57]. Pore sizes can be varied by intercepting the phase separation process. The mean ratio of pore diameter  $d$  over pore length  $l$  was found to be  $d/l \approx 0.23$  [57]. Density of Vycor was determined by measuring volume and weight of the as-produced samples and turned out as  $\rho = 1.40$  g/cm<sup>3</sup>. Porosity  $\Phi = 0.30$  is calculated from

$$\Phi = \frac{\rho - \rho_b}{\rho_b} \quad (2.1)$$

with the density of bulk fused silica  $\rho_b = 2.201$  g/cm<sup>3</sup>.

### 2.1.2 Gelsil

Gelsil monoliths are produced in a sol-gel process by hydrolization of silica containing precursors liquids, followed by condensation and heat treatment. Various precursors with various additional stabilizers (i.e. organic molecules), as well as different routes of production are in use to create highly porous Aerogels ( $\Phi \approx 0.9$ ), Xerogels like Gelsil or highly hierarchical organized porous silica [60]. Silica molecules condensate to spheres on stochastic sites within the hydrolyzed silica precursor. Subsequent gelation leads to a network-like arrangement of spheres. Via heat treatment the gel turns either into a bulk-like powder or monoliths. Thus, the dried and consolidated end product can be approximated as an assembly of stochastically arranged and monodisperse pure silica spheres [62]. Spheres are touching and also penetrating each other,





**Fig. 2.1:** schematic pore model of Vycor 7930 showing interconnected pores and pockets

as Fig. 2.2 sketches. The voids between these spheres constitute a random network of interconnected corridors and pockets and show a larger pore size distribution compared to Vycor 7930. Also bottle-neck shaped and closed pores do arise. Porosities range from  $0.5 < \Phi < 0.9$ , densities are typically  $1 < \rho < 1.5 \text{ g/cm}^3$ .

Until the late 1990s, a company called GelTech Inc. located in Alachua, Florida is an often cited supplier [63, 64, 65, 66]. But in 2001 the production of Gelsil was stopped. After weeks of searching we found out that there is only one company still producing Gelsil, which is 4F International Co. in Gainesville, Florida<sup>1</sup>. Preparation times are long, causing a minimum delivery period of 14 weeks. The price is about 1000 € per  $\text{cm}^3$ .

---

<sup>1</sup>contact: Jesse Wang, email: jwang.4f@gmail.com

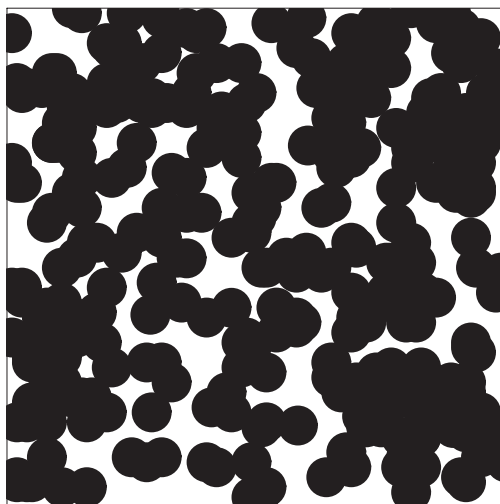


**Fig. 2.2:** Scheme of Gelsil structure: randomly placed spheres of  $r = 4$  in a  $(100 \times 100)$  square,  $\Phi=0.25$ .

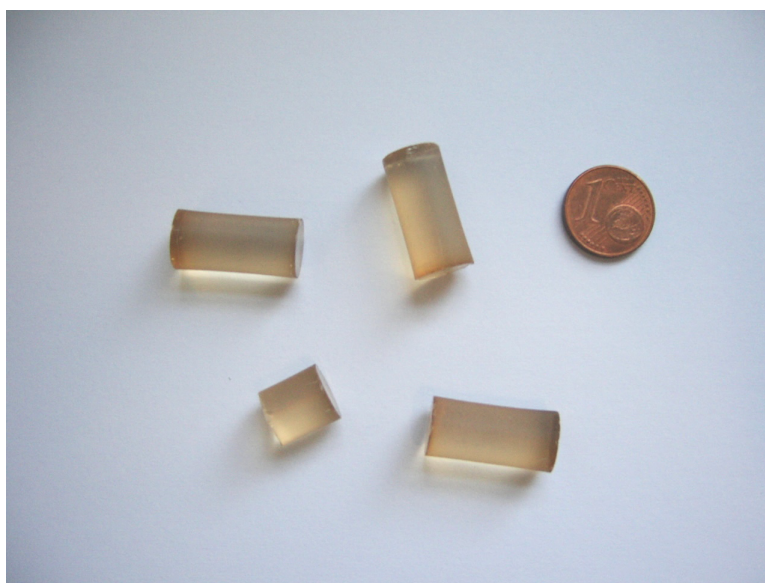


**Fig. 2.3:** Picture of Gelsil 2.6 nm rods as produced by 4F International. The change in color indicates small amounts of contamination, mostly organic molecules adsorbed by the pores along with air moisture. After cleaning samples appear clear and transparent.

## 2.2 Cutting, Sanding, Cleaning and Storage

Samples having orthogonal corners and parallel faces are crucial for DMA analysis, since calculations of Young's modulus  $Y$  in bending or compressing mode involves geometrical models calling for rectangular shapes. Of course in reality one cannot create perfect rectangular shapes, since corners of porous material tend to break and edges tend to chop. The most appropriate way to produce samples for dynamic mechanical analysis turned out to be cutting discs off the the as-produced rods with a diamond wire saw, and further cutting them into bars. Parallel faces and rectangular corners are gained using a steel u-formed shape (see Pict. 2.4), on which samples are clamped and sanded with finely grained sandpaper. Gluing samples on surfaces as used for polishing crystals is excluded, since the glue may permeate the samples' pores. By mounting the sample, sanding, checking angles and shape with an optical microscope, rotating and mounting the sample again and so on, rectangular rods or bars can be produced. The geometrical accuracy of this method, measured by height variations along as-prepared sample faces, is lower than  $10\text{ }\mu\text{m}$ .

Cleaning of all samples has been done in a 30% solution of  $\text{H}_2\text{O}_2$  for 24 hours as proposed by producers [57]. Small amounts of contamination, organic molecules adsorbed along with air moisture, are enough to turn a sample yellowish or brown [67]. The cleaning procedure removes this discolor. Afterwards samples are dried in a high vacuum chamber at  $10^{-6}$  mbar and  $120^\circ\text{C}$  for another 24 h. Multiple small plastic bags together with desiccant silica bags are used to store and transport cleaned samples. Storage for longer periods of time is done in distilled water.

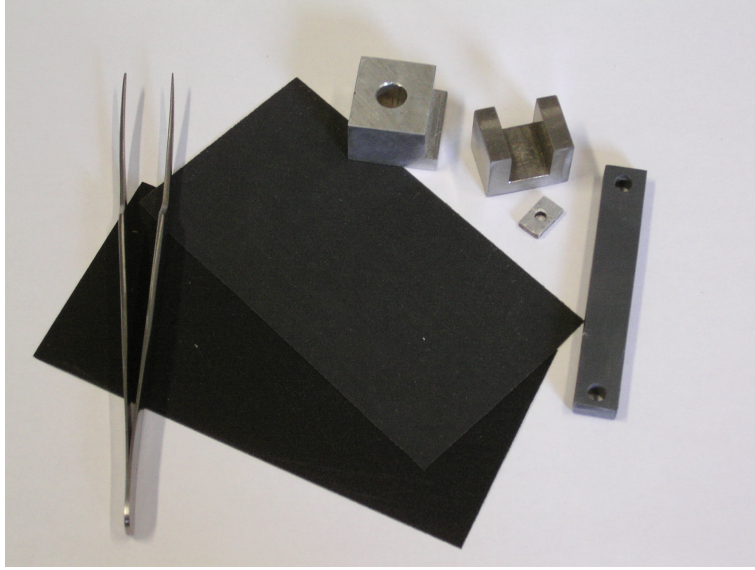


**Fig. 2.4:** holders, clamps and sand paper used for sample preparation

## 2.3 N<sub>2</sub>-Sorption characterization

Adsorption analysis is a standard method for characterizing porous materials. Clean samples are exposed to gaseous nitrogen. Upon rising relative gas pressure  $p/p_0$  nitrogen is adsorbed on inner pore walls. In an ideal case monomolecular layers develop upon the inner surface, and as  $p/p_0 \rightarrow 1$  adsorption saturates. As gas pressure is lowered again, nitrogen is desorbed until the initial state is reached. The quantity of adsorbed/desorbed nitrogen is plotted against relative pressure leading to characteristic - so called - adsorption/desorption isotherms. Shape and hysteresis give hints to pore geometry. Following the IUPAC classification [68] Vycor (see Fig. 2.5) shows a H1-hysteresis pointing at rather uniform cylindrical pores of a certain diameter and length. Gelsil (see Figs. 2.5b and c) shows a H2-hysteresis pointing to a broader PSD, a large interconnectivity and the presence of blocked bottle-neck shaped pores. [69].

A method based on a work of Brunauer, Emmet and Teller [70] is used to derive inner surface and pore volume (BET-analysis). Pore size distribution (PSD) is computed via an approach of Barrett, Joyner, and Halend [71] which is only appropriate down to a pore diameter of 2nm. Below that a method called mercury intrusion is used. For a comprehensive introduction to adsorption characterization see Ref. [72].

Untreated Vycor shows a much sharper PSD, see Fig. 2.6a, than untreated Gelsil in Figs. 2.6b and c. In the range  $2 < d < 10$  nm BJH analysis yields for untreated Vycor a mean value

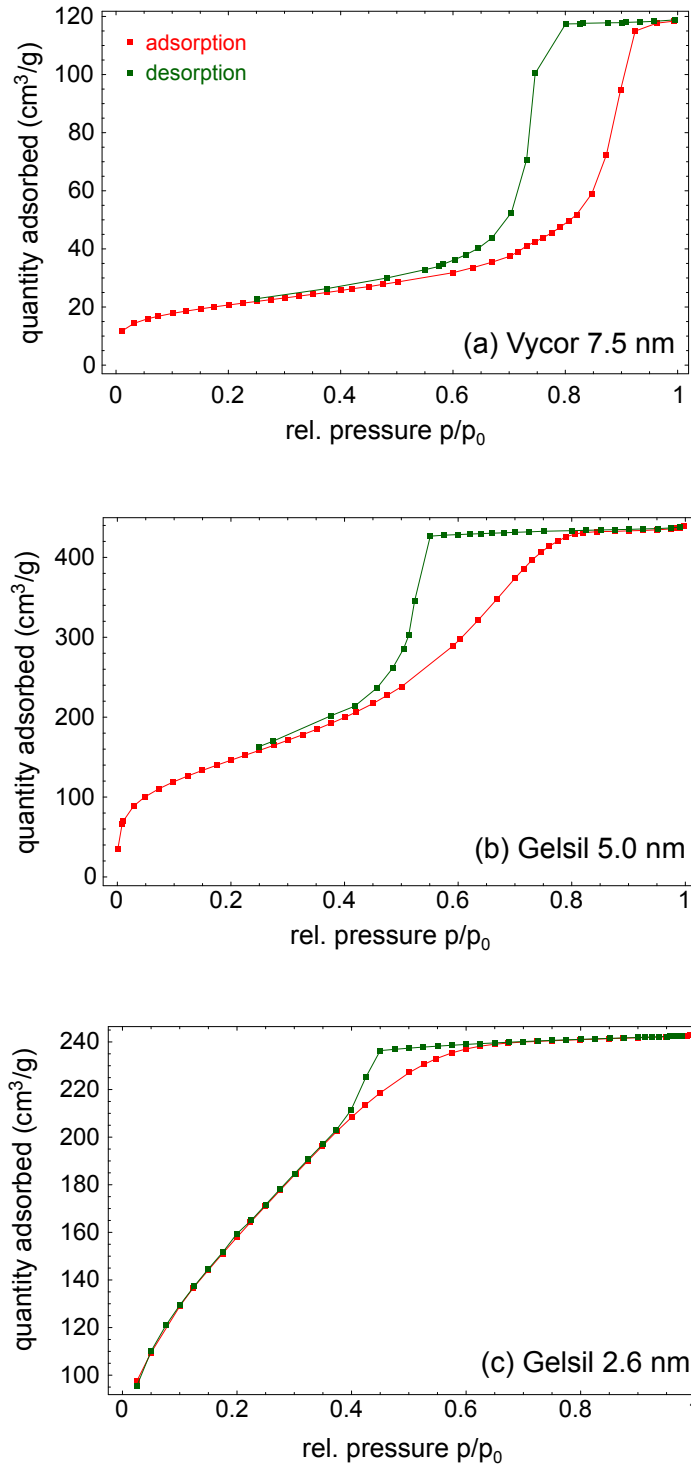


**Fig. 2.5:** Adsorption/Desorption isotherms of porous silica measured by Marie-Alexandra Neouze and coworkers at the Institute of Materials Chemistry at the Vienna University of Technology.

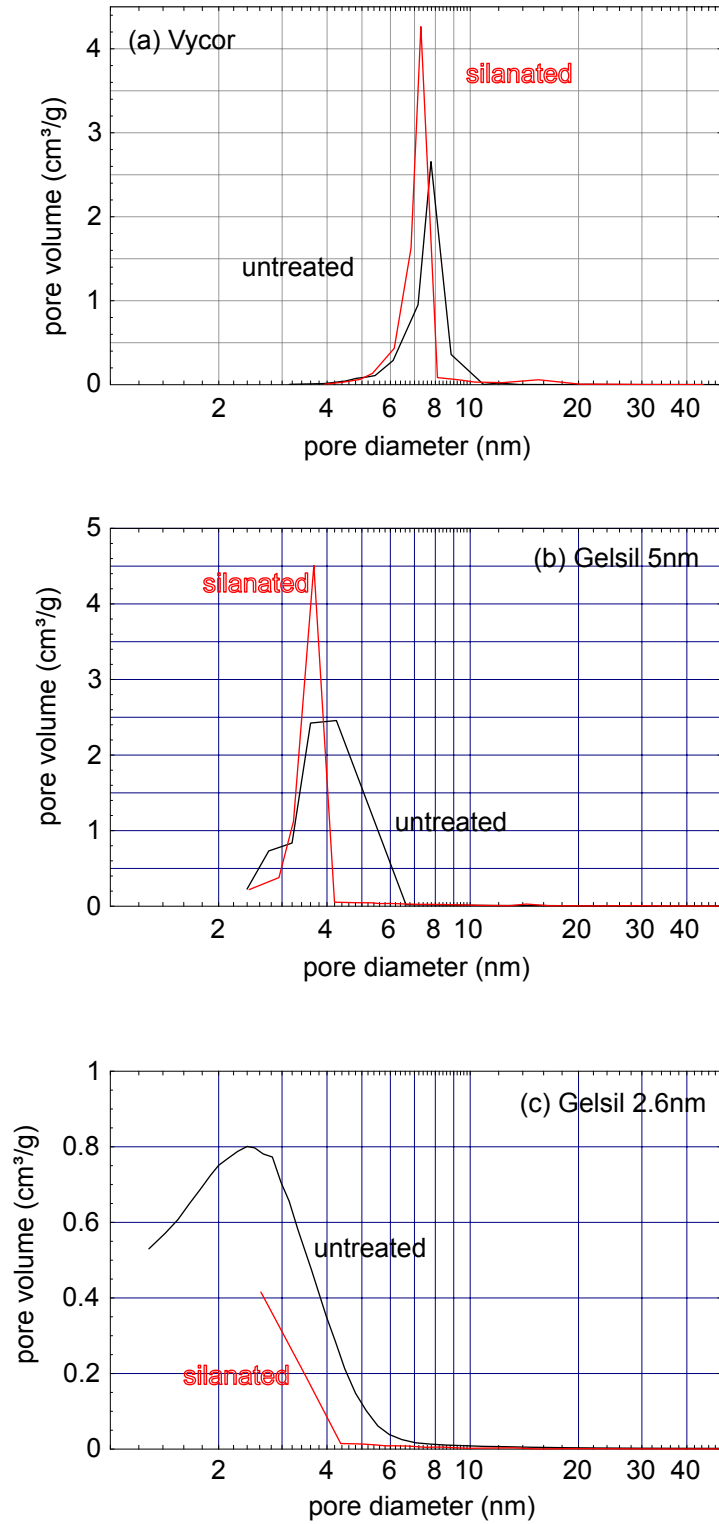


**Fig. 2.6:** Pore size distribution of untreated and silanated samples obtained by BJH/BET analysis of the individual desorption isotherms. Red lines show data of silanated samples (see Sec. 2.4).

of  $d = 7.5$  nm. For Gelsil samples mean diameters 5.0 and 2.6 nm are obtained. All of those values are very close to manufacturers data. For pore diameters smaller than 2 nm, so called nanopores, nitrogen adsorption does not give reliable data any more and BJH analysis cannot be used [67].

The effect of silanation on pore geometry is also shown in Fig. 2.6 (red lines) and Tab. 2.1. Vycor and Gelsil 5 nm show an even sharper PSD, whereas for Gelsil 2.6 nm (Fig. 2.6c) no peak of pore volume can be found due to the narrowness of the pores. A narrowing of PSD due to silanation as seen for Vycor 7.5 nm and Gelsil 5 nm (Fig. 2.6a and b) can be understood in terms of smoothing a prior rough inner surface. HMDS was adsorbed and first filled pockets and blocked bottle neck-formed pores. This idea is supported by the decrease of surface area and total pore volume and porosity (see Tab. 2.1), which is found for all silanated samples.

BJH analysis for both silanated Vycor and Gelsil samples yields a mean diameter of 7.3 nm, 4.8 nm and 2.3 nm respectively. Hence, the thickness of the HMDS layer within pores can be estimated as 0.1 nm (see also Sec. 6.2.1). For comparison Kremer et al. [73] estimated the thickness of the silan layer from analysis of dielectric strength data as 0.38 nm.

**Tab. 2.1:** N<sub>2</sub> adsorption characteristics and porosities of untreated and silanated porous silica samples.

	Gelsil 2.6	Gelsil 5	Vycor
untreated			
av. pore diameter (nm)	2.6	5.0	7.5
surface area (m <sup>2</sup> /g)	590	510	70
pore volume (cm <sup>3</sup> /g)	0.38	0.68	0.21
porosity $\phi$	0.36	0.54	0.40
silanated			
av. pore diameter (nm)	2.4	4.8	7.5
surface area (m <sup>2</sup> /g)	260	325	65
pore volume (cm <sup>3</sup> /g)	0.15	0.4	0.19
porosity $\phi$	0.30	0.49	0.33

## 2.4 Silanation Process

Silanation is the process of coating a hydrophilic surface and replacing charged surface molecules by uncharged ones, and so creating a hydrophobic inner surface. In our case hydroxyl  $\text{OH}^-$  groups on the  $\text{SiO}_2$  silica pore walls are replaced by  $\text{OSi}(\text{CH}_3)_3$  trimethylsilyl groups (see Fig. 2.7). This is achieved by exposing cleaned and dried samples to gaseous hexamethyldisilazane (HMDS, by Sigma-Aldrich, purity 99.9%) as sketched in Fig. 2.8.

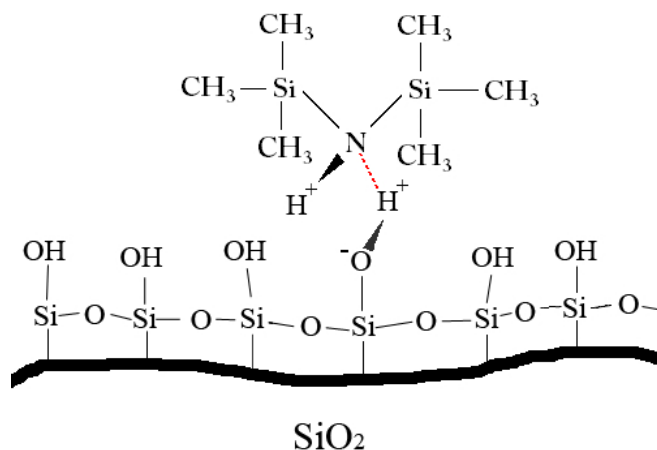


**Fig. 2.7:** Hexamethyldisilazane molecule replacing  $\text{OH}^-$  on a silica surface.

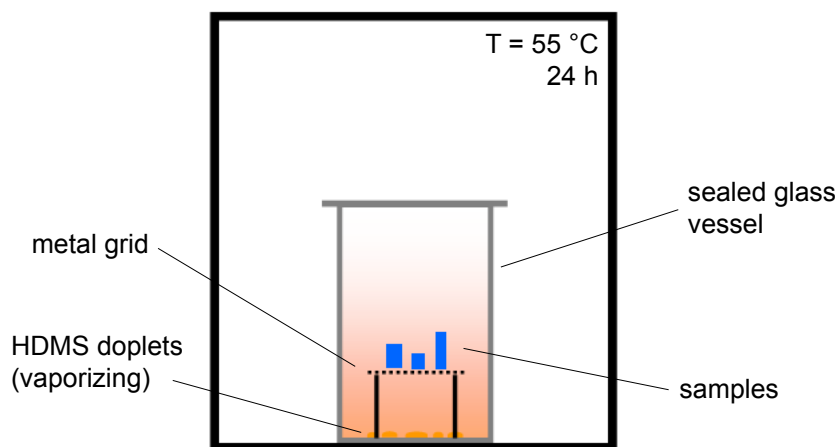


**Fig. 2.8:** Sketch of silanation process: Placed on a metal grid the cleaned samples are exposed to HMDS vapor in a closed glass vessel.

First a few droplets of HMDS are put on the bottom of a cleaned glass vessel. At room temperature HMDS is a clear, slightly yellow, volatile and corrosive liquid. Handling it calls for an exhaust hood, gloves and protection goggles. A metallic grid is put in the vessel and



the samples are placed on top of it. Afterwards the glass vessel is closed, sealed and put into a heating chamber at 55°C for 24 h.

During this process samples turn yellow to brown dependent of the inner surface (see Tab. 2.1). Silanated Vycor still was transparent, whereas Gelsil samples turned yellow (Gelsil 2.6 nm) and even brown (Gelsil 5nm). Silanated samples afterwards were evacuated once more at  $10^{-6}$  mbar at room temperature in order to remove any excessive liquid HMDS from the pores. Finally samples are filled with salol.

## 2.5 Filling procedure

In order to fill porous samples with the low molecular glass forming liquid salol (phenyl salicylate,  $C_{13}H_{10}O_3$ ) capillary forces are utilized. In capillary tubes pressure reduction is known [74] as  $P_c = 2\sigma/r$  with surface tension  $\sigma$  and pore radius  $r$ . As demonstrated in Sec. 5.3.2 for salol ( $\sigma = 1.73 \times 10^{-2}$  N/m) in a pore of 2.6 nm in diameter this would lead to  $P_c = 26$  MPa and a hypothetical capillary rise of 1.8 km. So capillary forces are strong in our samples and can be used to fill up most of the pore space, as we shall show below.

Simple submersion in liquid salol and contact with the whole sample surface leads to a remaining "bubble" of unfilled pores in the center which cannot be filled further. A more efficient way is to let the sample soak up single droplets, always taking care of only one side of the sample being in contact with the liquid. Thus for the following DMA measurements one can guarantee that none of the faces in contact with the measurement geometry have ever got in touch with salol and the effects observed definitely arise from salol *within* the pore system.

Filling fractions can easily be determined by weighing clean and filled samples. With the difference in weight  $\Delta w$  and the density of salol  $\rho_{sal}$  the filling fraction  $f$  is determined as

$$f = \frac{\Delta w}{\rho_{sal}} \cdot \frac{1}{V_{por}} \quad 0 < f < 1 \quad (2.2)$$

with the total pore volume  $V_{por} = V_{sample} \cdot \Phi$ . Porosities  $\Phi$  see Tab. 2.1. The error of this method estimated by Gaussian error propagation is  $\sigma_f \approx 0.02$ . Whereas Vycor samples are filled up to  $f = 0.95$  within minutes, the pore space of Gelsil samples takes about 1 h to be filled up to  $f = 0.5$ . Possible reasons are the plugging of bottle-neck pores and a significant part of closed pores (see Fig.2.2), which cannot be reached by the liquid.

The filling process itself has been observed via the simultaneous volumetric growth of the

porous matrix. A Perkin Elmer series 7 DMA has been used in a static so called TMA mode in parallel plate geometry. At RT crystalline salol has been placed next to and around a clean and empty sample (see Fig. 2.9). The quartz rod was placed on top of the sample with zero force. Next, the temperature was increased to reach the melting temperature  $T_m = 317$  K of salol. A sudden voluminal growth sets in and the samples height  $h$  was recorded with a resolution of 10 nm. The result (see also Sec. 5.3.2) shows the typical  $\sqrt{t}$  behavior known for filling of a single capillary as described by Lucas [75] and Washburn [76]. This result is also in agreement with findings of Huber et al. [77] and was published in Ref. [38] (chapter 5).

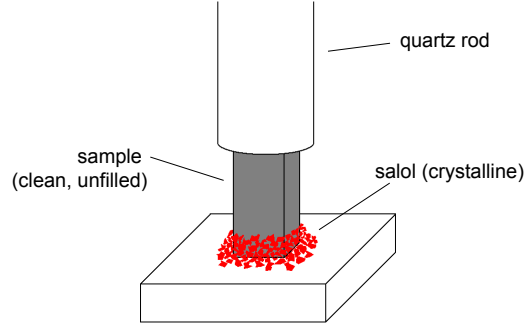


**Fig. 2.9:** Sketch of adsorption swelling measurements. Crystalline salol is placed next to the samples bottom and the quartz rod is placed on top of the sample with  $F = 0$  N. As temperature is raised to  $T_m = 317$  K of salol, the sample adsorbs the melted liquid.

## Chapter 3

# Laboratory equipment and details

This chapter focuses on technical details and handling of both DMA devices used: a DMA series 7 built in 1989 and the newly installed Diamond DMA built in 2005, both by Perkin Elmer Inc. Calibrations, cooling devices and self designed measurement extensions are presented. Furthermore, the method itself is explained and an estimation of stress and strain is developed.

### 3.1 Method

A dynamic mechanical analyzer in most of all applications and measurement geometries tests Young's modulus defined as

$$Y = \frac{\sigma_z}{\epsilon_z} \quad (3.1)$$

with stress  $\sigma$  and strain  $\epsilon$  in direction  $z$ . The main difference to a bulk modulus  $K$  is its uniaxial character. Applied stress in direction  $z$  generates strain along  $z$ . The force  $F$  is given by a motor and transferred upon the samples surface via a metallic or quartz rod. The created deformation is recorded using electromagnetic inductive coupling within an so called LVDT. A linear variable differential transformer (LVDT) uses a symmetric arrangement of primary and secondary coils i.o. to resolve the rod's movement by 10 nm. The generated deformation is calculated from the rods position change dependent of the geometry in use, and compared to the force which then yields Young's Modulus.

Force on the one hand can be applied constant and static. This case realizes the so called TMA (thermo-mechanical-analyzer) mode used e.g. for static stress-strain relations (Sec. 7.2) or thermal expansion measurements (Sec. 5.3.3). Another mode (the DMA mode) uses a static plus a dynamic force

$$F = F_{stat} + F_{dyn} \cdot e^{i\omega t} \quad (F_{stat} > F_{dyn}) \quad (3.2)$$

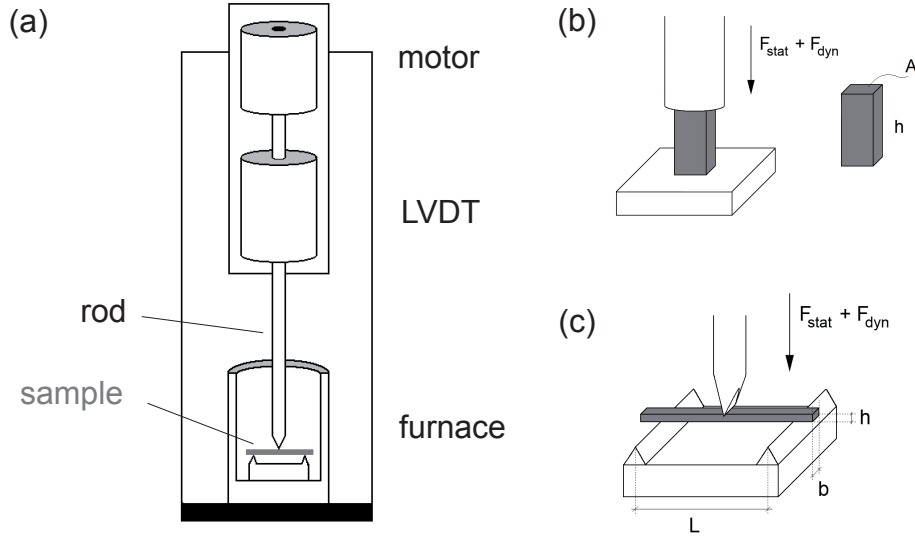


**Fig. 3.1:** Sketch of a DMA analyzer (a) and measurement geometries parallel plate (b) and three point bending (c).

with circular frequency  $\omega = 2 \cdot \pi \cdot \nu$ . A sinusoidal force at low frequency ( $1 \text{ Hz} < \nu < 100 \text{ Hz}$ ) is applied and usually the response of the sample is a sinusoidal deformation. There can be a delay between force and generated deformation. This phase lag  $\delta$  is a measure of kinetic energy lost within the sample and transferred into heat and is resolved by  $0.01^\circ$ . Metallic samples usually respond fast. Their oscillation is in most cases nearly lossless and the phase lag (usually given as  $\tan \delta$ ) apart a phase transition is close to zero. Polymer samples like PVC, PET or PMMA usually show a larger attenuation and  $\tan \delta$ , especially near phase transitions.

The DMA originally has been built for measurements of soft matter like plastics, polymers, rubber etc. Using different geometries as e.g. bending mode and forces up to 18 N allowed to reach the needed amount of strain and made it possible to exploit the amazing resolution also for the study of rather hard single crystals [43, 42] or metallic samples [78, 79, 80].

Different geometries are in use. The most straight-forward one is a parallel-plate geometry as shown in Fig. 3.1b. The complex Young's modulus in this case is

$$Y^*(t) = \frac{h}{A} \cdot \frac{F(t)}{\Delta h(t)} \quad (3.3)$$

with samples height  $h$ , contact surface  $A$  and the generated change in sample height  $\Delta h$ . The analyzer delivers real and imaginary part of  $Y^* = Y' + i \cdot Y''$  as storage modulus  $Y'$  and loss modulus  $Y'' = Y' \cdot \tan \delta$ .

Parallel plate measurements especially are subject to losses due to imperfect contact of sample and rod. The samples surface will never be a perfectly flat plane and samples are never shaped perfectly rectangular. The microscopic details of this contact are unknown. Thus, the modulus measured by the apparatus is usually below literature values. Contact errors can never be avoided and since they are unknown, DMA cannot supply absolute values for elastic moduli. A detailed discussion is given by D. Havlik [81] and also found in Ref. [36] and Sec. 4.3. In the present work this drawback was avoided by the use of RUS yielding very accurate moduli values at RT, which then were used to calibrate DMA results.

Especially the parallel plate geometry is subjected to a large contact error due to the large contact area  $A$ . This leads to a poor resolution in  $Y$  and  $\delta$ . Parallel plate geometry within this thesis was used for static measurements only to determine thermal expansion or adsorption swelling, for which of course it is the preferred geometry.

The geometry mostly used is three-point-bending, shown in Fig. 3.1c. The sample is sustained by a support of span  $l$ . Force perpendicular to the samples surface leads to flexure of depth  $m$ . The flexural modulus derived via

$$M(t) = \frac{3}{12} \frac{l^3}{w h^3} \frac{F(t)}{m(t)} \quad (3.4)$$

is determined by Young's and shear modulus as

$$M = \left[ S_{11} + \frac{3}{2} \left( \frac{h}{l} \right)^2 S_{55} \right]^{-1} \quad (3.5)$$

with the inverse elastic tensor components  $S_{ij} = C_{ij}^{-1}$  known as compliances. For cubic and homogeneous media  $S_{11}$  can be written as

$$S_{11} = \frac{C_{11} + C_{12}}{(C_{11} + 2C_{12})(C_{11} - C_{12})} \quad (3.6)$$

showing that a combination of elastic constants is probed. Eqn. (3.5) displays that the influence of shear  $S_{55} = 1/C_{55}$  is small as long as  $l \gg h$ . That's why for 3PB geometry the modulus derived by Eqn. (3.4) is identified with the Young's Modulus [41, 42, 81]

$$Y := \frac{1}{S_{11}}. \quad (3.7)$$

## 3.2 Perkin Elmer DMA series 7

The dynamic mechanical analyzer series 7 was built in 1989 . Via a combination of static and dynamic forces it tests a samples Young's modulus  $Y$  as well as damping  $\tan \delta$  dependent on temperature, applied force and frequency (see Sec. 3.1). A maximum force of 2.5 N can be applied in a frequency range of  $0.01 \leq \nu \leq 51$  Hz. A sketch is given in Fig. 3.1. 3PB, PP, tension and cantilever accessories made of steel as well as of quartz glass are available. Temperature can be varied using heating or cooling furnaces. Purge gas nitrogen is controlled via a flowmeter.

The DMA 7 is very sensitive to building vibrations, especially during dynamical measurements ( $F_{dyn} > 0$ ). Oscillations within the building disturb the measurements since their frequency coincides with the DMAs frequency range. In order to decouple the apparatus from the ambient building ideally it should be placed on an air suspension table. Since air tables are very expensive, another solution had to be found. The apparatus was placed on a 100 kg granite plate resting on 2 cm sized pieces of rubber. Measurements using an acceleration sensor showed that vertical accelerations were diminished noticeably. Interaction with the 50 Hz oscillation of the mains voltage have not been observed since all electronics within the analyzer is shielded.

### 3.2.1 Temperature control

Heating the sample is done with a heater surrounding the sample chamber which itself is surrounded by a water bath. The water bath is continuously flushed. Both heating and cooling runs from RT up to 600°C were executed satisfyingly as programmed. Heating runs from 180 K to RT also worked as supposed. A temperature hold allowing isothermal measurements is also performed satisfactory within  $\pm 0.1$  K.

Cooling is done in a furnace which - by hand - is filled with liquid nitrogen until the lower start temperature, in our case  $\approx 180$  K, is reached. For this reason an automated cooling run starting at RT with the DMA 7 is not advisable. The furnace itself drifts without heating to RT by roughly 0.5 K/min, which determines lower limit of the possible heating rates starting at LT. Due to the necessary change of furnaces, a continuous run from 180 to 900 K cannot be done.

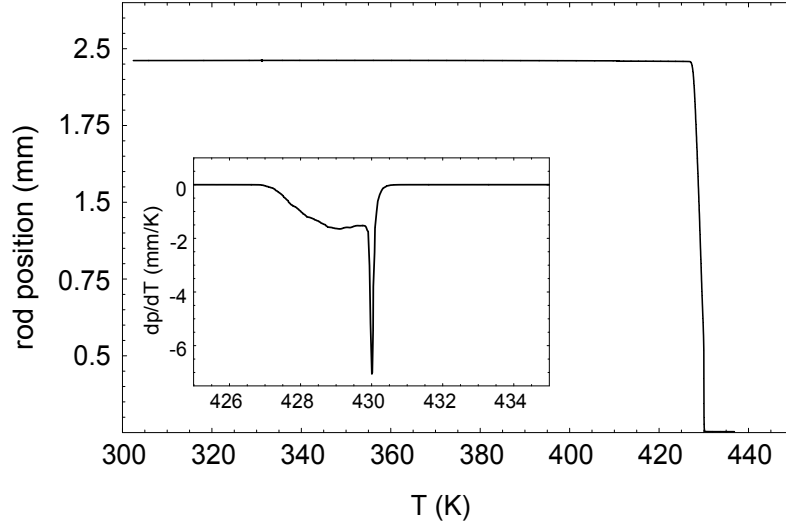


**Fig. 3.2:** Position signal of the DMA7's rod placed on a cylindrical piece of indium upon heating. Inset shows the first derivative w. r. to temperature and melting at  $T = 430.0$  K.

### 3.2.2 Calibration

Calibration of force and height reading and eigendeformation is done following the standard procedure [82] and by the use of standard calibration samples made of steel or quartz. Those three calibrations have to be repeated every time the measuring geometry is changed. (PP, 3PB, tension,...).

The thermocouple placed near the sample is calibrated using the melting point of indium. Standard indium pieces provided by Perkin Elmer Inc. are placed in a aluminium cup and the rod in PP geometry is placed on top with a small force of 50 mN i.o. to ensure proper contact. Afterwards, in a TMA mode temperature is raised by 1 K/min up to 500 K. The melting will show up as a sudden decrease in rod position  $p$  (Fig. 3.2). Comparing the found melting point to the literature value of  $T_m = 429.75$  K yields the new temperature calibration.

A melting point of  $T_m^{TMA} = 430.0$  K was found which is only 0.25 K off the expected  $T_m$  which is in the range of the temperature stability of the temperature controller of  $\pm 0.1$  K and the estimated  $T$ -resolution of  $\pm 0.1$  K. All further measurements are corrected according to this result.

### 3.2.3 Measurement procedure

After turning on the whole setup of DMA, controller and computer, a waiting time of at least 40 min is required, since especially the LVDT and the probe position signal needs to equilibrate. The constancy of  $p(t)$  should be rechecked afterwards, since at certain circumstances a slow drift of 1  $\mu\text{m}/\text{h}$  was observed which was hard to explain or to eliminate.

The 3PB quartz extension setup was used for all measurements herein. The Pyris Software Version 3.03 in use allows control of all important control parameters as probe position, forces, temperature program and furnace temperature. After positioning the quartz rod is placed on top of the sample without any force. A certain waiting time assures equilibration of the probe position signal. The probe position is set to zero (for 3PB experiments this is not necessary). At RT and closed furnace a small static force is applied which has to be accompanied by a downshift of rod position signal.

Turning on dynamic forces (e.g. at a standard frequency of 1 Hz) yields preliminary storage and loss moduli. At least by order of magnitude those values should be comparable to literature values. At any time  $F_{dyn} < F_{stat}$  since otherwise, the rod will loose contact, go up and when going down may crack the sample.  $F_{stat}$  and  $F_{dyn}$  are chosen as high as possible, since a large deformation amplitude increases resolution. At the same time, forces are chosen as close as possible (a minimum difference of 50 mN is advisable). In that way, forces are increased until a dynamic deformation of at least 2  $\mu\text{m}$  is achieved.  $\tan \delta$  at the same time should at least rise above 0.02.

After setting sample dimensions, file name and temperature program, the furnace can be closed. A short waiting time for temperature equilibration is recommended since the samples temperature will change as soon as the furnace is raised. During that time the purge gas (99.9% dry nitrogen) is turned on at 25 l/min i.o. to remove air moisture around the sample. Furthermore, the measurements end conditions need to be set which define temperature and forces applied after the measurement run is completed. A static force of 50 mN and holding temperature at current is advisable. After all the measurement run can be started. Strong vibrations in the room should be avoided, also measurements during construction works within the building. Most of the measurements shown here had to be done over night.

For cooling runs the analyzer has to be programmed and liquid nitrogen has to be poured into the furnace bit by bit and by hand, roughly every 2 minutes. Especially for filled porous silica samples, a cooling ramp of 2 K/min should not be exceeded. Faster cooling in some cases



led to cracks and destruction of the sample. In between, frequency is chosen, sample dimensions, temperature program and end conditions are set. In principle data can be gathered during cooling, but pouring in liquid N<sub>2</sub> leads to vibrations, and a smooth cooling curve is hard to achieve. A typical cooling run down to 170 K takes about 90 min. Once the intended low temperature is reached (limit: 90 K), a short waiting time is necessary to let the temperature equilibrate. As temperature starts rising again by itself, the heating run (e.g. at 2 K/min) is started. From that moment on, all vibrations within the room have to be minimized. It turned out as most advisable to start measurements late at night.

### 3.3 Perkin Elmer Diamond DMA

The Perkin Elmer Diamond DMA also used in the present thesis was built in 2005. It is a follower of the 7 and 7e series and actually designed for large polymer samples. We have modified the apparatus by an extension for small glass or metallic samples during this thesis. Its maximum static force is 10 N and the maximum dynamical force is 8 N giving 18 N of maximum overall force. Its main difference to the DMA series 7 is its nearly automated measurement procedure. Far less options can be controlled turning it into a "black box" for the user. E.g. there is no way to read out the probe position. Furthermore, an unknown computer controlled procedure creates pairs of forces which improve the resolution on  $Y$  and  $\tan \delta$ . These forces are altered during the measurement and cannot be controlled, so the instrument rather often destroys samples. However, once working, the resolution achieved is brilliant in comparison to DMA 7 data (see for example Fig. 4.3 vs. Fig. 5.5).

Bending, single cantilever, tension, shear and compression attachments made of steel are available only for large samples (cm-range). A steel made 3PB attachment for small samples (rods of 5mm in length,  $< 1$  mm thickness) using parts of a DMA 7 was designed, constructed and implemented within this thesis (see chapter 10).

The frequency range is  $0.01 \text{ Hz} \leq \nu \leq 100 \text{ Hz}$ , and can be chosen from  $200/n$ ,  $n$  being an integer between 2 and 20000. The accessible temperature range is  $-150^\circ\text{C} \leq T \leq 600^\circ\text{C}$  with possible heating rates from 0.01 to 20 K/min. The displacement resolution is 10 nm, and damping  $\delta$  is read within 0.005, which is two times better than the DMA 7's  $\delta$ -resolution. Force is controlled with a resolution of  $10^{-5}$  N.

The Diamond DMA is a heavy instrument and due to mechanical damping within the construction itself is much less sensitive to building vibrations. The furnace is lifted up and down automatically and cooling and heating runs can be performed within one run. The attached cooling setup uses liquid nitrogen, which is vaporized by a heating element and channeled into the furnace cooling it down. This method is quite inefficient and uses a lot of liquid nitrogen, also, the lowest temperature of  $-150^\circ\text{C}$  is only reached very slowly using some 30 l of nitrogen. Isothermal runs at low temperature are also very costly in  $\text{N}_2$ . The lowest heating rate achieved for the low temperature regime was 0.1 K/min. A lower rate would call for refilling the  $\text{N}_2$  tank which cannot be done during the measurement run. Furthermore, all measurements runs below RT are stopped by the temperature controller, if the liquid  $\text{N}_2$  level falls below 1/4.

In order to achieve reliable temperature control the Diamond DMA uses precalibrations.



Perkin Elmer DMA series 7



Perkin Elmer Diamond DMA

**Fig. 3.3:** Photos of Perkin Elmer DMA 7 and Diamond DMA.

These empty runs have to be done separately for the corresponding temperature range and heating rate before the actual measurement. Using these precalibrated temperature ramps every temperature scan is performed with great accuracy.

### 3.3.1 Calibrations

The module needs to be calibrated according to the attachment in use. Again, there is an automated procedure for height reading, force and eigendeformation using different steel plates and aluminum films.

Temperature calibration, as a standard procedure recommended by Perkin Elmer, is done by the melting of PMMA in both bending and tension mode. Perkin Elmer report a  $Y''$  peak temperature of  $T_{peak}=390.2$  K for their standard PMMA samples. The peak position found for bending is  $T_{peak}^{bend} = 387.1$  K and  $T_{peak}^{tens} = 391.5$  K for tension at 1 Hz upon 2 K/min heating. Measurements following all given instructions [83] are shown in Fig. 3.4. Perkin Elmer suggests to derive a mean peak position  $\bar{T}_{peak} = (1/2) \cdot (T_{peak}^{bend} + T_{peak}^{tens}) = 389.3$  K and to use its deviation from  $T_{peak}$  as the temperature correction term. According to this procedure the correction term would be  $\Delta T_{corr} = 0.9$  K.

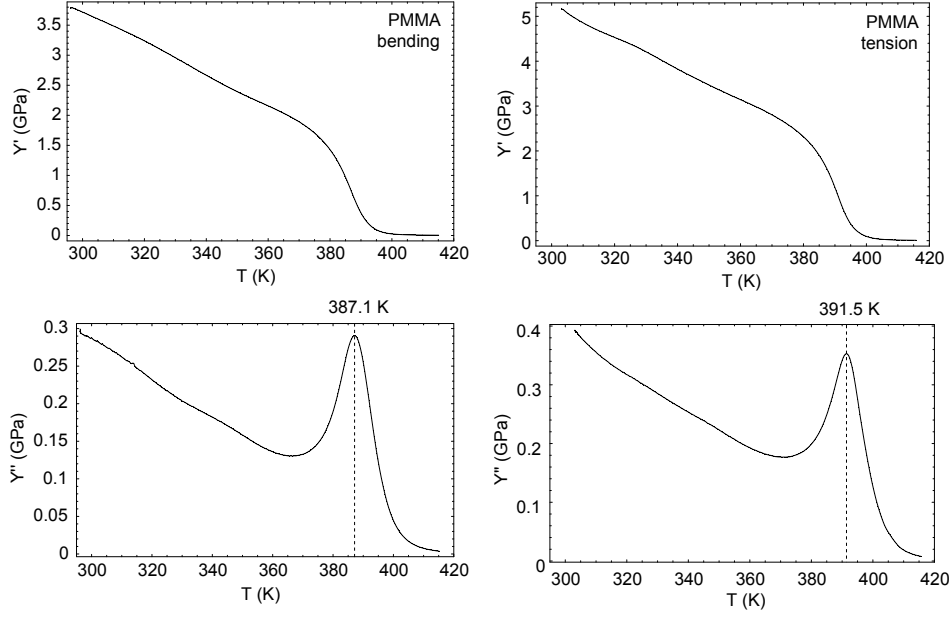


**Fig. 3.4:** Diamond DMA calibration: a standard PMMA sample measured in bending and tension geometry at 1 Hz.

The main point of criticism here is that at high temperature PMMA performs a transition from a glassy into a liquid state. This is not a proper phase transition and  $T_g$  not only depends on heating rate and measurement frequency, but also on the thermal history of the sample [84]. In literature several transition temperatures ranging from 393 K to 413 K are given [85]. Furthermore, the attachments in use (3PB DMA series 7) are different from the original ones and show different contact areas between sample and attachment.

These problems were bypassed via a calibration using indium and the attachment later in use for small samples (see chapter 10), which also is comparable to the method used for the DMA series 7 in Sec. 3.2.2. The Diamond DMA does not provide access to probe position data, so a dynamical test at 1 Hz and 0.5 K/min in PP mode was performed. The peak in  $\tan \delta$  is used for detection of  $T_m^{exp} = 429.0$  K as shown in Fig. 3.5. This is very close to the literature melting point of Indium  $T_m^{lit} = 429.75$  K. Therefore a correction term of  $\Delta T = +0.75$  K was used for all further measurements.

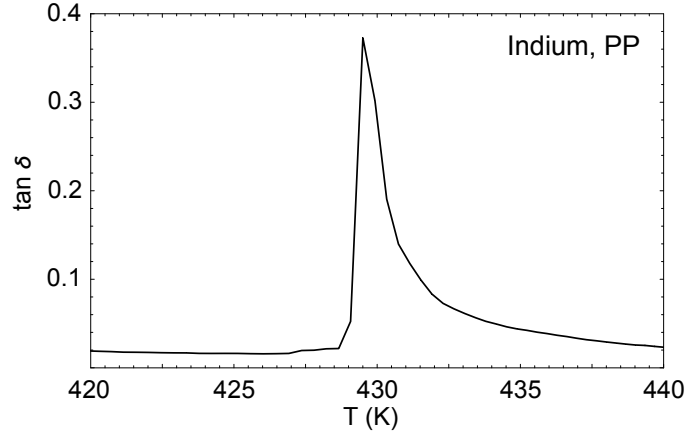


**Fig. 3.5:** PP test of indium at 1 Hz showing a narrow  $\tan \delta$  peak at 429.0 K.

### 3.3.2 Measurement procedure for 3PB

- The 3PB attachment is mounted. The parallel alignment of the probes lower edge relative to the support edges is done with the DMA7's alignment tool for the 5 mm 3PB steel attachment.
- The module is initialized. During this automated procedure the apparatus determines the offset load of the probe (i.e. the weight the probe plus attachment) and searches for the probes "zero" position.
- The sample is positioned on the support orthogonal to edges which is checked using the alignment tool and by visual inspection. It is helpful to lower the probe in small steps near to the samples surface i.o. to control the arrangement.
- The furnace is closed and the purge gas  $N_2$  is turned on at 25 l/min.
- Sample name and dimensions and a file name are entered. A temperature program is set up and a measurement frequency  $\nu$  is chosen.
- Default static and dynamic forces are entered. Static and dynamic forces can only be chosen as starting values for  $F_{base}$ ,  $F_0$  and the tension/compression gain  $g$ , where  $F(t) = F_{base} + g \cdot F_0 \cdot e^{i\omega t}$ . During measurements  $F_{base}$  is held constant and  $F_0$  is chosen automatically and  $\propto$  the found storage modulus. For soft materials, a gain  $g$  of 1 is recommended, for metals 1.5. For porous silica  $g = 1.2$  was chosen.
- The apparatus is geared to the deformation amplitude called "L Amp." which it tries to reach and hold constant. A value of 10  $\mu m$  to 20  $\mu m$  worked fine for all porous silica

samples. A "L Amp." set too high will destroy the sample during the measurement, especially in 3PB, even if initial test showed good results.

- Maximum deformation is entered (  $20\text{ }\mu\text{m}$ ) and the appropriate temperature precalibration file is loaded.
- Setup is saved and the test-function will give a single RT measurement using the setup parameters. Changing parameters and testing again is repeated several times until reproducible results are achieved which are in the range of expectations.
- The measurement run is started.

From time to time the Pyris software (Muse Version 3.9) controlling the DMA reports an "unknown software error" and recommends a software restart. In this case, the measurement run has to be stopped, since no more data are collected. A restart requires removing the sample (at room temperature) and initializing the module. A measurement run will be stopped automatically if the sample breaks.  $F_{dyn}$  is set to zero and  $F_{stat}$  will turn back to initial values. Cooling / heating is also stopped and the module will return to RT by thermal equilibration.

### 3.3.3 Optimizing sample dimension

Since our samples have rather large Young's moduli (several 10 GPa), we are always working close to the resolution limit of the DMA. I.o. to achieve good results we have to optimize the sample geometries.

In any case a dynamic mechanical measurement calls for a certain amount of dynamic deformation in the  $\mu\text{m}$  range. If this minimum deformation is barely achieved, the resolution in storage and loss modulus will be poor. If it is not achieved, the rods position change is too small and the phase lag  $\delta$  may not be resolved any more. The Diamond DMA stops the run automatically. On the other hand, a deformation too large may destroy the sample, even with the minimum deformation setup. That's why the shape of the sample is crucial and has to be calculated before preparation. The following considerations are done for 3PB geometry:

Young's modulus  $Y$  is derived by comparing stress and strain and has to be independent of sample shape, or deformation mode. Stress  $\sigma$  is proportional to the amount of force  $F$  by  $\sigma = c_f \cdot F$ . Strain is proportional to the amount of linear deformation  $\Delta x$  by  $\epsilon = c_s \cdot \Delta x$ . Factors  $c_f$  and  $c_s$  represent the sample shape and measurement geometry via the shape factor  $\alpha$ :

$$Y = \frac{\sigma}{\epsilon} = \frac{c_f \cdot F}{c_s \cdot \Delta x} = \frac{1}{\alpha} \cdot \frac{F}{\Delta x} \quad (3.8)$$

For 3PB geometry with rectangular cross section the shape factor is

$$\alpha = \frac{4wt^3}{l^3} \quad [\alpha] = \text{m} \quad (3.9)$$

with sample width  $w$ , thickness  $t$  and length  $l$  (which is identical with the span with of the 3PB suspension). Using the apparatus' limits [83] of  $10^2/\alpha < Y < 10^7/\alpha$  this relation can be put in a log-log diagram showing the link between a sample shape and the DMA's Young's modulus range shown in Fig. 3.6. Knowledge of the approximate Young's modulus of the sample allows to find the ideal sample shape i.o. to reach the maximum resolution.

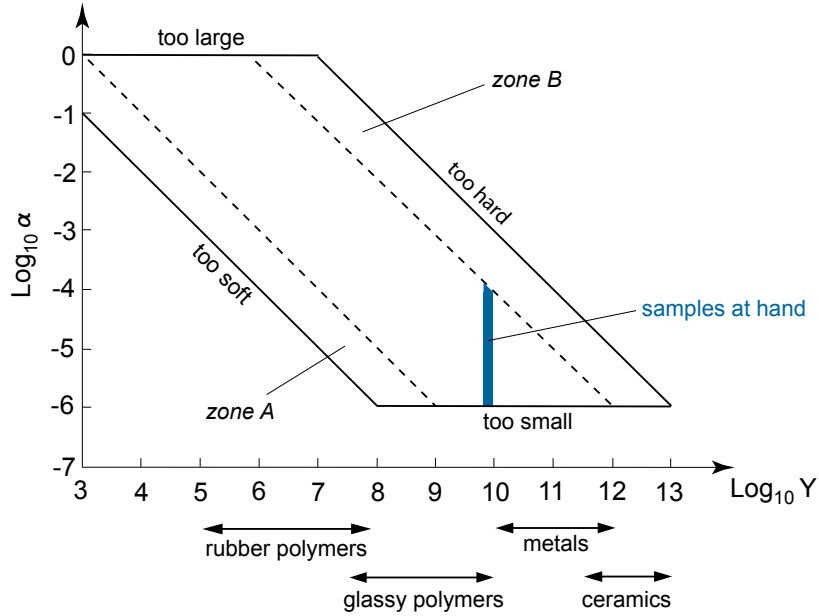


**Fig. 3.6:** Elastic measurement range of a Diamond DMA dependent on the sample's geometry factor  $\alpha$ . Zone A and B denote a probable loss of accuracy at high frequency [83].

For the samples in use within this thesis  $9 \text{ GPa} < Y < 20 \text{ GPa}$ , meaning that

$$10^{-6} < \frac{4wt^3}{l^3} < 10^{-4} \quad (3.10)$$

as shown in Fig.3.6. Assuming a sample width of  $w = 2 \text{ mm}$ , the thickness needs to be  $0.25 \text{ mm} < t < 1.2 \text{ mm}$ . Experience showed that especially Gelsil samples are broken by the

Diamond DMA is designed thinner than 1 mm. Therefore, the measurements presented within this thesis really were performed close to the resolution limit, partly within the called "zone B" of Fig. 3.6, denoting a possible loss of accuracy at high frequency, which in some cases indeed was observed (see e.g. Fig. 4.3b).



### 3.3.4 3PB measuring cell for small samples

Since the original Diamond DMA bending attachment provided by Perkin Elmer needs a minimum sample length of 40 mm, the bending geometry of the DMA series 7 was adapted (steel, span 5mm). Therefore a new support plate and a connection between Diamond DMA rod and DMA 7 rod attachments had to be built. The solution found is shown in chapter 10. It allows to mount DMA 7 attachments and bottom supports onto the Diamond DMA's geometry. The DMA 7's bending, parallel plate as well as tension attachment may then be used taking advantage of the higher force and resolution of the Diamond DMA.

All measurements of Ref. [40] (Sec. 6) and most of Ref. [38] (Sec. 5) have been done using this extension. Furthermore it was used for nanostructured copper, skutterudites [78], perovskites [79], the study of avalanches at the martensitic phase transition in CuAlBe [80] and magnetostrictive FeMn-alloys.



**Fig. 3.7:** Photo of Diamond DMA measurement cell designed for 3PB tests of small samples. A workshop drawing also is shown in chapter 10. The picture also shows the lowered furnace with the N<sub>2</sub> supply (black, in front).



## Chapter 4

# Heterogeneous relaxation dynamics of nano-confined salol probed by DMA, EPL 79, 36006 (2007)

Manuscript of published article

by

W. Schranz, M.R. Puica, J. Koppensteiner, H. Kabelka and A.V. Kityk

The contribution of J. Koppensteiner in this early stage of the present thesis has been

- experimental work: confirming results using the newly installed Perkin Elmer Diamond DMA
- development of relaxation models and fitting the data (together with W. Schranz).
- literature research (together with W. Schranz)

# Heterogeneous relaxation dynamics of nano-confined salol probed by DMA

W. Schranz<sup>1</sup>, M.R. Puica<sup>1</sup>, J. Koppensteiner<sup>1</sup>, H. Kabelka<sup>1</sup> and A.V. Kityk<sup>2</sup>

<sup>1</sup> Nonlinear Physics Group, Faculty of Physics of the University of Vienna, Boltzmanngasse 5, A-1090 Vienna, Austria

<sup>2</sup> Institute for Computer Science, Technical University of Czestochowa, Armii Krajowej 17, PL 42-200 Czestochowa, Poland

## *Abstract*

We present novel low-frequency (0.1 Hz - 50 Hz) measurements of the complex elastic susceptibility of the glass-forming liquid salol confined to nanoporous Vycor glass. Our data can be perfectly interpreted with the assumption of a radial distribution of Vogel-Fulcher temperatures  $T_0(r)$  inside the pores, resulting from an increase of the molecular relaxation time with decreasing distance from the rough pore surface as recently found by computer simulations [Scheidler et al., Europhys. Lett. 59, 701 (2002)]. The results show for the first time, that the dynamic elastic response is extremely sensitive for separating confinement-induced acceleration effects of the molecular dynamics and surface-induced slowing-down due to rough pore interfaces.

Pacs: 64.70.Pf, 61.20.Lc, 62.25.+g

## 4.1 Introduction

Dynamics in confined systems is a broad phenomenon. It appears in chemistry, physics, biology and material science. Basic questions concerning the modification of structural phase transitions [86, 50], crystallization [87], melting [21, 88, 89] or glass freezing [25] under confinement are a matter of active research. Near the glass transition temperature  $T_g$  a dramatic increase of the characteristic relaxation time  $\tau$  or the viscosity  $\eta$  over more than 14 decades is observed ( $\alpha$ -relaxation) [1, 2]. This can be most naturally interpreted as resulting from a cooperative behaviour of the relevant molecular motions ("cooperatively rearranging regions") characterized by a length scale  $\xi$ , which increases when approaching  $T_g$  [3]. Close to  $T_g$  this correlation length  $\xi_g$  is expected to be of the order of a few nanometers [34]. To search for such a characteristic length scale underlying the glass transition many experiments and computer simulations of glass-forming systems in spatial confinement of pores or ultrathin films have been performed over recent years [90]. This research is motivated by the following simple idea: If a growing correlation length  $\xi$  with decreasing temperature would be the origin of a glass transition, then a spatial limitation  $d$  should lead to a decrease of  $T_g$  (confinement induced acceleration of dynamics due to suppression of cooperatively interacting modes), and finally suppress the glass formation at all for  $d < \xi_g$ . Indeed dielectric spectroscopy and temperature modulated DSC measurements of polypropyleneglycol (PPG) and polydimethylsiloxane (PDMS) confined to nanoporous silica based host systems yield strong evidence for an inherent length scale relevant for glassy dynamics. The specific heat anomaly at  $T_g$  decreases with decreasing pore size and finally vanishes at  $d = 1.8$  nm for PPG and  $d = 5$  nm for PDMS [91]. From dynamic calorimetry across the glass transitions of polyethylene-terephthalate, benzoin-iso-butyl-ether and salol  $\xi(T_g) \approx 2$  nm was found [92]. For comparison, dielectric measurements of salol confined in nanoporous Gelsil yielded  $\xi(T_g) > 7$  nm [73]. The origin of such discrepancies is a matter of discussions in terms of calculating the correlation length either using the Gibbs or the von Laue approach [92].

A complication of the simple idea of above is due to the assumption that surface effects in the pores may balance or even overcome an intrinsic confinement effect. Samples with uncoated (natural) pores, where H-bonds between the molecules and the walls can form, correspond to the situation of a rough surface. Then the effect of this wall would be to block the molecular motion at the pore surface, slowing down the confinement-induced acceleration of dynamics. This seems to happen in toluene-d3, where it was argued that the surface-induced slowing-down of the molecular motions is transmitted quite far into the pore volume [93]. This implies, that the surface-induced slowing-down dominates over the finite-size induced acceleration and  $T_g$  is effectively shifted to higher temperatures due to confinement. Also for benzene an incre-

ase of  $T_g$  with decreasing pore size was reported [94]. Of course for such systems a discussion on the problem of length scales must distinguish between liquids with strong or weak wall interactions forming H-bonds with the pore surface or not, etc. [52].

If on the other hand the pore surface is coated, the molecules located near the walls would be highly mobile, and one expects an additional acceleration. Such surface effects were recently modeled by molecular-dynamics simulations of the relaxation dynamics of confined glass-forming liquids [33, 37, 16, 95]. Considering two types of confining walls, the authors found a slowing-down or an acceleration of the dynamics close to rough or smooth pore surfaces, respectively. Experimentally, dynamics in confinement is probed by a large variety of techniques like differential scanning calorimetry [26], dynamic calorimetry [96, 92], dynamic mechanical measurements [97], dielectric spectroscopy [98], neutron scattering [99] or NMR [100]. Despite the huge number of experimental and theoretical work which report increasing [28], decreasing [26], constant or even two glass transition temperatures [55] for various pore sizes, no final picture of the behaviour of glasses in confined media has been obtained up to now. This is partly due to the diversity of features which real systems show depending on the type and strength of interactions between the molecules and the pore surface, the measuring technique, etc. Excellent discussions concerning these questions can be found in Refs. [52] or [101].

## 4.2 Experimental results

In order to investigate the predicted confinement effects on dynamic elasticity, we performed detailed Dynamic Mechanical Analysis (DMA) measurements of the low molecular weight glass-forming liquid salol (phenyl salicylate,  $C_{13}H_{10}O_3$ ) confined to mesoporous Vycor glass (code 7930). Vycor is composed of nearly pure  $SiO_2$ . The confining morphology of Vycor (7930) can be described as a network of three-dimensional (3D) randomly connected pore segments with a mean pore diameter  $d \approx 7$  nm (Fig. 4.1), with a distribution width of  $\approx 0.5$  nm and an average length  $l \approx 30$  nm [57]. The pore segments are uniformly distributed in orientation and density.

Salol is a fragile (fragility parameter  $m = 73$ ) glass forming substance [102], which is considered as a model substance for the study of glass transition and molecular mobility in the supercooled liquid. It has been extensively studied by many experimental techniques, so that a great deal of information is available for comparison with new experimental and theoretical work. The glass transition temperature of salol ( $T_g \approx 220$  K for the bulk material) is moderately lowered in confined geometry. Trofymuk et al. [28] found a nonmonotonic dependence of  $T_g$  on pore size for salol confined in ordered mesoporous silica (MS). For pore sizes of

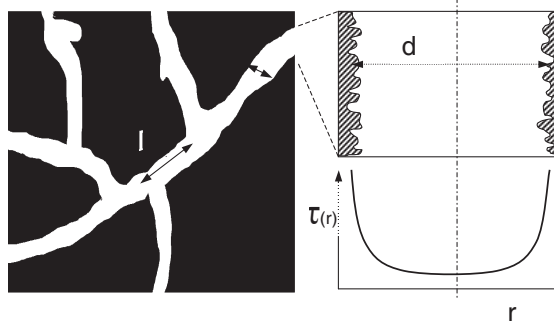


**Fig. 4.1:** Scheme of the pore structure of Vycor glass. On the right hand side the increase the relaxation time of confined salol molecules approaching the rough walls according to simulations of Ref. [37] is sketched.

5.6 – 26.4 nm they determined a  $T_g$  depression of 2-3 K. The authors also found that liquid salol does not crystallize in pores < 11.8 nm and easily vitrifies on cooling [28]. This allowed us to perform the experiments studying the glass transition with moderate cooling and heating rates (2 K/min). Unlike to the confined case bulk liquid salol easily crystallizes at about 290 K and it requires cooling rates of about 500 K/min to supercool it to the glassy state [103].

The present measurements have been performed using a Dynamic Mechanical Analyser (DMA7, Perkin Elmer). In this method a static or dynamic ( $\nu = 0.01 - 50$  Hz) force (1 - 2500 mN) is applied. The amplitude  $\Delta h$  (inset of Fig. 4.3) and phase lag  $\delta$  of the mechanical response are measured via electromagnetic inductive coupling with resolutions of better than 10 nm and 0.01°C respectively. This allows to determine the real and imaginary parts of the dynamic elastic susceptibility of a material at low frequencies as a function of temperature and applied force. The measurements are performed in so-called parallel-plate or three-point-bending geometries. In contrast to the relative accuracy, the absolute accuracy of the method is rather poor. There are two main sources for systematic errors, i.e. the error due to the DMA quartz rod-motor system (modeled by a spring constant  $k_{DMA} \approx 2 \times 10^4$  N/m) and an error due to non-perfect mechanical contact between the sample and the DMA quartz rod (we found typical values of  $k_{cont} \approx 10^6$  N/m). The first error is usually compensated by calibrating the DMA apparatus before measurements, but the contact error cannot be avoided and leads to a significant lowering of the effectively measured Young's modulus  $Y_{eff}$  which for parallel plate geometry is given as

$$Y_{eff} = k_{eff} \frac{h}{S}, \quad (4.1)$$

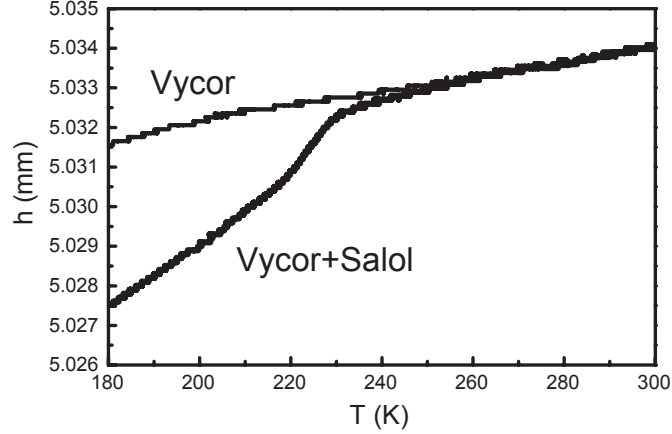


**Fig. 4.2:** Sample heights  $h(T)$  measured for pure Vycor and Vycor filled with salol, normalized at 300 K.

$$\frac{1}{k_{eff}} = \frac{1}{k_{sample}} + \frac{1}{k_{cont}}, \quad (4.2)$$

where  $h$  and  $S$  are thickness and contact surface of the sample. Further details of the experimental setup may be found in Refs. [41, 42].

Fig. 4.2 displays the temperature dependences of the sample heights of pure Vycor and Vycor filled with salol. For these thermal expansion measurements no force is applied at all. As expected for pure Vycor  $h(T)$  decreases almost linearly with decreasing temperature, whereas the salol filled sample shows a strongly nonlinear decrease of  $h(T)$  due to the vitrification of salol in the pores<sup>1</sup>. As already mentioned above the glass transition temperature  $T_g$  of confined salol appears to be similar to the bulk value of  $\approx 220$  K.

Fig. 4.3 gives an overview of dynamic parallel plate measurements of salol confined to Vycor glass of 7 nm sized pores. The real ( $Y'$ ) and imaginary ( $Y''$ ) parts of the complex Young's modulus  $Y^* = Y' + iY''$  show several characteristic features, which we shall qualitatively discuss before we present a detailed analysis of the data: As expected for a glass freezing transition with decreasing frequency the curves shift to lower temperatures. However the crossover region between the high- and low temperature limits (relaxed and unrelaxed moduli) of  $Y'$  and  $Y''$  appears to be rather broad ( $\approx 40$  K). This also shows up in a rather big tail on the high-temperature side of  $Y'$ , followed by a rather abrupt change on the low temperature

<sup>1</sup>An estimation using the density data of liquid and solid salol [104] shows, that the observed length change must originate from about 20 vol% of salol material, which implies that the measured response is due to the material inside the nanopores and not a result of residual material on the sample surface.



side, resembling a two-step (or double S-shaped) behaviour. In accordance with this the corresponding loss-moduli  $Y''$  show *two* rather broad peaks, which are separated by about 18 K in temperature. Three point bending measurements which we have performed as a function of temperature for various measurement frequencies show the same type of behaviour (inset of Fig. 4.3b). It should be noted, that pure Vycor displays no anomalies in  $Y'$  and  $Y''$ .  $Y'$  decreases linearly with decreasing temperature by about 2% in the whole covered temperature range and the loss modulus  $Y''$  is negligible and constant.

### 4.3 Interpretation and comparison with experiment

Measurements of the elastic response to an applied dynamical stress is a widely used technique for studying the slowing-down of the dynamics when approaching the glass transition temperature in the glass-forming materials [105, 106]. The DMA-technique was already successfully applied to study the glass transition dynamics in molecular glass forming liquids both in bulk materials [107] as well as confined in porous media [97]. A quantitative analysis of the elastic behaviour of composites can be done on various levels of sophistication [97, 108]. Using a simple mixing model one obtains for the Young's modulus  $Y_c$  of the composite salol+Vycor for serial mechanical coupling of Vycor and salol

$$Y_c = Y_v C_v + Y_s C_s \quad (4.3)$$

where  $Y_v, Y_s$  are the Young's moduli of Vycor and salol and  $C_v = 0.72, C_s = 0.28$  are the corresponding volume ratios. For parallel coupling one obtains

$$Y_c = \left( \frac{C_v}{Y_v} + \frac{C_s}{Y_s} \right)^{-1} \quad (4.4)$$

Using the values for the elastic moduli of  $\text{SiO}_2$  ( $Y_v = 72.4$  GPa) and salol in the liquid ( $Y_s = 2$  GPa) phase we obtain an estimation of Young's modulus of the composite at room temperature as  $6 \text{ GPa} < Y_c < 51 \text{ GPa}$ . Taking into account the above mentioned errors in Eqn. (4.1), we obtain for the effectively measured Young's modulus of the composite  $4.2 \text{ GPa} < Y_c^{eff} < 11.5 \text{ GPa}$ . Using Eqns. (4.3) and (4.4) and the value of the elastic modulus of salol in the liquid and the solid phase ( $Y_s = 5$  GPa) we obtain upper and lower bounds for the relative changes of the composite Young's modulus during vitrification of  $0.02 < \frac{\Delta Y_c}{Y_c} < 0.13$ . This estimation of the expected effect explains why the vitrification process of salol within the pores of Vycor can be so easily detected by DMA experiments. The measured relative change of the Young's modulus of about 10-20% (Fig. 4.3a) are well within the above calculated limits. Interestingly enough very similar conditions (with respect to the elastic moduli ratios) appear for a quite different system, i.e. for the transition of water into ice. There the bulk modulus

changes from about 2.2 GPa in the liquid state to about 9 GPa for polycrystalline ice [109]. In an early work Sellevold and Radjy [110] studied the freezing of water confined in porous Vycor by dynamic mechanical resonance measurements (300 Hz-1600 Hz). Very similar to our case they find a substantial increase of the Young's modulus up to 70% and an enhancement of internal friction associated with the freezing transition of capillary condensed water in the nanopores.

In order to explain the crossover from the liquid to the glass state of salol confined in Vycor we made several attempts to describe our experimental findings: A simple Kohlrausch or Cole-Davidson function even with extreme stretching parameters does not reproduce our data at all. Even in case where we can fit  $Y'$ , the peak in  $Y''$  appears to be shifted at about 20 K higher than the measured one! In fact all attempts to fit our data with a single relaxation time failed. This led us to the assumption that the dynamical behaviour of salol in the pores requires an *inhomogeneous* model taking into account a radial space dependence of the relaxation time (Fig. 4.1). In fact such a model was very recently applied to describe inelastic neutron scattering experiments of salol confined in nanoporous silica glass (Gelsil) [31]. In order to fit their data of the scattering function at all measured temperatures the authors assumed a shift of the Vogel-Fulcher temperature according to

$$T_0(r) = T_{00} + \frac{k}{R - r + r_p}, \quad (4.5)$$

where  $T_{00}$  is the Vogel-Fulcher temperature of the bulk liquid,  $R = d/2$  is the pore radius and  $r_p$  is a so called penetration radius, i.e. a distance beyond which it is very unlikely to find a particle of the fluid. Using a Vogel-Fulcher temperature dependence of the relaxation time  $\tau = \tau_0 e^{E/[T - T_0(r)]}$  one obtains a dependence  $\tau(r)$  on the position of a relaxing volume in the pore:

$$\tau(r) = \tau_0 \exp\left[\frac{E}{T - (T_{00} + \frac{k}{R - r + r_p})}\right]. \quad (4.6)$$

In fact such a parametrization is consistent with recent results from molecular dynamics simulations which predict an exponential dependence of the relaxation time when approaching the pore walls [37]. In Ref. [33] it was shown that close to the surface of the pores the  $r$ -dependence of the relaxation time can be described by the empirical ansatz  $\tau(r) \propto e^{\pm \Delta(T)/(R - r + r_p)}$  where the positive (negative) sign corresponds to systems with rough (smooth) surfaces (Fig. 4.1).

To calculate the macroscopic dynamic elastic response we integrate the dynamic complex Young's modulus - which here we assume to be of Cole-Davidson type - over the pore volume.

The averaged and normalized real and imaginary parts of  $Y^*(\omega\tau) \propto \frac{1}{[1+i\omega\tau(r)]^\gamma}$  then read

$$\begin{aligned} Y' &= 1 - \frac{2\Delta Y}{R^2} \int_0^R \frac{\cos[\gamma \tan^{-1}(\omega\tau(r))]}{[1 + \omega^2\tau(r)^2]^{\gamma/2}} r dr, \\ Y'' &= \frac{2\Delta Y}{R^2} \int_0^R \frac{\sin[\gamma \tan^{-1}(\omega\tau(r))]}{[1 + \omega^2\tau(r)^2]^{\gamma/2}} r dr. \end{aligned} \quad (4.7)$$

Inserting Eqn. (4.6) into Eqn. (4.7) we have fitted the frequency and temperature dependences of the real and imaginary parts of the complex Young's modulus (Fig. 4.3).

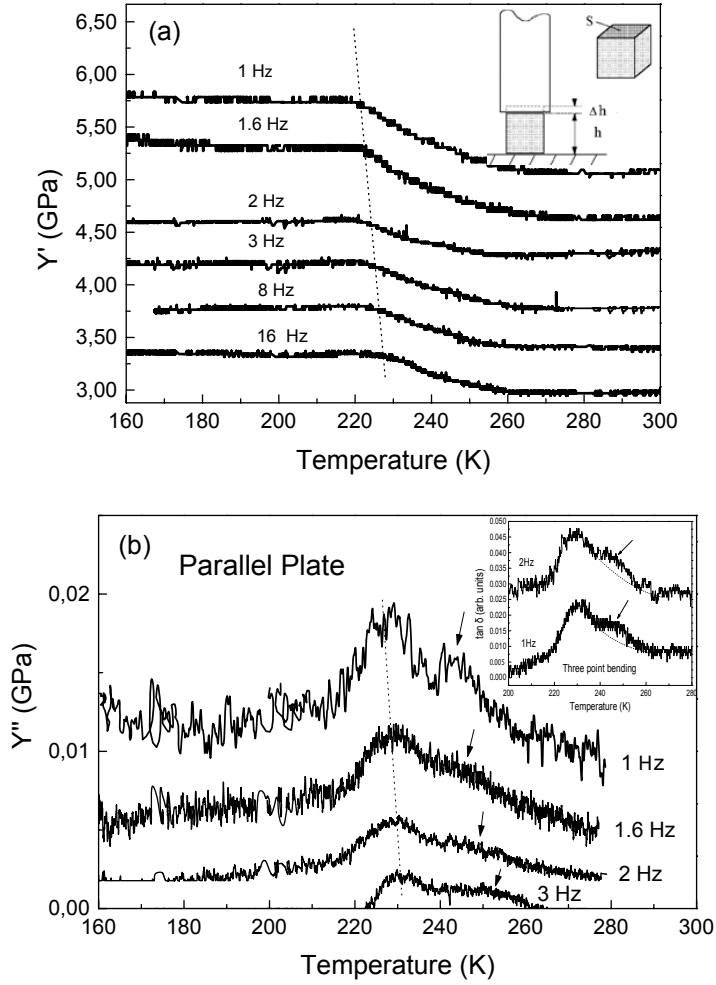


**Fig. 4.3:** Real (a) and imaginary (b) parts of the complex Young's modulus of salol confined to Vycor glass ( $d = 7$  nm) measured in parallel plate geometry. The curves are offset from the 1 Hz data for sake of clarity. The inset shows typical results from three point bending measurements.

The present model reproduces our measurement data excellently (Fig. 4.4) with fit parameters  $\gamma = 0.4$ ,  $T_{00} = 155$  K,  $E = 1750$  K,  $\tau_0 = 10^{-11}$  s and  $k = 25$  nmK. Broadband dielectric spectroscopy data [111] of salol in Gelsil of 2.5, 5.0 and 7.5 nm pore size were interpreted in terms of a two-states model with dynamic exchange between a bulk-like phase in the pore volume and an interfacial phase close to the pore wall. For the bulk-contribution and 7.5 nm pores the authors obtained  $\tau_0 = 10^{-15}$  s,  $T_0 = 177$  K and  $E = 1416$  K. The relaxation time of the surface contribution was shown to be two orders of magnitude higher. Of course these parameters cannot be directly compared with ours, since their fits were obtained from different equations, but a numerical evaluation of Eqn. (4.6) with our set of parameters also yields  $\tau(r = R)/\tau(r = 0) \approx 100$  in the temperature range covered by dielectric spectroscopy.

Very recently inelastic neutron scattering experiments of salol in Gelsil were performed [31]. The authors used the same approach of inhomogeneous dynamics as we do and obtained values of fit parameters for salol confined in 2.5 nm Gelsil:  $\gamma = 0.322$ ,  $T_{00} = 179$  K,  $E = 831$  K,  $\tau_0 = 10^{-13}$  s and  $k = 5$  nmK. Unfortunately these parameters also cannot be directly compared to ours since the pore size, the host matrix and the measurement technique is rather different from ours. Moreover in a previous work it was shown that the Vogel-Fulcher temperature can strongly depend on the low-frequency cutoff of the applied fitting range [112]. Using dielectric and specific heat spectroscopy the author has shown that the Vogel-Fulcher temperature  $T_0$  can vary from 220 K to 140 K for frequency cutoffs between  $10^7$  Hz and  $10^{-3}$  Hz. This may explain the different  $T_{00}$  values obtained from inelastic neutron scattering and low-frequency dynamic mechanical analysis. The other bulk values for salol reported in the literature [111] are  $\tau_0 = 10^{-13}$  s and  $E = 931$  K.

Interestingly in differential scanning calorimetry (DSC) measurements of salol confined to porous silica MCM-41 and SBA-15 a second anomaly at 14-16 K above the bulk glass transition was found [28]. The authors interpret this additional specific heat anomaly in terms of a second glass transition in the interfacial pore region. Our analysis of data however rather suggests that the additional peak in the temperature dependence of the loss modulus  $Y''$  is not related to the existence of a layer at the pore surface that is dynamically decoupled from the rest of the liquid, but is just the result of averaging over particles that have a distribution of relaxation times. A similar interpretation may also be appropriate for the additional specific heat anomaly of Ref. [28]. Indeed for increasing the pore size the present model yields a decrease of the second loss anomaly as well as a shift in temperature (inset of Fig. 4.4), which very much resembles the findings of Ref. [28].

Part of the above mentioned complication i.e. the increasing or decreasing  $T_g$  with varying

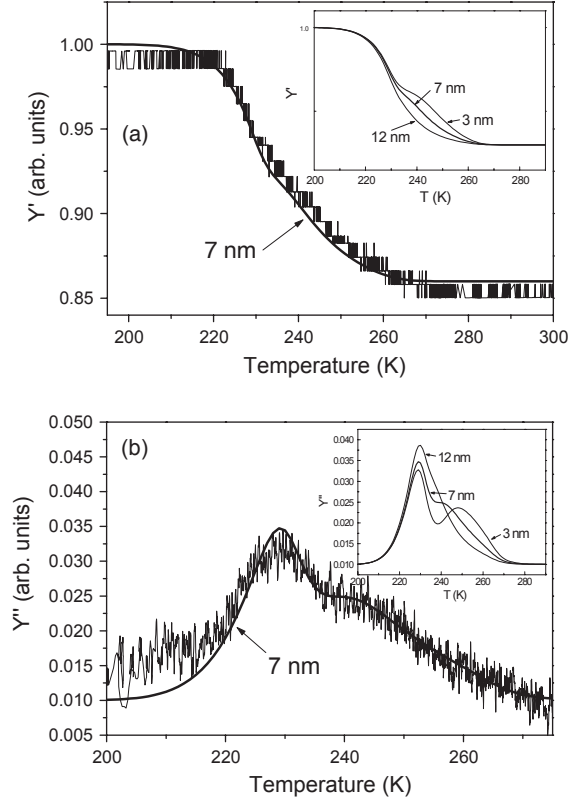


**Fig. 4.4:** Fit of the dynamic ( $f=1.6$  Hz) elastic response of salol confined to 7 nm pores with the inhomogeneous model – Eqn. (4.7) – described in the text. The inset shows calculations with different pore sizes.

pore sizes may originate from a transmission of surface-induced slowing-down or acceleration of molecules quite far into the pore volume. However, salol seems to be a system, where the surface-induced slowing-down can be separated from the confinement-induced acceleration of the dynamics. Indeed in the framework of our model the extrapolated "core" Vogel-Fulcher temperature  $T_0(r = 0) = T_{00} + k/(R + r_p) \approx 160$  K, is about 35 K below the bulk value (194 K) measured by dielectric spectroscopy [111]. It implies that although the motion of molecules is slowed down near the rough surface of the pores, the relaxation times near the center of the pores are smaller at all temperatures compared to bulk salol. The present results for salol are consistent with the view that the  $\alpha$ -relaxation is faster in confined geometries. Very recently Zorn et al. [31] arrived at the same conclusion from elastic neutron scattering experiments of salol confined in nanoporous Gelsil with various pore sizes.

## 4.4 Conclusion

Summarizing, our measurements demonstrate that Dynamic Mechanical Analysis provides a very sensitive method to test the dynamic behaviour of glass-forming liquids in confined systems. In favorable cases it allows to study the question of whether or not there is an "intrinsic" size or confinement effect that is balanced by surface effects. Indeed the result of salol (inset of Fig. 4.4) show that for decreasing pore size the second anomaly in  $Y''$  becomes more pronounced, making it easier to separate confinement and surface effects for the interesting case of pore sizes approaching the correlation length  $\xi(T_g)$ . Experiments are under way to measure the glass transition dynamics of salol for various pore sizes of the host matrix.

**Acknowledgements:** Support by the *University of Vienna* within the research focus *Materials Science* ("Bulk Nanostructured Materials") and the Austrian FWF (P19284-N20) is gratefully acknowledged.

## Chapter 5

# Confinement effects on glass forming liquids probed by dynamic mechanical analysis, PRB 78, 054203 (2008)

Manuscript of published article

by

J. Koppensteiner, W. Schranz and M.R. Puica

The contribution of J. Koppensteiner has been

- all experimental work: sample preparation, DMA, RUS, adsorption swelling and thermal expansion measurements
- analysis of RUS data and all other data processing
- further development of relaxation models and fitting the data (together with W. Schranz)
- literature research (together with W. Schranz)
- design of all sketches, figures and tables
- composing a raw version of the article and taking it to its final version under supervision of W. Schranz.

# Confinement effects on glass forming liquids probed by dynamic mechanical analysis

J. Koppensteiner, W. Schranz and M. R. Puica

Nonlinear Physics Group, Faculty of Physics of the University of Vienna, Boltzmanngasse 5, A-1090 Vienna, Austria

## *Abstract*

Many molecular glass forming liquids show a shift of the glass transition  $T_g$  to lower temperatures when the liquid is confined into mesoporous host matrices. Two contrary explanations for this effect are given in literature: First, confinement induced acceleration of the dynamics of the molecules leads to an effective downshift of  $T_g$  increasing with decreasing pore size. Secondly, due to thermal mismatch between the liquid and the surrounding host matrix, negative pressure develops inside the pores with decreasing temperature, which also shifts  $T_g$  to lower temperatures. Here we present novel dynamic mechanical analysis measurements of the glass forming liquid salol in Vycor and Gelsil with pore sizes of  $d = 2.6, 5.0$  and  $7.5$  nm. The dynamic complex elastic susceptibility data can be consistently described with the assumption of two relaxation processes inside the pores: A surface induced slowed down relaxation due to interaction with rough pore interfaces and a second relaxation within the core of the pores. This core relaxation time is reduced with decreasing pore size  $d$ , leading to a downshift of  $T_g \propto 1/d$  in perfect agreement with recent DSC measurements. Thermal expansion measurements of empty and salol filled mesoporous samples revealed that the contribution of negative pressure to the downshift of  $T_g$  is small ( $< 30\%$ ) and the main effect is due to the suppression of dynamically correlated regions of size  $\xi$  when the pore size  $d$  approaches  $\xi$ .

Pacs: 64.70.pm, 61.20.Lc, 62.25.-g



## 5.1 Introduction

When approaching a glass transition some physical properties like viscosity or relaxation times change up to 14 orders of magnitude [1, 2]. An explanation for the observed slowing down of the dynamics is the formation of collectively dynamically rearranging clusters [113, 3] or regions, with growing size  $\xi$  and increasing relaxation times as  $T_g$  is approached [4]. The idea of an increasing dynamic correlation length  $\xi$  when approaching a glass transition is strongly supported by recent computer simulations [14, 15, 16], although not strictly proven, since computer simulations cannot treat the time range of the  $\alpha$ -process. Very recently a breakthrough was achieved in this field. G. Biroli, et al. [17] found first-time evidence that the Mode Coupling Theory predicts a growing dynamic length scale approaching the glass transition of a supercooled liquid. The authors obtained a rather modest growth of the dynamical length scale  $\xi$  with decreasing temperature, which is in very good agreement with computer simulations [16] and experimental results. Indeed many experimental setups like heat capacity spectroscopy [5, 8], multidimensional NMR [9, 10, 11], multipoint dynamical susceptibilities [12], etc. have been used to monitor a possible growing length scale accompanying the glass transition. All these results agree in the fact, that the obtained dynamically correlated regions - although material dependent - are of the order of 1-4 nm and display - if at all - a weak temperature dependence.

An alternative experimental approach to get a reference to a possibly existing cooperation length  $\xi$  which increases when  $T \rightarrow T_g$  is by spatial limitation of a glass forming liquid. Spatially confining geometries as ultrathin films, mesoporous silica or zeolithes have already been used to study phase transitions of water [19], hydrocarbons [20], noble gases [21, 22], liquid crystals [23] or alkenes [24]. But this concept also illuminated the old and still open question on the very nature of the glass transition and its dynamics [25]: In a pioneering work Jackson and McKenna [26] studied the glass transition of organic liquids in controlled pore glasses (CPG) for various pore sizes  $d$ . They found a reduction of the glass transition temperature  $T_g$  for liquids in confinement as compared to the bulk material. The downshift of  $T_g$  was larger for smaller pore sizes, i.e.  $\Delta T_g \propto 1/d$ , an effect similar - but not as strong as - the suppression known for the melting temperature  $T_m$  in confinement. During the following two decades this effect was studied via calorimetry [28, 29], dielectric spectroscopy [30], neutron scattering [31], light scattering [32] and molecular dynamics [33]. It was shown that in many cases confinement below a characteristic length impedes [29] the transition, implying that molecules within a region of the size  $\xi_g$  (approaching  $T_g$  typically some nm [34, 35]) have to cooperate and rearrange in order to create the glassy state. Hindering this cooperation first leads to a downshift of  $T_g$  if  $d \sim \xi_g$  and finally to a suppression of the transition if  $d < \xi_g$  [29].

However, although this shift of  $T_g$  with decreasing confinement size was found in numerous studies, there are complications which blur this simple picture: E.g. in many molecular dynamics simulations of glass forming liquids at high temperatures above the empirical mode-coupling temperature  $T_c$  confinement is found to slow down the dynamics [114, 115]. Furthermore, in some systems a competition appears between slowing down of molecular motions due to pinning of the molecules at the pore surface and acceleration of the dynamics due to decreasing size of the confinement. Another effect occurs due to the difference in thermal expansion coefficients of the porous host matrix and the glass forming liquid. This may create negative pressure upon the confined liquid when the glass transition is approached. Some authors attribute the whole observed downshift of  $T_g$  to this negative pressure effect [32]. We will address these points in very detail below. For excellent reviews about these topics the reader is referred to Refs. [52] and [101].

Very recently the confinement effect on the glass-forming liquid salol was studied via dynamic mechanical analysis measurements (DMA) [36] in Vycor with  $d = 7$  nm pore size. It turned out that the dynamic elastic response is very sensitive to the glass transition of liquids confined to mesoporous samples. Based on the results of computer simulations [33, 37] we could disentangle acceleration effects due to confinement and slowing down of molecular motion due to interaction of the molecules with the rough pore surface. We could even predict the pore size dependence of the dynamic elastic response (see Fig. 4 of Ref. [36] or Fig. 4.4 of chapter 4). In order to test these predictions and to study the glass transition of salol for different pore sizes, further measurements have been performed. Here we present novel experimental results of the temperature and frequency dependence of the complex dynamic elastic susceptibility of salol confined in mesoporous matrices of  $d = 7.5$  nm, 5.0 nm and 2.6 nm. In addition, thermal expansion measurements have been performed, which now allows us to take a new look at the often discussed negative pressure effect on glass forming liquids in confinement and to separate this effect from an intrinsic size effect.

The present paper is organized as follows: Section 5.2 yields insight into sample preparation and some technical details of DMA analysis. Section 5.3 displays a compilation of the experimental data and results of modeling and interpretation of the present data. It also contains a calculation of the effect of adsorption swelling and the separation of the actual downshift of  $T_g$  in salol into the negative pressure effect and the confinement effect. Section 5.4 concludes the paper.

## 5.2 Experimental

### 5.2.1 Sample preparation

Porous Vycor samples are made by Corning Inc., NY, and sold under the brand name "Vycor 7930". Via phase separation and leaching a three dimensional random network of pores in nearly pure silica is fabricated [61]. Pores are uniformly distributed in length, direction and density Levitz. The mean ratio of average pore diameter  $d$  and pore length  $l$ , is  $d/l \approx 0.23$ . Gelsil is a mesoporous xerogel consisting of pure silica with a very narrow pore radius distribution. Gelsil rods were made by 4F International Co., Gainesville, FL. Results on pore sizes derive from BJH analysis of the individual  $N_2$ -desorption isotherms [72] and are summarized in Tab. 5.1.

**Tab. 5.1:**  $N_2$  adsorption characteristics of porous silica samples.

	Gelsil2.6	Gelsil5	Vycor
av. pore diameter (nm)	2.6	5.0	7.5
surface area ( $m^2/g$ )	586	509	72
pore volume ( $cm^3/g$ )	0.376	0.678	0.214
porosity $\phi$	0.51	0.66	0.30

All samples were cut and sanded in order to gain parallel surface plains. The typical size of a sample was  $(2 \times 2 \times 8) \text{ mm}^3$  for parallel plate and about  $(2 \times 1 \times 7) \text{ mm}^3$  for three point bending DMA-measurements. Cleaning was done in a 30% hydrogen peroxide solution at  $90^\circ\text{C}$  for 24 h, drying at  $120^\circ\text{C}$  in a high-vacuum chamber at  $10^{-6}$  bar, also for about 24 h. The guest glass forming material was salol (phenyl salicylate,  $C_{13}H_{10}O_3$ ), a low molecular weight liquid, whose melting temperature is  $T_m = 316 \text{ K}$ . Salol is a standard, so called fragile [102], glass former ( $m=73$ ) known [28] to form a glass either at extreme cooling rates of 500 K/min or in pores smaller than 11.8 nm. Filling was done at 317 K via capillarity wetting. By comparing the weight of clean and filled samples the filling fractions  $f$  were determined (see Table 5.1).

### 5.2.2 Dynamic mechanical analysis (DMA)

In this method a static and a dynamic force  $F_{stat} + F_{dyn} \cdot e^{i\omega t}$  (0.001-16 N at 0.01-100 Hz) are applied on a sample using a quartz or steel rod (see Fig. 5.1). The response of the sample is measured via the displacement of the rod. Absolute height  $h$ , height amplitude  $\Delta h$  and phase lag  $\delta$  are read via electromagnetic inductive coupling (LVDT) with a resolution of 10 nm and  $0.01^\circ$  respectively. These data allow direct access to real and imaginary part of the complex

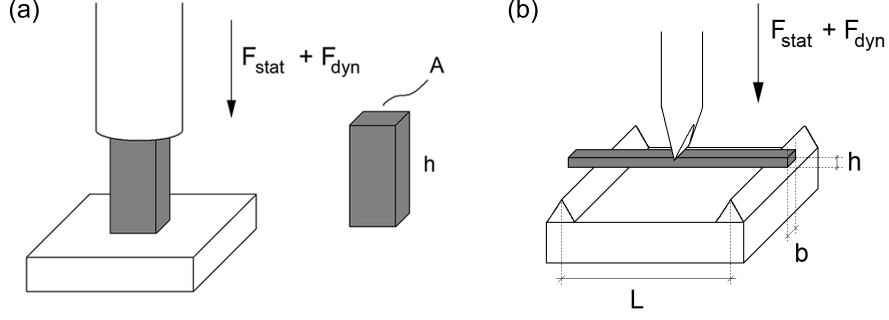


**Fig. 5.1:** Sketch of (a) parallel plate and (b) three point bending geometry.

elastic susceptibility at low frequency and as a function of temperature and applied force. In addition, the thermal expansion of a sample can be determined in the so called TMA-mode, where no external force is applied. Two devices are used: a DMA 7 and a Diamond DMA, both from Perkin Elmer Inc. Two measuring geometries are applied: parallel plate compression (PP) and three-point bending (3PB), see Fig. 5.1.

Parallel plate geometry reveals purely the complex Young's modulus  $Y^* = Y' + iY''$ , where  $Y'$  and  $Y''$  are the storage and the loss modulus, respectively. The three point bending geometry delivers Young's modulus plus a small (geometry dependent) contribution of a shear elastic constant. More details on measurement geometry may be found in Refs. [41] and [42]. The absolute accuracy of resulting real and imaginary parts  $Y'$  and  $Y''$  is rather poor, mainly because of contact losses between the quartz rod and the sample. A discussion of these systematic errors may be found in Ref. [36]. In contrast the relative accuracy is excellent and the DMA-method is estimated to be about 100 times more sensitive to detect glass transitions or other subtle phase transitions than DSC-measurements [116].

## 5.3 Results and Discussion

### 5.3.1 Dynamic elastic response

Diamond DMA-measurements (in parallel plate and three-point-bending geometry) of Vycor and Gelsil samples filled with salol are shown in Figs. 5.2 - 5.5. The loss modulus  $Y''$  (Fig. 5.2b) of salol in 7.5 nm pores clearly shows a "two peak structure", i.e. a peak with HWHM about 20 K, and a shoulder or second peak at about 15 K higher temperature (also see Fig. 5.5b). This is also reflected by the real part  $Y'$ , which displays a "two step like shape" with temperature (Figs. 5.2a and 5.5a). Both peaks in  $Y''$  shift to higher temperatures with increasing frequency

as expected for a glass transition. In smaller pores of Gelsil 5.0, peak and shoulder merge into one asymmetric peak of width  $\sim 30$  K (see Fig. 5.3b and 5.5e), also shifted with higher frequency to higher temperatures. In 2.6 nm pores the loss peak shows a rather symmetric form broadened up to about 60 K, see Figs. 5.4b and 5.5f.

While in large pores of 7.5 nm diameter vitrification of salol seems to happen decoupled (two peaks in  $Y''$ ) in regions near the pore surface and the pore center, things change in smaller pores. With decreasing pore diameter,  $Y''$  approaches a symmetric form and simultaneously  $Y'$  changes from a "double step shape" into a "single step shape", indicating only one type of relaxation process. Similar broadening effects as for the loss peaks of our DMA-measurements were observed in pores of decreasing size also by calorimetric [26] and dielectric measurements [117, 63]. This broadening as well as a shift of the glass transition to lower temperatures was calculated by Sappelt and Jäckle using kinetic Ising and lattice gas models [118], and shown to originate from confinement induced suppression of cooperative motion of molecules.

Pure Vycor and Gelsil, meaning exposed to air and therefore mostly filled with nitrogen, do not show any of these features.  $Y'$  decreases about 2% between 300 K and 180 K.  $Y''$  is constant within the corresponding temperature range.

Any standard relaxation model like Debye, Kohlrausch, Cole-Cole or Cole-Davidson fails to describe our dynamic elastic susceptibility data if only one type of relaxation process is assumed. One would have to use extreme stretching parameters to fit  $Y'$ , which then leads to improper temperature shifts of the peaks in  $Y''$  with respect to the experimental data and misfitting signal heights. The most efficient model to describe our data turned out to be a modification of the empirical Vogel-Fulcher-Tammann-law

$$\tau(T) = \tau_0 \cdot \exp\left[\frac{E}{T - T_0}\right], \quad (5.1)$$

where  $\tau_0$  is a preexponential factor,  $E \cdot k_B$  is an activation energy, and  $T_0$  is the Vogel-Fulcher (VF) temperature. Following computer simulations [33, 37] we take into account a shift of VF-temperatures along the pore radius  $r$ . In a recent paper Zorn et al. [31] suggest the empirical ansatz

$$T_0(r) = T_{00} + \frac{k}{R - r + r_p}, \quad (5.2)$$

with the bulk VF-temperature  $T_{00}$ , and the pore radius  $R = d/2$ . The so called penetration radius  $r_p$  is the radius beyond which it is very unlikely to find a particle in the fluid state [33].

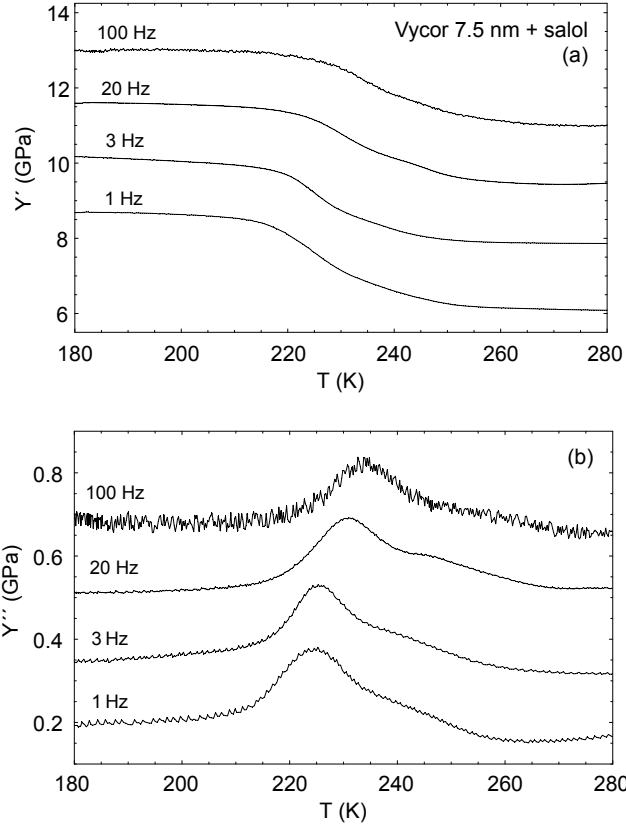


**Fig. 5.2:** Real (a) and imaginary parts (b) of the complex Young's modulus of Vycor 7.5 nm filled with salol (filling fraction  $f \approx 0.79$ ) measured in three point bending geometry. The curves are offset from the 1 Hz data for sake of clarity.

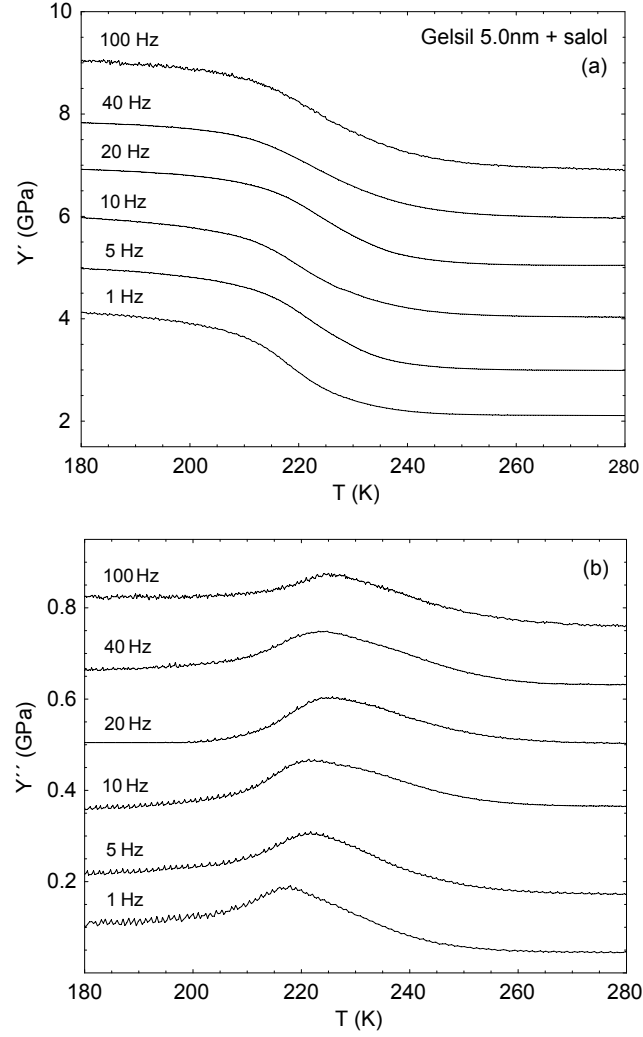


**Fig. 5.3:** Real (a) and imaginary (b) parts of the complex Young's modulus of Gelsil 5.0 nm filled with salol (filling fraction  $f \approx 0.75$ ) measured in parallel plate geometry (Diamond DMA). 1Hz signal are original data, other signals are offset for sake of clarity.

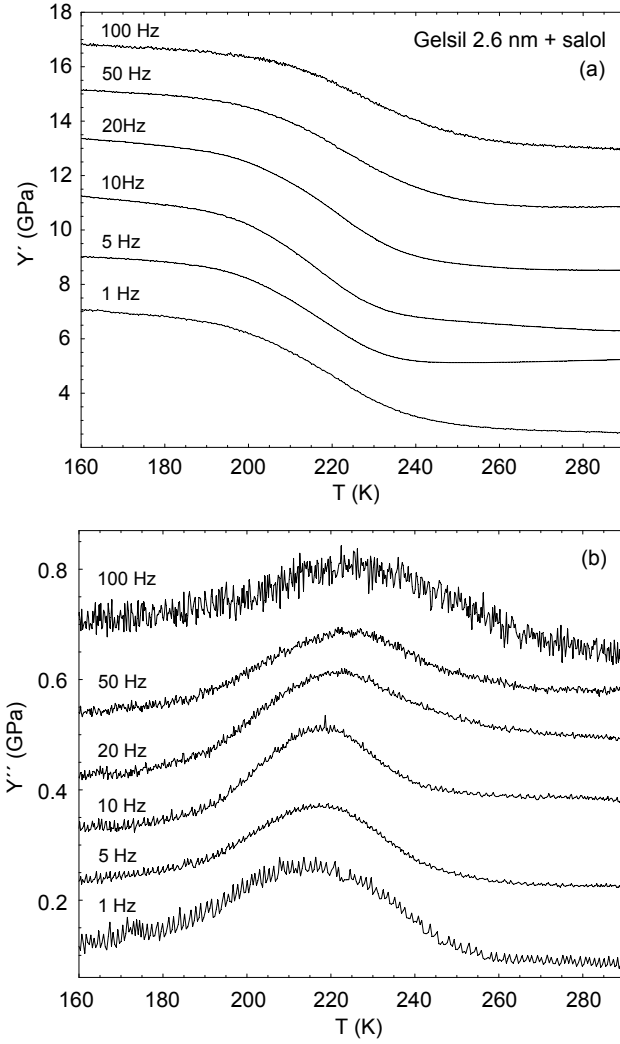


**Fig. 5.4:** Real (a) and imaginary (b) parts of the complex Young's modulus of Gelsil 2.6 nm filled with salol (filling fraction  $f \approx 0.65$ ) measured in three point bending geometry (Diamond DMA). 1 Hz signal are original data, other signals are offset for sake of clarity.



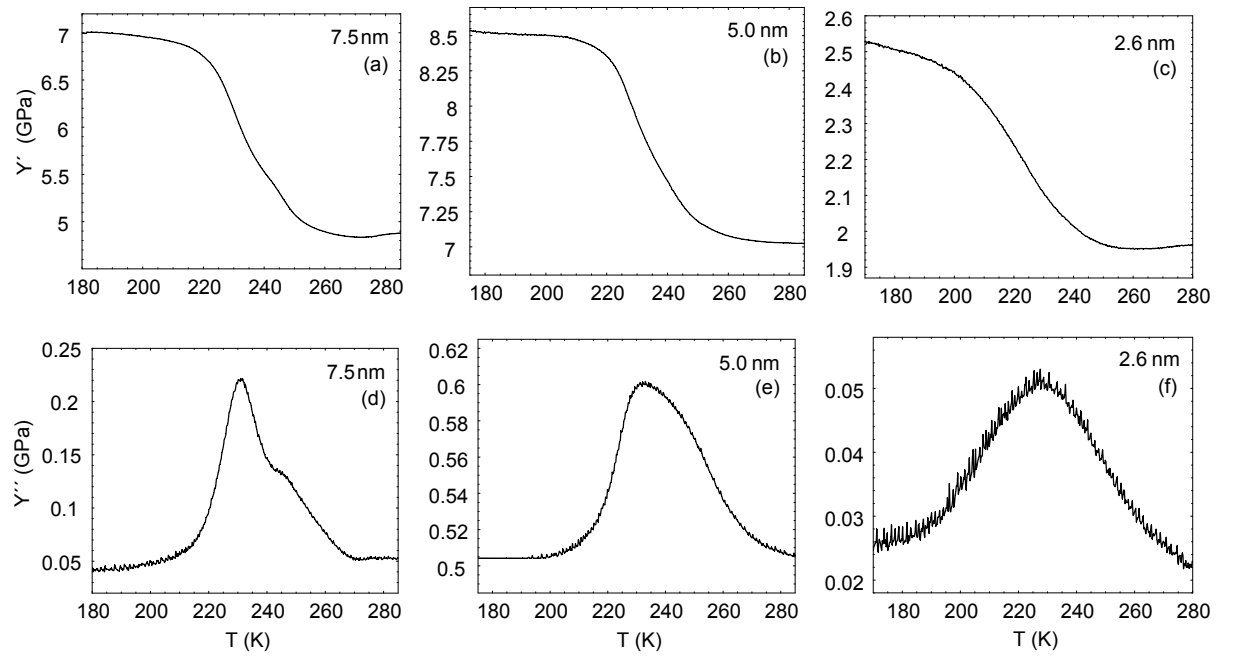


**Fig. 5.5:** Real (a) and imaginary (b) part of the complex Young's modulus of salol in Vycor or Gelsil for different pore sizes, all measured at 20 Hz.

The combination of Eqns. (5.1) and (5.2) leads to a radial distribution of relaxation times  $\tau$  inside the pore:

$$\tau(r, T) = \tau_0 \cdot \exp\left[\frac{E}{T - (T_{00} + \frac{k}{R-r+r_p})}\right] \quad (5.3)$$

Eqn. (5.3) describes the exponential increase of relaxation time when a rough pore wall is approached, and a growing influence of the pore wall with decreasing temperature, a behaviour which was also found by recent computer simulations [33, 37, 16, 95]. A temperature parametrized Cole-Cole-Plot of  $Y''$  vs.  $Y'$  of our data calls for a Cole-Davidson model of the complex dynamic elastic susceptibility

$$Y^*(\omega) \propto \frac{1}{(1 + i\omega\tau)^\gamma} \quad (5.4)$$

with  $\omega = 2\pi\nu$ ,  $\nu$  being the measurement frequency, and the broadening parameter  $\gamma$ . Using Eqn. (5.3), averaging over the pore radius  $R$ , and separating real and imaginary part of  $Y^* = Y' + i \cdot Y''$  by common procedures leads to

$$Y' = 1 - \frac{2 \Delta Y}{R^2} \int_0^R \frac{\cos[\gamma \cdot \arctan(\omega\tau(r, T))]}{[1 + \omega^2\tau(r, T)^2]^{\frac{\gamma}{2}}} r dr \quad (5.5a)$$

$$Y'' = \frac{2 \Delta Y}{R^2} \int_0^R \frac{\sin[\gamma \cdot \arctan(\omega\tau(r, T))]}{[1 + \omega^2\tau(r, T)^2]^{\frac{\gamma}{2}}} r dr \quad (5.5b)$$

As already mentioned above, the two peak structure in  $Y''$  of 7.5 nm and 5 nm confined salol (Figs. 5.2 and 5.3) suggests to split the dynamic elastic response into a core and a surface contribution: the molecules in the core (center of the pores) behave bulk-like and are dynamically decoupled from the molecules near the pore surface. This is modeled by inserting into Eqns. (5.5) the corresponding relaxation times  $\tau_0 \cdot \exp(E/(T - T_0))$  given by Eqn. (5.1) if  $r \leq R_c$  and  $\tau(r, T)$  given by Eqn. (5.3) if  $r > R_c$  (see also Fig. 5.7). The sum of the two contributions perfectly describes our  $Y'$  and  $Y''$  data on salol in 7.5 nm and 5 nm pores simultaneously (see Fig. 5.6).

In 2.6 nm pores we do not expect any molecule to behave like the bulk liquid any more, since the pore radius is of the same order as the estimated surface shell (see Tab. 5.2), implying that every molecule is influenced by the near surface. Therefore we use Eqns. (8.5a,b) with no bulk term which reproduces one single peak and also fits our data very well (Fig. 5.5c and f and Fig. 5.6c and f).

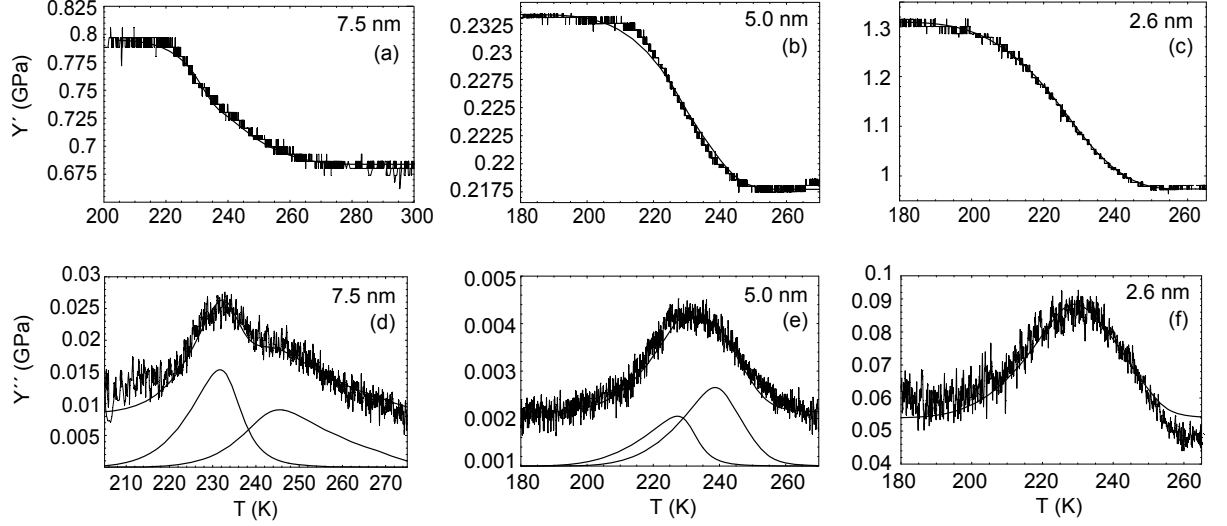


**Fig. 5.6:** Real part  $Y'$  and imaginary part  $Y''$  of different porous samples filled with salol. Lines are fits using Eqs. (8.5a,b) with parameters of Tab. 5.2.

The radius of the "core" of bulk-like interacting molecules turned out to be  $R_c = 2.5$  nm and 1.35 nm in 7.5 nm and 5.0 nm pores, respectively, see Tab. 5.2. This implies that the thickness of the shell of molecules being slowed down by wall interaction  $R - R_c = 1.25$  nm and 1.15 nm for 7.5 nm and 5.0 nm pores respectively.

Additional loss peaks, attributed to molecules forming H-bonds to the inner pore surface, have also been reported from dielectric measurements of salol in 7.5 nm pores [119, 73]. The work of Kremer and Stannarius [119] also revealed that the typical size of a shell of molecules interacting with the pore surface is about 2 or 3 molecules. Since the size of a salol molecule is estimated as  $(1.4 \times 0.6 \times 0.4)$  nm<sup>3</sup> in Ref. [64] or as 0.282 nm<sup>3</sup> in Ref. [120], both corresponding to a mean diameter of 0.8 nm, this shell size is in the order of 1.6 to 2.4 nm. This is in very good agreement with our findings (see Tab. 5.2). The core size  $R_c$  decreases with decreasing pore radius (see Tab. 5.2 and Fig. 5.7), also in very good agreement with the results of Kremer et al.

The fitted Vogel-Fulcher temperature  $T_{00}$  is reduced with respect to the bulk and with decreasing pore size (see Tab. 5.2). In order to compare our results with published data, we plotted the relaxation time in the pore center  $\tau(r = 0, T)$  for various pore sizes  $d$  and determined the corresponding  $T_g(d)$  by using the common procedure [121] for finding the laboratory glass transition temperature, i.e. a cut with a horizontal line at  $\tau = 100$  s (see Fig. 5.8). As shown in Fig. 5.11, this leads to glass transition temperatures decreasing  $\propto 1/d$  in very good

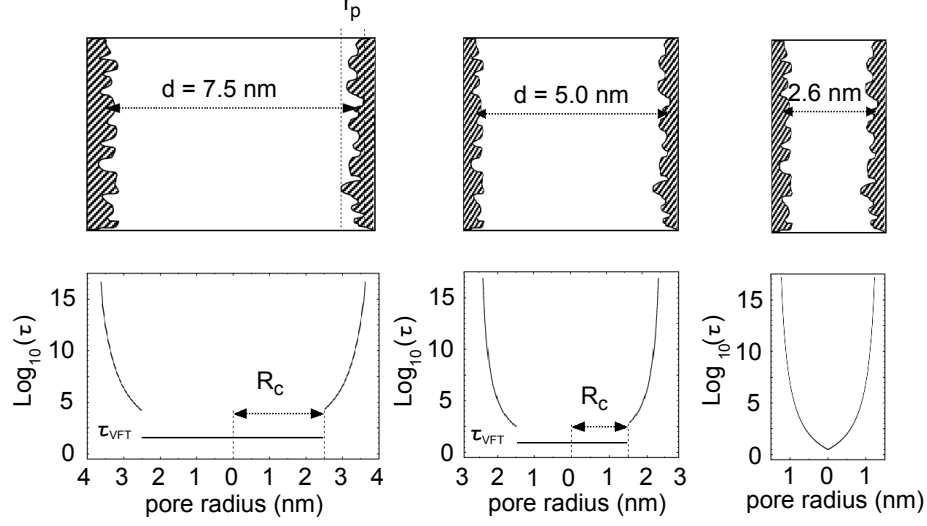


**Fig. 5.7:** Modeled relaxation time distributions in pores of diameter 7.5 nm to 2.6 nm from Eqn. (5.3) used in Eqns. (8.5a,b) for fits of Fig. 5.6.

**Tab. 5.2:** Fit parameters used in Eqns. (8.5a,b) for fits of Fig. 5.6.

	Vycor	Gelsil5	Gelsil2.6
$R$ (nm)	3.75	2.50	1.28
$r_p$ (nm)	0.36	0.25	0.28
$E$ (K)	1750	1750	1750
$T_{00}$ (K)	158.5	156.2	136.0
$\tau_0$ (s)	$10^{-11}$	$10^{-11}$	$10^{-11}$
$\gamma$	0.33	0.18	0.15
$k$ (nm·K)	18	11	25
$R_c$ (nm)	2.5	1.35	-
shell $R - R_c$ (nm)	1.25	1.15	1.28

agreement with published data of DSC measurements [32].

On the other hand there are molecular dynamics simulations [114, 115] of glass forming liquids pointing to the fact that at higher temperatures above the mode coupling temperature  $T_c = 260$  K of salol [122] confinement slows down the dynamics. However within the present experimental frequency range (0.01 Hz - 100 Hz) we are not able to detect such a crossover

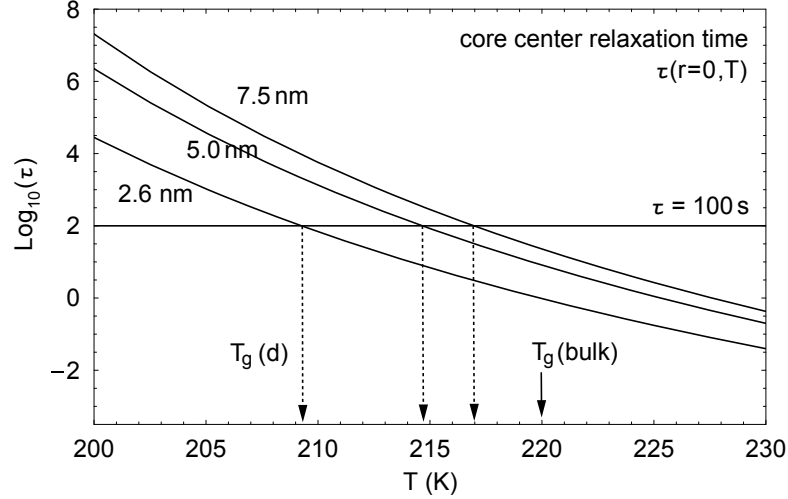


**Fig. 5.8:** Relaxation time in pore centers calculated from Eqns. (5.1) and (5.3) with corresponding parameters from Tab. 5.2. Horizontal line shows  $\tau = 100$  s.

to confinement induced slowing down by heating the sample from  $T_g$  to temperatures above  $T_c$  for the following reason: An extrapolation of the relaxation times of Fig. 5.8 to these temperatures shows that  $\tau(T > 260 \text{ K}) < 10^{-4} \text{ s}$ , implying that  $\omega\tau < 1$  within this temperature range even at the highest available measurement frequency of 100 Hz. Therefore the dynamic elastic susceptibility given by Eqn. (5.4) is actually independent of  $\tau$  and we have to extend our frequency range to higher frequencies. Work in this direction using resonant ultrasound spectroscopy (RUS,  $50 \text{ kHz} < \nu < 1.5 \text{ MHz}$ ) is in progress.

### 5.3.2 Filling process and accompanying effects

By using a DMA in a static TMA mode one can detect small changes in a sample's height with a resolution of 10 nm. We measured the time dependent swelling of the Vycor and Gelsil samples during filling with salol and the thermal expansion of empty and filled samples in the following way: In parallel plate mode, the quartz rod is placed on top of the sample with force  $F = 0 \text{ N}$ , and just height and temperature signals are read out. A clean piece of Vycor/Gelsil sample is cooled down to 170 K. Afterwards the sample is heated slightly above the melting temperature  $T_m = 316 \text{ K}$  of salol and kept there isothermally. Crystalline, powder-like salol placed right around the sample melts and percolates the Vycor/Gelsil sample due to capillarity (Fig. 5.9). After filling until saturation, the sample is cooled down to 170 K again (Fig. 5.10).

The time-dependence of the filling process is displayed in Fig. 5.9 for Vycor. While salol is percolating the sample, the temperature is held constant and the sample's height is measured.

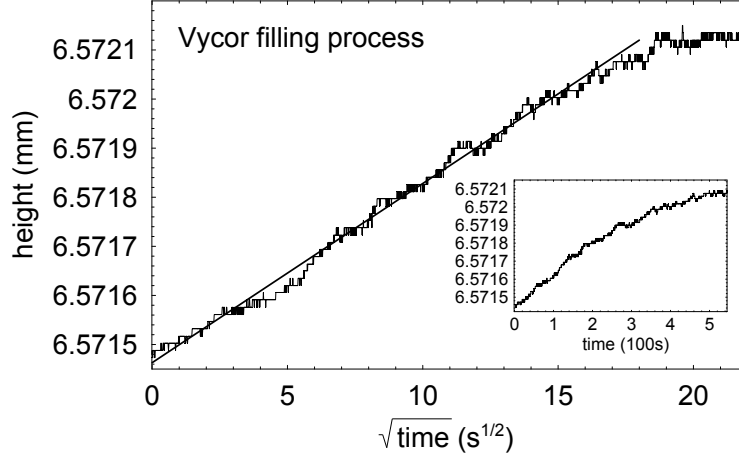


**Fig. 5.9:** Height of Vycor sample during the filling process against  $\sqrt{t}$ . Inset shows sample height against time.

Charts for Gelsil 5.0 nm and Gelsil 2.6 nm look very similar. The diagrams in all cases show the typical  $\sqrt{t}$ -behavior as expected for a single capillary rise experiment, following Lucas [75] and Washburn [76]. This result is in concordance with findings of P. Huber et al. [77], who investigated the mass uptake of porous silica samples and its time dependence, leading to the Lucas-Washburn  $\sqrt{t}$  behaviour of the mass uptake with time. Very recently it was shown that the Lucas-Washburn equation (with small modifications) works well even at the nanoscale [123], which is in harmony with our results.

The expansion of a porous sample during adsorption of gases or water has already been investigated in the 1920s [124]. As a liquid/gas intrudes the sample it is subject to a negative hydrostatic pressure inside the pores, which leads to an expansion of the porous sample during adsorption of gases or water. Mesoporous media have enormous inner surfaces up to some 100 m<sup>2</sup>/g (see Tab. 5.1). This leads to a considerable stress reduction within the whole matrix and a sudden voluminal growth, which slows down and stops as all pore space is filled (see Fig. 5.9). The change in height due to the adsorption swelling can even be calculated quantitatively. The pressure reduction of the liquid in a capillary is known [74] as  $P_c = 2\sigma/r$ , with the surface tension  $\sigma$  and the capillary radius  $r$ . With  $\sigma = 1.73 \cdot 10^{-2}$  N/m from Ref. [32], this yields a capillary pressure of 26.6 MPa in 2.6 nm pores. This would lead to a hypothetical capillary rise of 1.8 km for salol. The linear strain  $\epsilon = \Delta h/h$  accompanying the filling process can be computed by the equation [125]:

$$\epsilon = \frac{f \cdot P_c}{3} \left( \frac{1}{K} - \frac{1}{K_s} \right) \quad (5.6)$$

with the filling fraction  $f$ , the bulk modulus  $K$  of the empty host matrix, and the bulk modulus of the material building the solid frame  $K_s$  (which is nearly pure  $\text{SiO}_2$ ). The bulk moduli  $K$  have been determined by resonant ultrasound spectroscopy (RUS). Tab. 5.3 shows parameters used to calculate  $\epsilon = \Delta h/h$ . The calculated values for the adsorption swelling agree rather well with the experimental results.

**Tab. 5.3:** Variables of Eqn. (5.6).

	Vycor	Gelsil5	Gelsil2.6
$d$ (nm)	7.5	5.0	2.6
porosity $\Phi$	0.31	0.66	0.51
$P_c$ (MPa)	9.2	13.8	26.6
$K$ (GPa)	8.1	3.9	9.6
$f$	0.77	0.62	0.32
$\epsilon_{calc}$	$2.3 \cdot 10^{-4}$	$6.6 \cdot 10^{-4}$	$2.2 \cdot 10^{-4}$
$\epsilon_{exp}$	$1.0 \cdot 10^{-4}$	$4.1 \cdot 10^{-4}$	$3.5 \cdot 10^{-4}$

### 5.3.3 Negative pressure effect

The downshift of the glass transition in nm-confining pores is often reported to obey a  $1/d$  law, see Refs. [26], [32], [28] and [126]. At first this was proposed by Jackson and McKenna [26], following their former results on the shift of the melting transition  $T_m$  in confinement [27]. But the supposed suppression of molecular cooperation when the pore diameter approaches an inherent length scale is not the only possible reason for a downwards shift of  $T_g$  in confinement. Zhang et al. [126] proposed the increase of negative hydrostatic pressure within the pores due to mismatching thermal expansions of liquid and host matrix as the main driving force for the downshift of  $T_g$ . This idea is also discussed by Patkowski et al. [32] and Simon et al. [39], and was reviewed by Alcoutlabi and McKenna [52].

As Fig. 5.10a shows, for large pores and in a cooling process starting at RT, at higher temperatures the Vycor matrix is not affected by its filling. It contracts like the empty Vycor matrix with a thermal expansion coefficient  $\alpha = \Delta h/(h \cdot \Delta T) = 5.1 \cdot 10^{-6} \text{ K}^{-1}$ . Patkowski al. [32] proposed the possible flow and equilibration of the confined liquid well above  $T_g$ , which we also consider to be the case here. But as vitrification sets in at about 230 K, the filled Vycor matrix is subject to a contraction which is stronger compared to the empty Vycor sample. Strong interaction (H-bondings) between salol and the pore surface might be the reason for

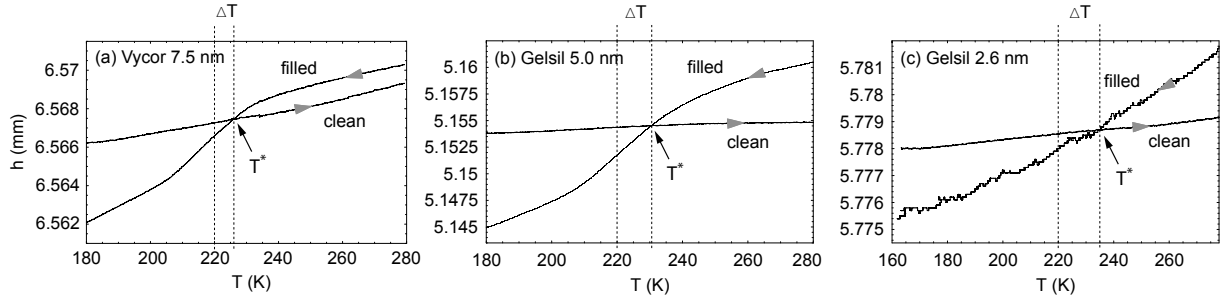


**Fig. 5.10:** Linear thermal expansion of empty and salol filled samples with pore diameters of (a) 7.5 nm, (b) 5.0 nm and (c) 2.6 nm.

this. At smaller pores of filled Gelsil samples (Fig. 5.10b and c) additional contraction already starts at higher temperatures. For an estimation of the process developing negative pressure upon the filling liquid, the strain misfit between the glass and the host matrix is

$$\Delta\epsilon^{mf} = 3(\alpha_1 - \alpha_2)\Delta T \quad (5.7)$$

with  $\alpha_i$ , the thermal expansion coefficients of the host matrix (1) and salol (2). Negative pressure then derives from  $\Delta P = \Delta\epsilon/\kappa_T$ , where  $\kappa_T$  is the bulk compressibility of salol. The resulting shift of  $T_g$ , i.e.

$$T_g(P) = T_g(P=0) \cdot \left. \frac{\partial T_g}{\partial P} \right|_{P=0} \cdot \Delta P \quad (5.8)$$

crucially depends on the choice of  $\Delta T$ , the temperature range, in which the effective negative pressure upon salol develops. This effective temperature range can be estimated from our data as follows: As calculated from Eqn. (5.6) the host porous matrix expands with filling due to the negative capillary pressure which acts on the confined liquid. Since with cooling the liquid salol contracts, this stress relaxes and the composite is stress free if the filled sample height is the same as for the empty matrix which occurs at  $T = T^*$  (see Fig. 5.10). So  $\Delta T \approx T^* - T_g$ . Results of these estimations are given in Tab. 5.4. Parameters used for salol are  $\kappa_T = 5 \cdot 10^{-10} \text{ Pa}^{-1}$  from Ref. [104], the thermal expansion coefficient  $\gamma_1 = 3\alpha_1 = 7.36 \cdot 10^{-4} \text{ K}^{-1}$  from Ref. [1], and  $\partial T_g / \partial P = 0.204 \text{ K/MPa}$  from Ref. [127]. Our measurements are in accordance with enthalpy recovery results of S. L. Simon et al. [39]. Their model shows that effective negative pressure develops 2 to 2.5 K above the reduced glass transition for samples with 11.6 nm and 25.5 nm pore sizes. Further, they state "...if negative pressure were the cause of the depressed  $T_g$ , the temperature at which isochoric conditions are imposed would have to be  $\sim 20$  to 40 K above  $T_g$ ." For comparison we obtain a necessary  $\Delta T = 10$  to 40 K for  $d = 7.5$  to 2.6 nm pores, which is in very good agreement with Simon et al.



**Tab. 5.4:** Parameters of  $\Delta T_g$  estimations,  $\Delta T_g^{exp} = \Delta T_g^{np} + \Delta T_g^{conf}$ .

	Vycor	Gelsil5.0	Gelsil2.6
$d$ (nm)	7.5	5.0	2.6
$\alpha_2$ (K <sup>-1</sup> )	$2.1 \cdot 10^{-5}$	$4.6 \cdot 10^{-5}$	$1.1 \cdot 10^{-5}$
$\Delta T$ (K)	6	10	15
$\Delta \epsilon^{mf}$ (%)	-0.40	-0.60	-1.06
$\Delta P$ (MPa)	-8.1	-12.0	-21.1
$\Delta T_g^{np}$ (K)	-1.6	-2.4	-4.3
$\Delta T_g^{conf}$ (K)	-1.4	-2.9	-6.4
$\Delta T_g^{exp}$ (K)	-3.0	-5.3	-10.7

In our opinion our calculated  $\Delta T_g^{np}$  is still overestimated for two reasons: First, using the bulk value  $\alpha_2$  of the host matrix from Fig. 5.10 does not take into account internal pore walls being affected by the negative pressure inside, relaxing to some extent and so reducing pressure. Secondly, thermal expansions of other glass forming liquids e.g. toluene have been reported 1.5 times smaller in confinement [128] compared to bulk. Moreover, thermal expansion of liquid salol drops [1] to a *quarter* of its value at the glass transition. So, as the glass transition sets in,  $\alpha_1$  starts to decrease and a purely pressure induced downshift  $\Delta T_g$  would be even more diminished. Apart from this the reason for the size dependence of the thermal mismatch effect (see Fig. 5.11, open circles) is not clear at all.

## 5.4 Conclusions

The glass transition of salol confined to porous host matrices of Vycor and Gelsil with pore sizes of 7.5, 5.0 and 2.6 nm has been measured for the first time by Dynamic Mechanical Analyzers (DMA 7 and Diamond DMA, Perkin Elmer). The dynamic complex elastic susceptibility data can well be fitted assuming two types of dynamic processes: A "bulk" relaxation in the core of the pores and a radially increasing "surface relaxation" of molecules near the pore surface. The calculated core relaxation time shows a typical Vogel-Fulcher temperature dependence and decreases with decreasing pore size  $d$ . This confinement induced acceleration of dynamics leads to a shift of the glass transition temperature  $T_g \propto 1/d$ , which is in perfect agreement with recent DSC results [32]. Measurements of the sample height with filling (adsorption swelling) and thermal expansion are used to calculate the effect of "negative pressure" due to thermal mismatch between the porous host matrix and the glass forming liquid. Such negative pressure

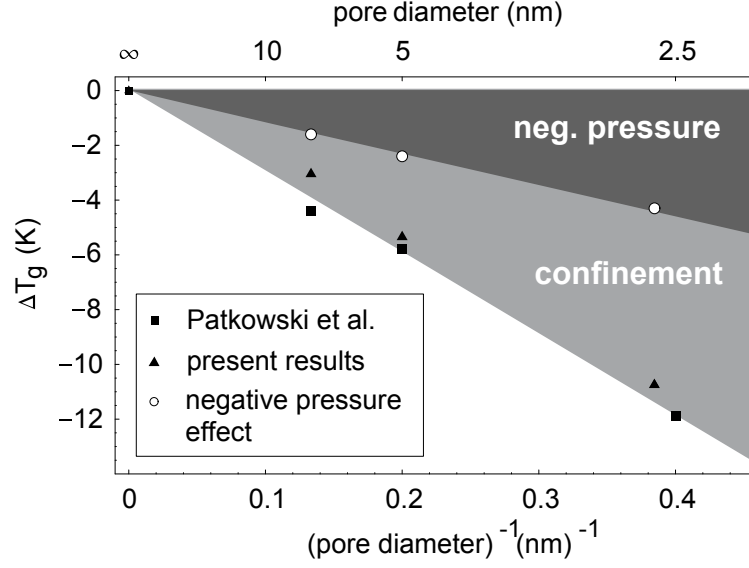


**Fig. 5.11:** Shift of glass transition temperature against  $(\text{pore diameter})^{-1}$ . Boxes are  $T_g$ s from Fig. 5.8, triangles show literature values from Ref. [32], open circles display the maximum negative pressure contribution (see section 5.4).

could at least partly explain a shift of  $T_g$  in confined glass forming liquids [32, 52, 39]. Our data show that for salol this effect of thermal mismatch could describe at most 30% of the observed downshift of  $T_g$ , which is in harmony with enthalpy recovery experiments [39].

In our opinion the main cause for the shift of  $T_g$  is a hindering of cooperativity due to confinement. This is also supported by an estimation of this effect using the results of Hunt et al. [129]. They calculated the finite size effect of the glass transition from percolation and effective medium models, which yields

$$T_g(d) = T_g(\text{bulk}) - \frac{0.5 \cdot E}{\ln(t \cdot \nu_{ph})} \cdot \frac{r_0}{L}. \quad (5.9)$$

Inserting  $t = 100$  s,  $\nu_{ph} = 1/\tau_0$ , and our fit parameters from Tab. 5.2, and assuming that the typical distance between molecules  $r_0$  is about the diameter of a salol molecule [120] ( $d_0 \approx 0.8$  nm), we obtain  $\Delta T_g^{Hunt}$  as 3.2, 4.8 and 9.1 K for 7.5, 5.0 and 2.6 nm pores, respectively. These calculated values agree surprisingly well with the measured confinement induced downshifts of  $T_g(d)$  (see Fig. 5.11 and  $\Delta T_g^{exp}$  in Tab. 5.4).

Moreover Eqn. (5.9) predicts [129] that the size dependence of  $\Delta T_g$  increases with increasing fragility [130]

$$m = \frac{E \cdot T_g}{\ln(10) (T_g - T_0)^2} , \quad (5.10)$$

since  $m \propto E$ . Indeed, this correlation between  $\Delta T_g(d) \sim m$  was verified experimentally for many systems, i.e. for glycerol [126] ( $m = 53$ )  $\Delta T_g(d = 2.5 \text{ nm}) \approx -4 \text{ K}$ , benzyl-alcohol [26] ( $m = 65$ )  $\Delta T_g(d = 2.5 \text{ nm}) \approx -9 \text{ K}$ , salol [32] ( $m = 73$ )  $\Delta T_g(d = 2.5 \text{ nm}) \approx -11 \text{ K}$ , o-terphenyl [32] ( $m = 81$ )  $\Delta T_g(d = 2.5 \text{ nm}) \approx -25 \text{ K}$ .

We think that these considerations, i.e. the downshift of  $T_g$  calculated via percolation theory, as well as the clear correlation between the magnitude of induced  $T_g$  shift and the fragility of a glass forming liquid, both confirm our other findings (see Fig. 5.11) that the main effect of the confinement is to suppress cooperative motion. Negative pressure effects although always present contribute only little.

**Acknowledgements:** Support by the Austrian FWF (P19284-N20) and by the University of Vienna within the IC Experimental Materials Science ("Bulk Nanostructured Materials") is gratefully acknowledged. We thank Marie-Alexandra Neouze and the Institute of Materials Chemistry from the Vienna University of Technology for the  $N_2$ -characterization of our samples. We are grateful to J. Bossy (CNRS Grenoble) for supplying us with Gelsil samples.



## Chapter 6

# Revealing the pure confinement effect in glass forming liquids by dynamic mechanical analysis, accepted by PRB (2009)

Manuscript of accepted article

by

J. Koppensteiner, W. Schranz and M.A. Carpenter

The contribution of J. Koppensteiner has been

- all experimental work: sample preparation including silanation, DMA and RUS experiments, the latter under supervision of M.A. Carpenter
- analysis of RUS data and all other data processing
- Application of the existing theoretical models and fitting of data. Applying the new found method of Berthier et al. [12] as proposed and pretested by W. Schranz to determine the dynamic correlation length from elastic susceptibility data.
- further development of molecular relaxation models (together with W. Schranz)
- literature research (together with Prof. Schranz)
- design of all sketches, figures and tables
- composing a raw version of the article and taking it to its final version under supervision of W. Schranz

# Revealing the pure confinement effect in glass-forming liquids by dynamic mechanical analysis

J. Koppensteiner<sup>1</sup>, W. Schranz<sup>1</sup> and M. A. Carpenter<sup>2</sup>

<sup>1</sup> Nonlinear Physics Group, Faculty of Physics of the University of Vienna, Boltzmanngasse 5, A-1090 Vienna, Austria

<sup>2</sup> Department of Earth Sciences, University of Cambridge, Downing Street, Cambridge CB2 3EQ, UK

## *Abstract*

The dynamic mechanical response of mesoporous silica with coated inner surfaces confining the glass forming liquid salol is measured as a function of temperature and frequency (1-100 Hz) for various pore sizes (2.4-7.3 nm). Compared to former results on natural pores, a distinct acceleration of dynamics due to the removal of surface-related retardation of molecular dynamics is found now, which can be fitted by a homogeneous relaxation using an unmodified Vogel-Fulcher-Tammann relation. This lubrication effect leads to a stronger decrease of the glass transition temperature  $T_g$  with decreasing pore size. The present data allow to quantify and separate competing side effects as surface bondings and negative pressure from the pure confinement induced acceleration of molecular dynamics with decreasing pore size. We analyze the dynamic elastic susceptibility data in terms of a recently proposed procedure [C. Dalle-Ferrier et al. , Phys. Rev. E **76**, 041510 (2007)], which relates the number  $N_{corr,T}$  of molecules, whose dynamics is correlated to a local enthalpy fluctuation, to the three-point dynamic susceptibility  $\chi_T$ . The observed increase of  $N_{corr,T}$  with decreasing temperature strongly indicates that the size  $\xi$  of dynamic heterogeneities increases when approaching the glass transition.

Pacs: 64.70.P-, 61.20.Lc, 62.25.-g

## 6.1 Introduction

Glass-forming materials have been produced by mankind for more than 6000 years. Despite several decades of intense research the transition of a liquid into its glassy state is still lacking a universal theory explaining both the increase of viscosity  $\eta$  and molecular relaxation rates by 14 orders of magnitude [1, 2] without creating any long range order. A widely used explanation which goes back to Adam and Gibbs [3] is based on the assumption of cooperative rearrangement of molecules ("cooperative rearranging regions, CRR"), forming compact clusters of a typical size  $\xi$ . Such a subsystem of molecules can rearrange into another configuration independently of its environment.

The size of these groups of molecules is considered to grow to some nm as  $T_g$  is approached [5]. E.g. random first order transition theory of glasses [6, 7] predicts  $\xi = r_0 0.51 (\ln \frac{\tau}{\tau_0})^{\frac{2}{3}}$ . At  $T_g$  where  $\tau \approx 100$  s one obtains for typical values of  $\tau_0 \approx 10^{-12}$  s and  $r_0 \approx 1$  nm,  $\xi(T_g) \approx 5$  nm. Measuring such dynamic heterogeneities is one of the most important but at the same time difficult issues in the field of glass formation. Experimental setups like specific heat spectroscopy [5, 8], multidimensional NMR [9, 10, 11] and dielectric spectroscopy [12], etc. have been used to determine a possible growing length scale accompanying the glass transition. All these results agree in the fact, that the obtained cooperative regions are of the order of several nm near  $T_g$ , and are displaying a weak temperature dependence [13]. Recent computer simulations also confirm a rather modest growth of the dynamically correlated regions when approaching the glass transition from above [16]. Very recently in a groundbreaking work Biroli et al. [17] found direct evidence for a growing dynamical length in supercooled liquids by applying inhomogeneous mode-coupling theory. Based on this theory these authors have recently developed a method to quantify the size of the correlated regions [12] by analyzing three-point dynamic susceptibilities. For a large number of supercooled liquids they could indeed confirm growing of the correlated regions when approaching the glass transition [18].

However, direct measurements of  $\xi$  are extremely difficult, sometimes even impossible and one has to resort to indirect investigations. A widely used approach is confining the glass-forming liquid spatially, either in the form of thin films or by using mesoporous host matrices for confinement. If the size  $d$  of the confinement is finite the cooperatively rearranging regions cannot grow beyond any bound, becoming saturated at  $\xi = d < \infty$ . This should lead to a confinement induced acceleration of the dynamics resulting in a downshift of the glass transition, and even impeding it [29] as  $\xi > d$ .

Since the pioneer work of Jackson and McKenna [26] in 1991, uncovering a reduction of

the glass transition temperature  $\Delta T_g \propto 1/d$  in confinement of size  $d$ , a variety of confinement geometries and experimental methods have been used. Both weak and strong glass forming liquids, showing strong and weak interaction with the 2D or 3D confinement media were investigated. Single, double, even multiple transitions have been observed. Extensive topical overviews are found in Refs. [52], [101] and [30].

The abundance and diversity of experimental findings shows that an accurate discussion of side effects in discussing results of glass forming liquids in confinement is essential. Negative pressure due to mismatching thermal expansion coefficients of liquid and confining matrix is such a side effect. It was discussed by various authors [32, 39] and sometimes even made responsible for the whole downshift of  $T_g$  in confinement [32]. Being true, it would disprove the idea of a growing length scale of cooperativity. In a former paper [38] the authors have determined negative pressure effects for salol in natural un-coated pores of size 7.5 to 2.6 nm from high resolution thermal expansion measurements. An upper bound for the contribution of negative pressure to the total downshift of  $T_g$  of  $\approx 30\%$  was found.

A second, and much larger effect on the glass transition of liquids in confinement arises from the interaction of the molecules with the huge inner surface of confining host matrices which can take values up to 600 m<sup>2</sup>/g (see Tab. 6.1). Confined liquids tend to form H-bonds with the hydrophilic pore surface, which leads to an immobile surface layer of molecules and a retarded relaxation behavior when approaching the glass transition.

In recent dynamic elastic measurements [36, 38] of salol filled into matrices of Vycor and Gelsil with natural untreated pores we studied this competition between surface induced slowing down and confinement induced acceleration of the dynamics. Here we present new results of salol confined in mesoporous Vycor and Gelsil with silanated pore surfaces. The results clearly show that silanation removes the liquid-surface interaction to a large extend, leading to an enhancement of the molecular dynamics in the pores, resulting in a stronger downshift of  $T_g$  as compared to the uncoated pores. These findings allow to separate the surface effect from confinement induced acceleration, and a simultaneous quantitative statement about negative pressure (no change due to silanation) within one and the same measurement technique and confinement geometry. A comparison with previous dielectric spectroscopy data [73, 131, 132] of salol in mesoporous matrices yields excellent agreement.

Using the recently proposed method of Berthier et al. [12] we determine the number  $N_{corr,T}$  of dynamically correlated molecules as a function of temperature and pore size.



## 6.2 Experimental

### 6.2.1 Sample preparation

Vycor by Corning Inc., NY is produced via phase separation within a  $\text{Na}_2\text{O-B}_2\text{O}_3\text{-SiO}_2$  melt, and subsequent acid leaching [61], which leaves a 98% pure  $\text{SiO}_2$  skeleton containing interconnected pores of random length, direction and density. A very narrow pore size distribution and an average ratio of pore length  $l$  over pore diameter  $d$  of  $l/d \approx 4.35$  is reported [57]. Gelsil samples result from a sol-gel process [133] and consist of randomly formed pure fused  $\text{SiO}_2$  monodisperse spheres [62], touching and penetrating each other, resulting in a mesoporous structure with a rather broad distribution of pore diameters, as  $\text{N}_2$ -sorption results showed. Samples are cut and sanded to gain the required orthogonal shapes, and cleaned in a 30%  $\text{H}_2\text{O}_2$  solution at 363 K for 24 h. Drying is done under high vacuum ( $10^{-6}$  mbar) at 393 K for another 24 h.

In order to deactivate inner surfaces,  $\text{OH}^-$  groups are replaced by  $\text{OSi}(\text{CH}_3)_3$  trimethylsilyl groups via exposing cleaned samples to gaseous hexamethyldisilazane (HMDS, from Sigma Aldrich, purity 99.9%) in a closed vessel at 330 K for 24 h. Afterwards samples are again evacuated for 24 h at 300 K. In order to check pore geometry and pore radius after silanation, mesoporous samples have been tested via  $\text{N}_2$ -sorption and BET/BJH analysis of the individual desorption isotherms [72] experiments before and after HMDS treatment (Tab. 6.1). The samples surface area, pore volume and porosity were found to decrease due to silanation. The effect of silanation on the pore diameter is  $\approx 0.2$  nm, corresponding to a HMDS layer thickness of  $\approx 0.1$  nm. For comparison Kremer et al. [73] estimated the thickness of the silan layer from analysis of dielectric strength data as 0.38 nm.

Filling with the fragile low molecular weight glass former [28] phenylsalicylate (salol,  $\text{C}_{13}\text{H}_{10}\text{O}_3$ ,  $T_m^{\text{bulk}} = 316$  K) is done by capillary wetting at 333 K for 12 h. Filling fractions  $f$  are evaluated via weighing clean and filled samples. Vycor pore space can usually be filled up completely ( $f \approx 1$ ), whereas for Gelsil samples  $f \approx 0.9$  is usually achieved due to blocking of bottle-neck shaped pores and closed pores which cannot be reached by the liquid.

Some characterizing parameters for the glass-freezing behavior of bulk salol are: fragility index  $m$  – which usually varies from  $m = 17$  for strong glass formers to  $m = 150$  for fragile ones – takes for salol [102] the value  $m = 73$ ,  $T_g^{\text{bulk}} = 220$  K (glass transition temperature defined at  $\tau=100$  s) and  $T_0 = 175$  K [121] (bulk Vogel-Fulcher temperature). The volume of a salol molecule is estimated [120] as  $0.282 \text{ nm}^3$  corresponding to a mean diameter of about 0.8 nm.

**Tab. 6.1:** N<sub>2</sub> adsorption characteristics and elastic moduli of untreated and silanated porous silica samples.

	Gelsil 2.6	Gelsil 5	Vycor
untreated			
av. pore diameter (nm)	2.6	5.0	7.5
surface area (m <sup>2</sup> /g)	590	510	70
pore volume (cm <sup>3</sup> /g)	0.38	0.68	0.21
porosity $\phi$	0.36	0.54	0.40
bulk mod. $K$ (GPa)	9.6	3.9	8.1
shear mod. $G$ (GPa)	7.7	3.3	6.7
Young's mod. $Y$ (GPa)	18.2	7.7	15.8
silanated			
av. pore diameter (nm)	2.4	4.8	7.3
surface area (m <sup>2</sup> /g)	260	325	65
pore volume (cm <sup>3</sup> /g)	0.15	0.4	0.19
porosity $\phi$	0.30	0.49	0.33
bulk mod. $K$ (GPa)	9.6	3.3	9.1
shear mod. $G$ (GPa)	9.0	3.9	9.0
Young's mod. $Y$ (GPa)	20.6	8.9	20.3

### 6.2.2 Dynamic mechanical analysis

The dynamic mechanical response of samples of a typical size of 1 x 2 x 8 mm<sup>3</sup> in three point bending (3PB) mode yields the real and imaginary part of the complex Young's modulus  $Y^* = Y' + iY''$  within a frequency range of 0.01 to 100 Hz applying static and dynamic forces up to 9.8 N. For further details see Refs. [38], [36], [41] and [42]. Temperature is controlled by gaseous nitrogen flow from 120 K to RT. DMA analyzers are decoupled from building vibrations, and electronics are shielded from a possible interference with the 50 Hz mains voltage frequency. The analyzers used are a series 7 DMA and a Diamond DMA, both built by Perkin Elmer Inc.

### 6.2.3 Resonant ultrasound spectroscopy

Due to contact errors a DMA experiment does not yield absolute values for elastic moduli. Therefore resonant ultrasound spectroscopy (RUS) was used to determine bulk and shear moduli of both natural and silanated mesoporous samples at room temperature. Orthogonal parallel-

epipeds of about  $2.9 \times 3.0 \times 3.1 \text{ mm}^3$  were used to gather resonance spectra from 50 to 1100 kHz. For each sample 25 peaks resulting from excited resonant eigenmodes and corresponding overtones then were fitted via a Lagrangian minimization routine gaining bulk modulus  $K$  and shear modulus  $G$  (see Tab. 6.1) with an accuracy of less than 1%. For further experimental details see e.g. Ref. [134]. Young's modulus  $Y$  was calculated from  $Y = 9KG/(3K + G)$  and used to calibrate DMA raw data at room temperature (see Figs. 6.1, 6.2 and 6.3).

### 6.3 Results and Discussion

As an example, the dynamic elastic response (1 Hz - 100 Hz) of salol in Gelsil with silanated pores of 4.8 nm diameter is shown in Fig. 6.1. The data for 2.4 and 7.5 nm pores look very similar and are hence not presented here.

Fig. 6.2 gives a comparison between the recent results of salol in natural untreated pores [38] and the new data on silanated samples. The most striking feature of the silanated samples is the absence of a double peak structure in  $Y''(T)$  and the steplike shape in  $Y'(T)$ . In untreated samples a significant part of the confined liquid sticks to the pore surface due to hydrogen bonding, thus being retarded in relaxation dynamics. This leads to a local dependence of relaxation times across the pore section (see Fig. 6.4) causing an extra glass transition at higher temperature relative to the one of the core molecules. Assuming a spatial distribution of Vogel-Fulcher temperatures [31]  $T_0(r) = T_{00} + k/(R - r + r_p)$ , which translates via  $\tau(r) = \tau_0 \cdot \exp[E/(T - T_0(r))]$  to a distribution of relaxation times we were able to fit the stepwise change in  $Y'(T)$  and the double-peak-structure in  $Y''(T)$ . A detailed analysis can be found in Ref. [38].

For silanated surfaces we now find only bulk-like relaxation, i.e. just one step in  $Y'(T)$  and one single narrow peak in  $Y''(T)$ . Peaks do shift with measurement frequency, as Fig. 6.1 shows. Since the liquid-surface interaction is removed now, we do not take into account any radial dependence of the relaxation time (see Fig. 6.4), but use a single homogeneous Vogel-Fulcher-Tammann equation

$$\tau(T, d) = \tau_0 \cdot \exp \left[ \frac{E}{T - T_0(d)} \right] \quad (6.1)$$

with the pre-exponential factor  $\tau_0$ , the activation energy  $E$  and the Vogel-Fulcher temperature  $T_0(d)$ , which depends on the pore diameter  $d$ .

Similar as in our previous work [38, 36] a Cole-Davidson relaxation is used to model

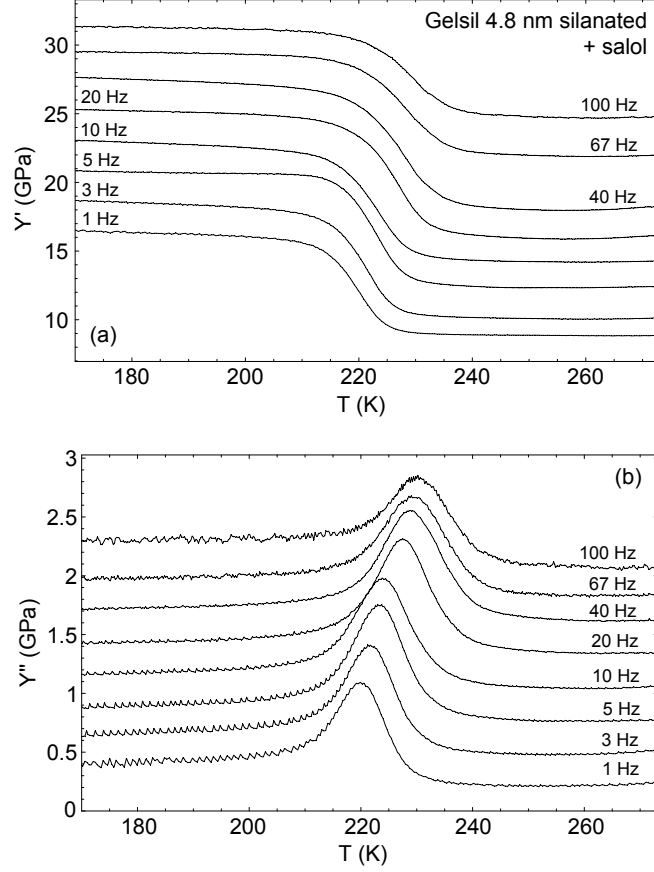


**Fig. 6.1:** Real (a) and imaginary (b) parts of the complex Young's modulus of silanated Gelsil (4.8 nm) filled with salol (filling fraction  $f = 0.87$ ) measured in three point bending geometry (Diamond DMA). 1Hz signal are original data, other signals are offset for sake of clarity since there is no frequency dependence of low and high temperature values aside the glass transition.

dynamic mechanic susceptibility in terms of (now radially monodisperse) relaxors

$$Y^*(\omega) \propto \frac{1}{(1 + i\omega\tau)^\gamma} \quad (6.2)$$

with  $\omega = 2\pi\nu$ ,  $\nu$  being the measurement frequency, and the broadening parameter  $\gamma$ . Separating real and imaginary part of  $Y^* = Y' + iY''$  leads to

$$Y'(T, d) = 1 - \Delta Y \cdot \frac{\cos[\gamma \cdot \arctan(\omega\tau(T, d))]}{[1 + \omega^2\tau(T, d)^2]^{\frac{\gamma}{2}}} \quad (6.3a)$$

$$Y''(T, d) = \Delta Y \cdot \frac{\sin[\gamma \cdot \arctan(\omega\tau(T, d))]}{[1 + \omega^2\tau(T, d)^2]^{\frac{\gamma}{2}}} \quad (6.3b)$$

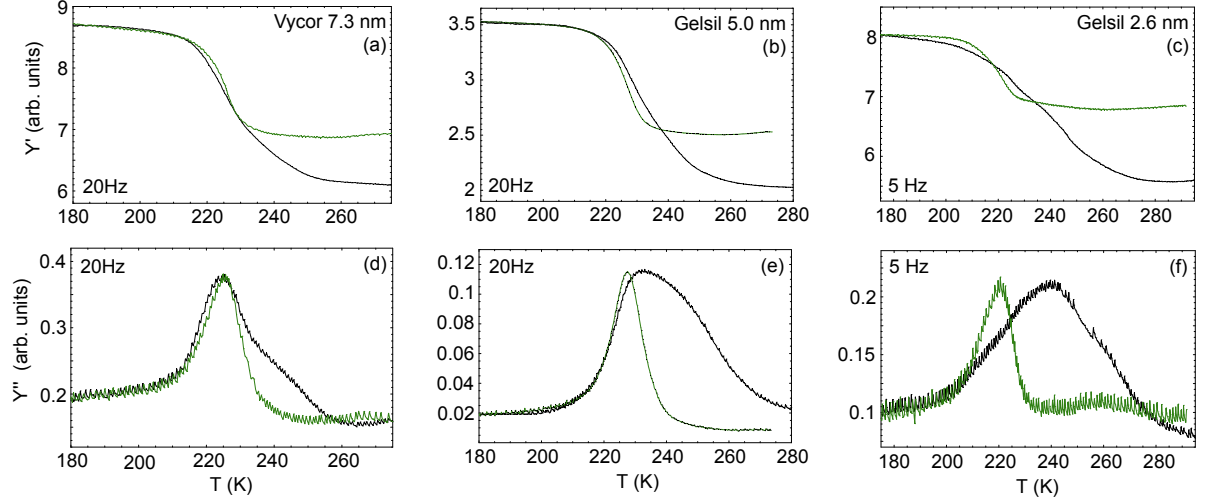


**Fig. 6.2:** Comparison of DMA data: black lines represent untreated samples, green lines are new data for silanated pore surface. Since contact losses inhibit direct comparison,  $Y'$  and  $Y''$  signals of silanated samples were scaled i.o. to match  $Y''$  peak heights.

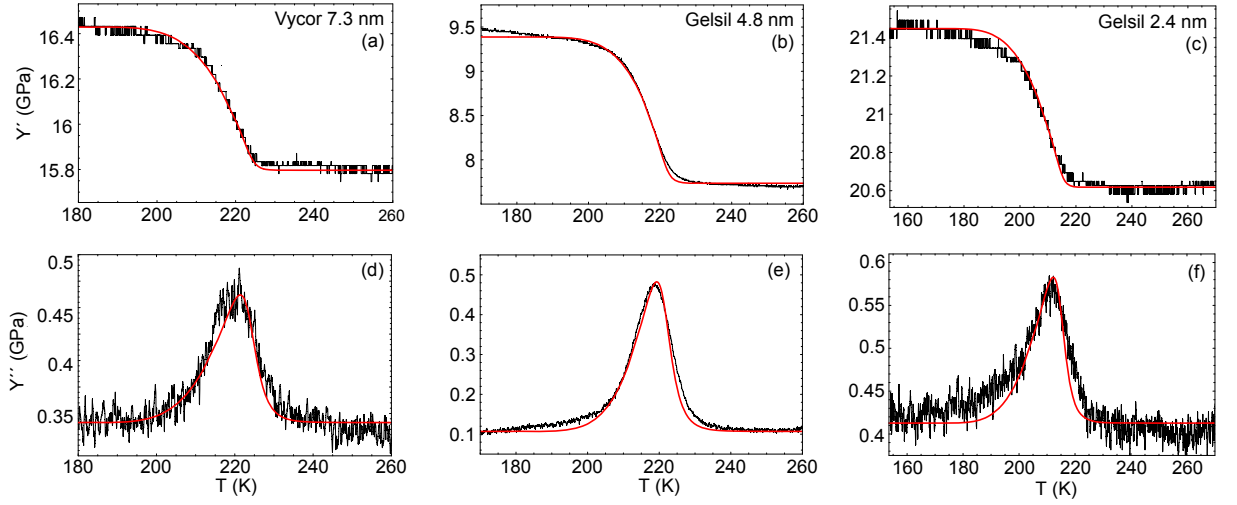


**Fig. 6.3:** Real part  $Y'$  and imaginary part  $Y''$  of different porous samples filled with salol, calibrated using RUS results at room temperature. Lines are fits using Eqns. (9.3a,b) and (6.1) with parameters of Tab. 6.2.

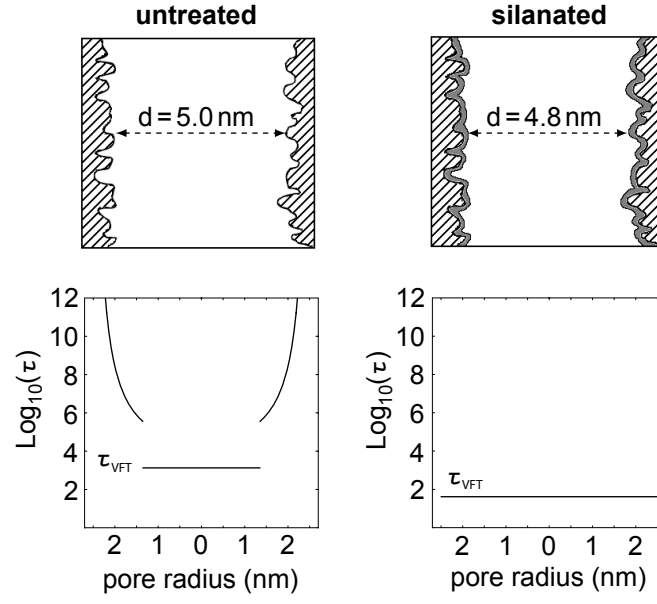


**Fig. 6.4:** Modeled relaxation time in untreated and silanated pores of Gelsil 5 from Eqn. (6.1) used in Ref. [38] and in Eqns. (9.3a,b) for fits of data in Fig. 6.3b and e herein, at  $T = 220 \text{ K}$ .

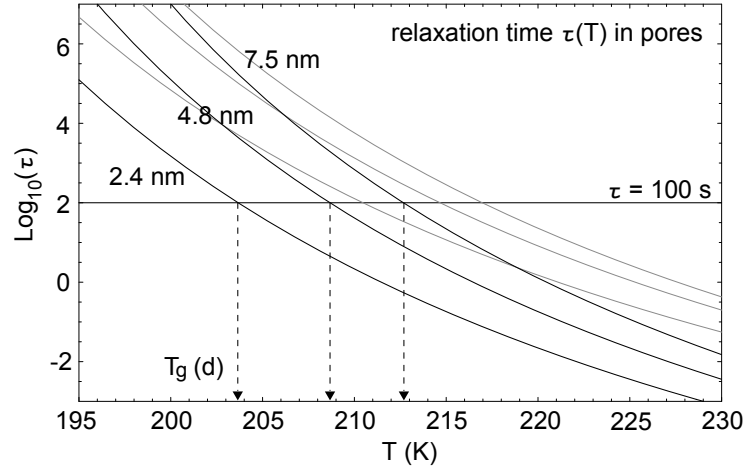


**Fig. 6.5:** Relaxation time in pore centers calculated from Eqn. (6.1) with corresponding parameters from Tab. 6.2. Horizontal line shows  $\tau = 100 \text{ s}$ . Gray lines are relaxation times in untreated pores from Ref. [38].

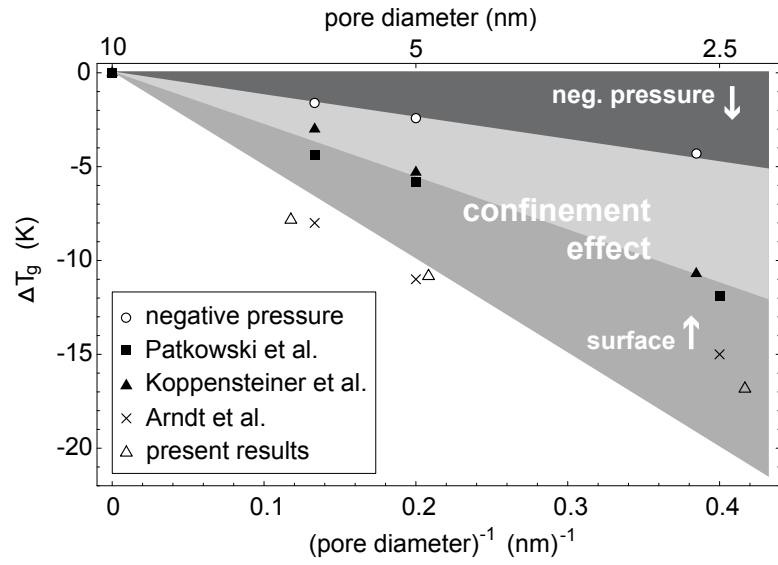


**Fig. 6.6:** Shift of glass transition temperature against inverse pore diameter. Open circles display the maximum negative pressure contribution (see Sec. III. C. of Ref. [38]), boxes are  $\Delta T_g$ 's Ref. [38], filled triangles show literature values from Ref. [32]. Open triangles are the present results, and crosses mark corresponding literature data from Ref. [73].

Eqns. (9.3a,b) and Eqn. (6.1) are used to fit the data given in Figs. 6.1 and 6.2. We point out that  $T_0$  enters as a fit parameter depending on the pore size  $d$ . Fits and corresponding parameters are shown in Fig. 6.3 and Tab. 6.2, respectively.

Silanation causes two main effects on the dynamics of the molecules within the pores: 1.) For untreated surface, we had to consider pore center relaxation times about two orders of magnitude higher [38] than obtained from the present analysis of silanated pores. Such an enhancement of mobility of molecules due to the absence of surface blocking in silanated pores was also observed in previous studies [132, 135]. It probably reflects the fact, that the surface blocking of molecular mobility in uncoated pores slows down the dynamics of molecules also in the center of the pores.

2.) Present results and used fit parameters (Tab. 6.2) show that the acceleration of the dynamics in silanated pores now leads to a much stronger downshift of  $T_g$  with decreasing pore size as compared with the results of uncoated pores [38]. It reflects the pure confinement effect - i.e. free of surface contributions - which leads to a downshift of  $T_g$  due to limitation of the correlated regions by the pore diameter.

On the other hand, silanation does not seem to have an effect on negative pressure within pores: Thermal expansion experiments using silanated samples were performed as already done for untreated samples in Ref. [38]. The result for Gelsil 5.0 nm is displayed in Fig. 6.7. Whereas silanated samples show less adsorption swelling probably due to a reduced surface tension (see Eqn. (6) of Ref. [38]), the temperature  $T^*$  at which thermal contraction again balances swelling and no pressure is applied upon the liquid, is not changed by silanation. This is possible due to a less steep contraction and smaller thermal expansion coefficient of the filled silanated sample. The calculated negative pressure induced downshift  $\Delta T_g$  following the procedure of Sec. III. C of Ref. [38] is -2.6 K compared to -2.4 K deduced for untreated pores. Also for silanated Vycor we found the same negative pressure contribution as compared to untreated Vycor. Thus the enhancement of the size effect of  $\Delta T_g(d)$  in coated pores results from the reduction of the chemical bonding of the glass forming liquid with the pore surface due to silanation.

Unfortunately there is no unique theory which clearly relates these finite size effects to parameters characterizing the glass transition. However in recent computer simulations [136] of supercooled polymer films confined between two separated walls of distance  $d$  it was shown that confinement leads to faster dynamics. The authors parametrized the size dependence



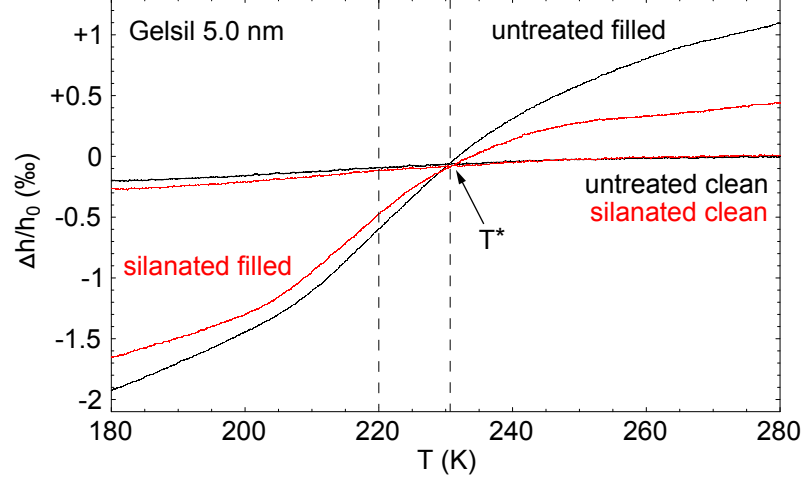


**Fig. 6.7:** Linear thermal expansion of untreated (black) and silanated (red) Gelsil 5.0 nm, both empty and filled. Sample height is normalized at 280 K.

of the relaxation time as  $\tau(T, d) \propto \exp \left[ \frac{E(d)}{T - T_0(d)} \right]$  and found similar  $d$ -dependencies for the mode-coupling critical temperature  $T_c(d)$  and the Vogel-Fulcher temperature  $T_0(d)$  arguing, that  $T_g(d)$  should also follow a similar curve (see Fig. 14 of Ref. [136]). As already mentioned above we here use the same dependence of the relaxation time (Eqn. (6.1)) to fit our data, and obtain a very similar size dependence of  $T_g(d)$  and  $T_0(d)$  (Fig. 6.8) as Varnik et al.

A. Hunt [129] has calculated finite size effects on the glass transition temperature in glass-forming liquids analytically using percolation theory. Assuming a Gaussian distribution of barrier heights  $n(E) \propto \exp[(E - E_m)^2/2\sigma^2]$  with  $E_m \approx \sigma$  (Eqn. (6) of Ref. [129]) it was found that

$$T_g^{bulk} = \frac{1.75 \sigma}{k_B \ln(t/\tau_0)} \quad (6.4)$$

where  $t$  defines the laboratory time scale  $\approx 100$  s of the glass transition. for the confinement induced shift of the glass transition temperature the author obtained

$$T_g(d) = T_g^{bulk} \left[ 1 - \frac{0.5 \sigma}{k_B \ln(\frac{100}{\tau_0} T_g^{bulk})} \cdot \frac{r_0}{d} \right] \quad (6.5)$$

where  $r_0$  is the typical distance between molecules, which we approximate here as the diameter of a salol molecule  $r_0 \approx 0.8$  nm. Inserting Eqn. (6.4) into Eqn. (6.5) yields

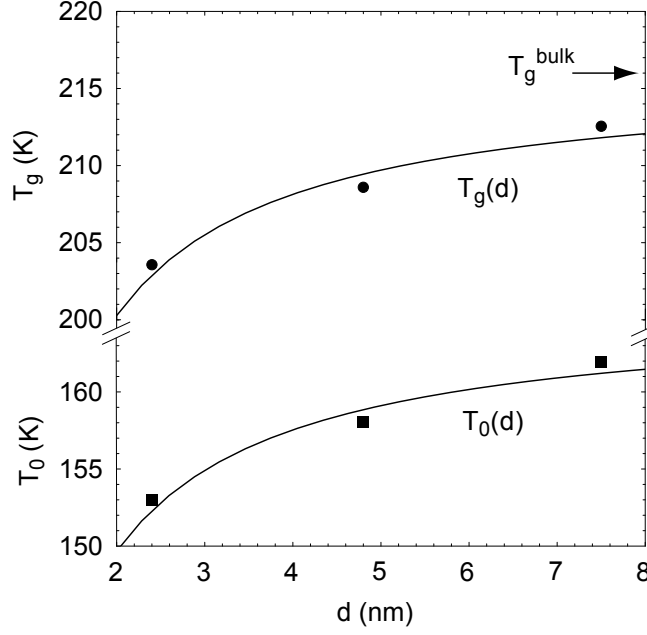


**Fig. 6.8:** Shift of glass transition temperature  $T_g$  and Vogel-Fulcher temperature  $T_0$  against pore diameter  $d$ . The points are determined from fitting the experimental data with Eqns. (9.3a,b) and (6.1), where  $T_g(d)$  is obtained from  $\tau(T, d) = 100$  s, as shown in Fig. 6.5. The lines are fits using Eqn. (6.6) yielding  $c = 0.13$  and  $T_g^{bulk} = 216$  K. For calculating  $T_0(d)$  the relation  $T_g - T_0 = \frac{E}{\ln(100/\tau_0)} = 50.6$  K was used, as indicated in the text.

$$T_g(d) = T_g^{bulk} \left[ 1 - c \frac{r_0}{d} \right] \quad (6.6)$$

where  $c = 0.286$ . Given the semiquantitative character of this theory, the agreement with our determined value of  $c = 0.13$  is quite reasonable. In this picture  $T_g$  is reduced by confinement because the average barrier height for the molecules in pores is smaller than the so called "blocking" barrier, which is responsible for the glass freezing in the bulk. We have also plotted the values of  $T_0(d)$  of Table 6.2 in Fig. 6.8. The corresponding line was drawn using the relation  $T_g - T_0 = \frac{E}{\ln(100/\tau_0)} = 50.6$  K, which is obtained from Eqn. (6.1) using the fit parameters  $E = 1750$  K and  $\tau_0 = 10^{-13}$  s of Table 6.2.

As already mentioned above, Dalle-Ferrier et al. [18] have given an expression for the number  $N_{corr,T}$  of molecules that are dynamically correlated to local enthalpy fluctuations over a time interval of the order of  $\tau$  as

$$N_{corr,T}(T) = \frac{T}{\sqrt{\Delta C_p}} (\max_{\omega} |\chi_T(T, \omega)|) \quad (6.7)$$

where  $\chi_T(T, \omega) := \frac{\partial \chi(T, \omega)}{\partial T}$ ,  $\chi(T, \omega)$  is a normalized suitable dynamic correlation function and  $\Delta C_p$  in units of the gas constant  $R$  is the excess specific heat of the glass-forming liquid at constant pressure [18]. Very often glass-forming materials are studied by dielectric spectroscopy measurements and therefore the dynamic susceptibility is identified with the dielectric susceptibility. To estimate  $N_{corr,T}$ , we apply two different procedures: In the first one we are using  $\chi(T, \omega) := \frac{Y'(\omega) - Y'(\infty)}{Y'(0) - Y'(\infty)}$  in Eqn. (6.7) to analyze the data directly, i.e. without any fit procedure in between. In the second case we rewrite Eqn. (6.7) with Eqn. (6.2) yielding

$$N_{corr,T}(T) = \frac{T}{\sqrt{\Delta C_p}} f(\gamma) \left( \frac{\partial \ln \tau}{\partial T} \right) \quad (6.8)$$

where  $\tau(T)$  is obtained from fits of the data in Fig. 6.3 and  $f(\gamma) = \frac{\sin[\gamma \arctan(\frac{1}{\gamma})] + \frac{1}{\gamma} \cos[\gamma \arctan(\frac{1}{\gamma})]}{(1 + \gamma^{-2})^{1 + \gamma/2}}$  results from the Cole-Davidson dynamic response function and is the analog to the stretched exponential  $\beta$  of the KWW-response function used e.g. in Eqn. (8) of Ref. [137]. It should be noted that Eqn. (6.8) is only strictly valid, if  $\gamma$  is independent of temperature (see discussion in Ref. [18]). Fig. 6.9 compares the temperature dependence of  $N_{corr,T}$  calculated from the two different methods, which results in excellent agreement in the temperature range  $220 \text{ K} < T < 235 \text{ K}$ . This implies that at least in this temperature range  $\gamma$  is temperature independent.

Although it is not straightforward, it is tempting to estimate the size of  $\xi$  of dynamic heterogeneities for the present case i.o. to compare it with values determined from other types of experiments. As shown e.g. in Refs. [12] and [18] the height of the peak in the nonlinear susceptibility  $\chi_4$  yields the correlation volume, i.e.  $\chi_4 \approx (\frac{\xi}{a})^\zeta$ , where  $2 < \zeta < 4$  [138] and  $a$  is the molecular size, i.e. 0.8 nm for salol. Quite generally  $\chi_4 \geq \frac{T^2}{\Delta C_p} \chi_T^2$ . However, for most fragile liquids the equality  $\chi_4 \approx \frac{1}{\Delta C_p} T^2 \chi_T^2$  can be assumed [12, 18].

Assuming a compact correlation volume, i.e.  $\zeta = 3$ , we can estimate  $\xi = (N_{corr,T}^2)^{1/3} a$  yielding a growth of  $\xi$  from about 1.6 nm at  $T = 270 \text{ K}$  to 3.2 nm at  $T_g(d)$  which is nearly the same value for any measured pore size  $d$ . Although there are uncertainties about numerical prefactors [18], as well as the geometry for heterogeneities, i.e. the exponent  $\zeta$ , the overall behavior of  $\xi(T_g, d)$  is in remarkable agreement with calorimetrically determined characteristic lengths for salol in confined geometries [92], as well as with dielectric measurements [139].

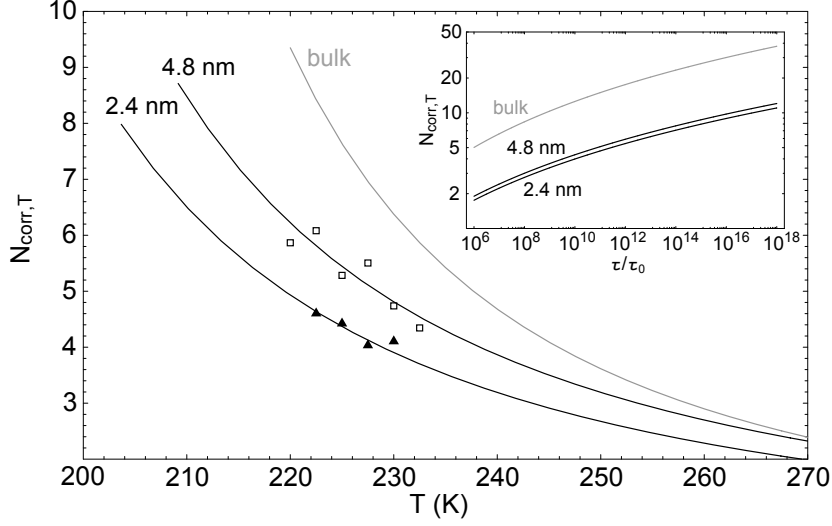


**Fig. 6.9:** Temperature dependence of  $N_{corr,T}$  for various pore sizes. Lines are calculated from Eqn. (6.8) using the procedure described in the text. Symbols are calculated from DMA data using Eqn. (6.7). Inset shows  $N_{corr,T}$  against relaxation time  $\tau/\tau_0$  in the corresponding temperature range on logarithmic scales.

## 6.4 Conclusions

Results of extensive dynamic mechanical measurements of the glass forming liquid salol confined in mesoporous silica with silanated pores are presented. It turns out that silanation is able to reduce the liquid-surface interactions drastically. At the same time high resolution thermal expansion measurements show that the negative pressure contribution to the downshift of the glass transition temperature  $T_g$  is the same as in uncoated pores. As a result the observed stronger (as compared to uncoated pores) downshift of  $T_g$  with decreasing pore size can be fully attributed to the confinement induced acceleration of the dynamics, which occurs due to

**Tab. 6.2:** Fit parameters used in Eqns. (9.3a,b) for fits of Fig. 6.3.

	Vycor	Gelsil5	Gelsil2.6
$E$ (K)	1750	1750	1750
$T_0$ (K)	161.5	158.5	154.5
$\tau_0$ (s)	$10^{-13}$	$10^{-13}$	$10^{-13}$
$\gamma$	0.19	0.25	0.17

the hindering of cooperativity. Using the results of percolation theory [129] we have calculated the downshift of  $T_g$  with decreasing pore size, which fits our data very well. In Ref. [129] it is also shown that finite size effects are expected to set in when the pore size  $d \approx 7r_0 - 10r_0$  yielding 4.8–8 nm for salol with  $r_0 \approx 0.8$  nm. This is in very good agreement with our observations.

We also have analyzed our dynamic elastic data obtained for the different pore sizes in terms of a newly proposed theory [12] which relates the number of dynamically correlated molecules  $N_{corr,T}$  to the temperature derivative of the dynamical two-point correlation function, which in our case can be identified with the dynamic elastic susceptibility  $Y(\omega, T)$ . The results clearly show an increase of  $N_{corr,T}$  with decreasing temperature approaching  $T_g$ . In spite of the fact that the precise relation between  $N_{corr,T}$  and a corresponding length scale is hampered due to unknown prefactors and exponents [18], this implies that the pore size  $\xi$  of dynamically correlated regions increases when approaching  $T_g$ .

For smaller pore sizes  $\xi(T', d)$  at a given temperature  $T'$  shifts to smaller values which is concomitant to the systematic decrease of the relaxation time  $\tau(T', d)$  and the resulting downshift of  $T_g(d)$ . However at the glass transition temperature the dynamic correlation length is almost independent of the pore size with  $\xi(T_g, d) = 3.2$  nm, a value which was also found by calorimetric [92] and dielectric [139] measurements. Very similar as already observed in Ref. [18], we found a modest growth of  $N_{corr,T}$  from about 2 at  $T = 270$  K to 8 at  $T_g$ , whereas the relaxation time  $\tau$  increases dramatically by about 12 orders of magnitude in this temperature interval (see inset of Fig. 6.9). This characteristic behavior was observed for all measured pore sizes.

Unfortunately at present there is no unique theory that relates the relevant parameters controlling the confinement effects in glass-forming materials to experimental data. The reason for this is that the microscopic mechanism behind the glass transition is still not completely understood and more theoretical (e.g. of the type presented in Ref. [140]) and experimental work is required to close the gap of knowledge and understand confinement effects in glass-forming liquids.

**Acknowledgements:** We thank Marie-Alexandra Neouze and the Institute of Materials Chemistry from the Vienna University of Technology for the N<sub>2</sub>-characterization of our samples. We also thank Irena Drevenšek-Olenik and Miha Devetak from the Jožef-Stefan-Institute in Ljubljana for help concerning silanation, which was done within the ÖAD-WTZ project SI 19/2009. RUS facilities in Cambridge were established with the support of grant to MAC from the Natural Environment Research Council of Great Britain, NE/B505738/1. Support by

the Austrian FWF (P19284-N20) and by the University of Vienna within the IC Experimental Materials Science ("Bulk Nanostructured Materials") is gratefully acknowledged.

# Chapter 7

## Unpublished Results

### 7.1 Overview

In addition to the results published and given in Secs. 4 - 6, we have worked on the following problems and obtained results which are not yet published:

- We searched for a possible nonlinear elastic behaviour of mesoporous materials (Sec. 7.2) at increasing stress.
- We investigated the glass transition of the molecular glass forming liquids toluene (Sec. 7.3) and orthoterphenyl (Sec. 7.4) in confinement.
- We performed Resonance Ultrasound Spectroscopy (RUS) measurements on the mesoporous empty and filled samples to determine the elastic constants of Vycor and Gelsil, i.e. as a function of porosity and to study confinement effects on the glass transitions also at high frequencies ( $10 \text{ kHz} < \nu < 1 \text{ MHz}$ ). These results are shown in chapter 8.

Both the DMA series 7, as well as the Diamond DMA were used to do the experiments. Dynamic measurements were done on both apparatus, static, i.e. thermal expansion measurements were done with the DMA 7, as the Diamond DMA does not allow to directly access probe position data. Diamond DMA data come with a much better resolution due to higher forces controlled and changed during measurements proportional to the samples elastic modulus. Furthermore, temperature control is very reliable, although the automatic cooling unit consumes huge amounts of liquid nitrogen. Further drawbacks are its "black-box" character: certain measurement signals simply can not be accessed, the applied forces cannot be controlled, and an error-prone software sometimes quits measurement runs by itself.

Concerning the DMA 7, forces are controllable, the measurements signals can be accessed and exported making it a transparent apparatus with straightforward handling. Unfortunately

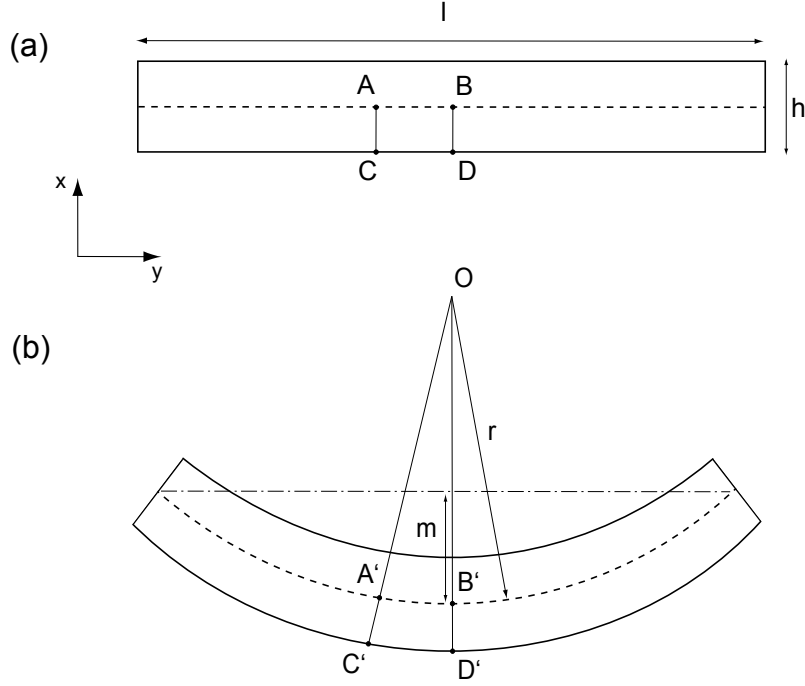


**Fig. 7.1:** Modeling of strain in a 3PB experiment. Straight undeformed bar (a) and bar under stress (b).

forces are limited to 2.5 N, making it even more important to think of proper sample shaping (see Sec. 3.3.3) i.o. to gain the required deformation and resolution. Further drawbacks are the absence of an automated cooling unit, its sensitivity to building vibrations and extended signal equilibration times.

## 7.2 Stress-strain relation in mesoporous silica in 3PB

An estimation of stress and strain in a 3PB experiment can be done by geometrical considerations and beam bending theory [141]. Fig. 7.1 shows an undeformed bar (a) and its bent state (b). The bending line is approximated as part of a circle. Strain is not homogeneous in  $y$  direction through the sample. Compression is present on the upper side, no change along the central axis (dotted line), and expansion on the bottom. In the similar triangles  $OB'A'$  and  $OD'C'$  we find

$$\frac{\overline{C'D'}}{\overline{A'B'}} = \frac{r + h/2}{r} \quad (7.1)$$

The strain along the samples bottom is



$$\epsilon = \frac{\overline{C'D'} - \overline{CD}}{\overline{CD}} = \frac{h/2}{r} \quad (7.2)$$

since  $\overline{CD} = \overline{AB} = \overline{A'B'}$ . The radius  $r$  can be given by the arch rise  $m$  (deflection) and arch length along the central axis  $l$  as

$$r = \frac{(l/2)^2 + m^2}{2m} \quad (7.3)$$

Then the strain induced by a given deflection  $m$  is

$$\epsilon(m) = \frac{h/2}{\frac{(l/2)^2 + m^2}{2m}} = \frac{4hm}{l^2 + 4m^2} \quad (7.4)$$

Deflection  $m$  is identical with a DMA's rod position change  $\Delta p$  at a given force.  $p$  is zero when at the beginning the rod rests upon the sample with force  $F = 0$ .

Stress  $\sigma$  along the  $y$ -axis of the sample due to a perpendicular punctual force on the samples surface can be estimated by classical beam bending theory [141] yielding a maximum stress of

$$\sigma_{max} = \frac{3Fl}{2wh^2} \quad (7.5)$$

on the samples bottom with sample dimensions length  $l$ , width  $w$  and height  $h$ . Stress-strain 3PB-measurements of Vycor and Gelsil samples are shown in Fig. 7.2. In 3PB geometry force upon the sample was increased linearly up to 2.5 N and bending depth  $m$  was read every second. The resulting data were converted to stress and strain using Eqns. (7.4) and (7.5), which are shown in Fig. 7.2.

Data were fitted using

$$\epsilon(\sigma) = S_1 \cdot \sigma + S_2 \cdot \sigma^2 \quad (7.6)$$

Used fit parameters  $S_1$  and  $S_2$  are shown in Tab. 7.2. Quantities  $S_i$  in general are called compliances which are inverse elastic constants.

As shown in Tab. 7.2, the mesoporous silica monoliths show a distinctively larger amount of nonlinear stress-strain behavior than the bulk material. Nonlinear compliances  $S_2$  are 6 to 25 times higher for porous Vycor and Gelsil samples as compared to bulk fused silica. A possible explanation is the deformation of inner structures like walls leading to less (macroscopic) strain at increasing stress [142]. Further work in this direction is in progress.

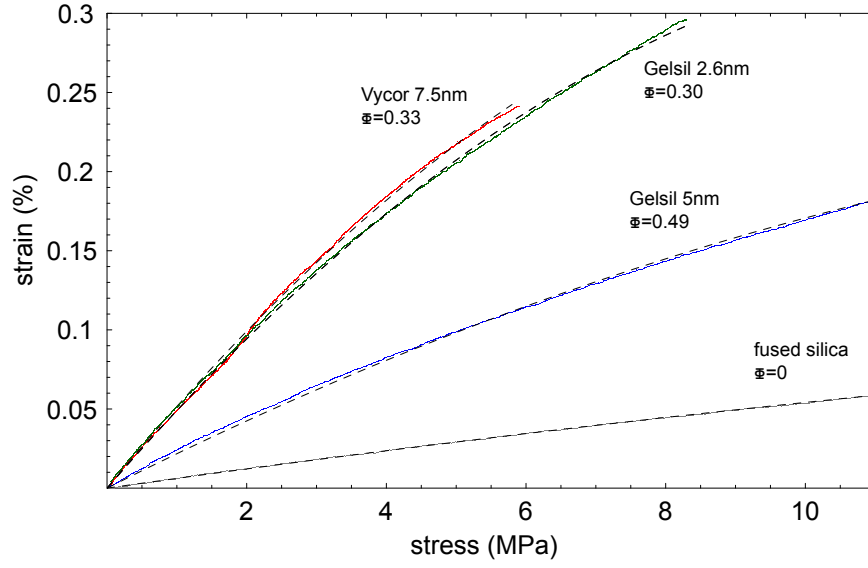


**Fig. 7.2:** Modeled strain due to stress of porous silica samples compared to fused silica. Points are calculated from raw data along Eqns. (7.5) and (7.4). Dotted lines are quadratical fits yielding parameters of Tab. 7.2.

**Tab. 7.1:** Comparison of fitted compliances and bulk moduli.

	fused silica	Vycor	Gelsil 5	Gelsil 2.6
$(S_1)^{-1}$ (GPa)	8.0	0.9	2.2	1.0
bulk modulus $K$ (GPa)	36.9	8.1	3.9	9.6

**Tab. 7.2:** Parameters of Eqn. (7.6) used for fits of Fig. 7.2.

	porosity $\Phi$	$S_1$ (GPa $^{-1}$ )	$S_2$ (GPa $^{-2}$ )
fused silica	0	0.12	-3.27
Vycor 7.5 nm	0.4	1.07	-81.77
Gelsil 5.0 nm	0.45	0.45	-20.91
Gelsil 2.6 nm	0.30	1.02	-75.85

### 7.3 Toluene in confinement

In order to test different glass forming liquids, toluene (methylbenzene,  $\text{C}_6\text{H}_5\text{CH}_3$ ,  $T_m = 180\text{ K}$ ) was filled into mesoporous silica and measured via DMA. In literature toluene is intensively discussed especially since a strong *upshift* of  $T_g$  by 37 K was found in confinement of 2.4 nm and similar results were found for benzene [94]. The authors suggested a particularly strong interaction of - in general - fragile liquids with the untreated silica surface. With decreasing pore size, the confinement effect is more and more superimposed. Comparable behavior was found in glycerol [28], polypropylene-glycol [91] and oTP [143].

The bulk glass transition temperature of toluene is  $T_g^{\text{bulk}} = 117\text{ K}$  which is out of the range of the Diamond DMA (lower limit 123 K). But the strong upshift found in calorimetric experiments would shift  $T_g$  into the temperature range accessible with the DMA. So, even if the whole transition may not be covered, at least an affirmation - or disprove - of this trend should be possible.

Samples were again filled via immersion using capillary forces (see Sec. 2.5). Filling fractions e.g. for Vycor turned out to be  $f \approx 0.95$ . Unfortunately, toluene in standard atmosphere is an extremely volatile liquid and a filled sample at RT within minutes is emptied, which easily can be observed on accurate scales. Lowering temperature suppresses vaporization, so the filled sample was positioned within the Diamond DMA 3PB attachment quickly, the furnace was closed and a steep cooling ramp of 20 K/min down to 225 K was applied. An estimated amount of 30% pore space was still filled with toluene as upon the following measurements the glass transition was tested.

**Tab. 7.3:** Fit parameters of Fig. 7.3

	Gelsil 2.6	Vycor
$d$ (nm)	2.6	7.5
$E$ (K)	2690	2690
$k$ (nm·K)	15	48
$r_p$ (nm)	0.25	0.5
$\gamma$	0.1	0.1
$\tau_0$ (s)	$10^{-11}$	$10^{-11}$
$T_{00}(K)$	33	20

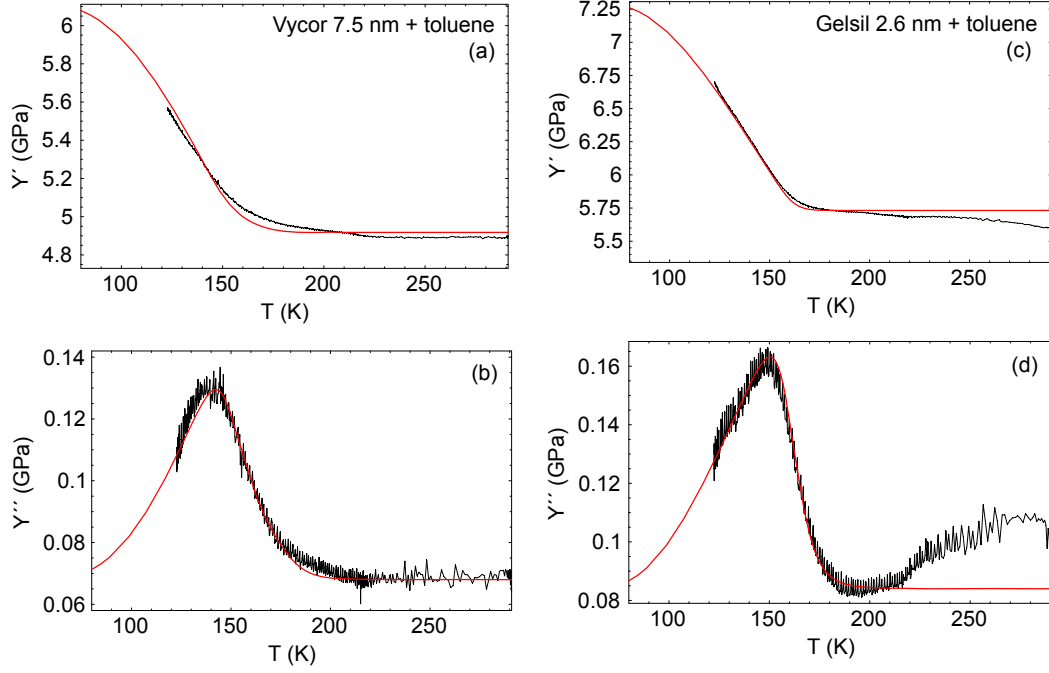


**Fig. 7.3:** Storage and loss modulus of Vycor (a,b) and Gelsil 2.6 nm (c,d) filled with toluene, both at 5 Hz. Both cooling runs performed at 10 K/min from RT  $\rightarrow$  225 K, and at 2 K/min 225 K  $\rightarrow$  120 K, the DMAs lower limit. Fits use Eqns. (4.7) with parameters of Tab. 7.3.

As done for salol, a Cole-Davidson-approach was used for fitting the data. Relaxation time was modeled using a modified VFT-equation (Eqn. (4.6)) as in Ref. [36] (chapter 4). Contrary to our observations for salol (see chapters 4 and 5), for toluene, from the point of view our limited data offers, no 2-step-like heterogeneous behavior can be detected. An interaction with the pore wall, expressed as an exponential decrease of relaxation time  $\tau(r, T)$  (Eqn. (4.6) and 4.5) is used across the whole pore up to the pore center as shown in Fig. 7.6. VFT-parameter  $E$  is derived from results presented in Ref. [144]. The resulting fits satisfyingly describe our (uncomplete set of) data.

A procedure following Ref. [38] or Sec. 5.3.1 yields glass transition temperatures well in the range of literature values. The results displayed in Fig. 7.4 support the measurements of Alba-Simionesco et al. [94] and also show a downshift of  $T_g$  in 7.5 nm pores, and an upshift in 2.6 nm pores, both less strong, but still present. This agreement is even more astonishing, since Alba-Simionesco et al. used an NMR technique and parallel cylindrical pores of MCM-41 and SBA-15 whereas we used Vycor and Gelsil and a dynamic mechanical approach. Due to limitation of time, further measurements and analysis on toluene had to be abandoned. But

certainly this is an interesting direction to continue the research.

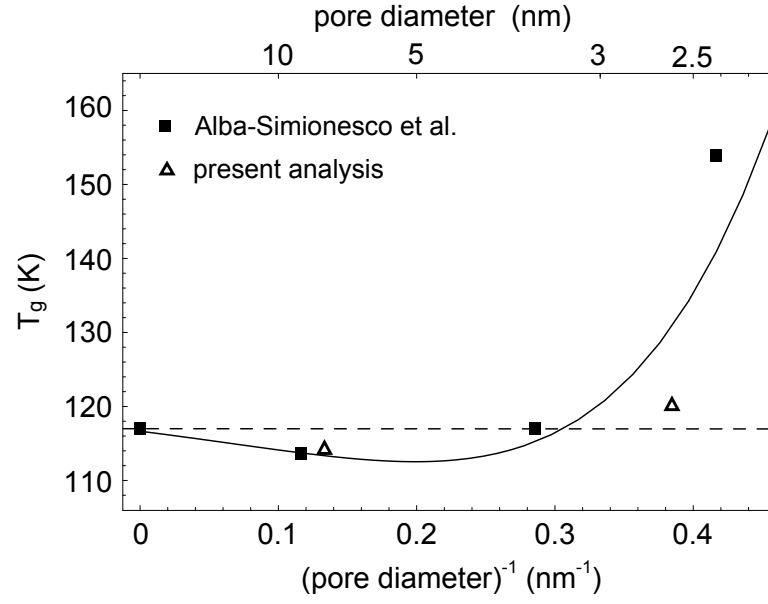


**Fig. 7.4:** Non-monotonic variation of  $T_g$  of nanoscopically confined toluene. Boxes stem from Ref. [94], open triangles indicate present data. Dotted line displays  $T_g^{bulk} = 117$  K. The line is a guide to the eyes.

## 7.4 Orthoterphenyl in confinement

The van-der-Waals liquid ortho-Terphenyl (oTP,  $C_{18}H_{14}$ ) is another extensively studied standard glass forming liquid ( $T_m = 329$  K). Molecules consist of three phenyl rings ( $C_6H_5$  -  $C_6H_4$  -  $C_6H_5$ ) arranged in a circle and tilted against each other [145], forming a nearly spherical non-polar molecule of radius  $r_{OTP} = 0.4$  nm [146]. The bulk glass transition temperature is  $T_g^{bulk} = 243$  K [147], fragility index  $m = 81$  [130].

In their pioneer work on the hindered glass transition, Jackson and McKenna [26] used oTP to show a downshift of  $T_g \propto (1/d)$  in pores of CPG of mean diameter  $d$ . Other calorimetric setups yielded similar behaviour in different host matrices: Gelsil [32], MCM-41 and SBA-15 [28]. A recent work by Le Quellec et al. [143] shows a strong influence of surface interaction in SBA-15 matrices, even displaying an upshift of  $T_g$  in untreated pores. This is in contrast to former authors which report distinct downshifts in untreated pores [26, 28, 32].

Up to now no report of a dynamic mechanical analysis of oTP in confined geometry is present in literature. Thus Vycor and Gelsil samples were prepared as described in Sec. 2.2 and filled via capillary wetting, which was done by Dr. Madalina Puica. oTP is a corrosive liquid and filling always has to be done under an exhaust hood and with special care. Secondly oTP is a volatile liquid and rather tends to evaporate and crystallize on the container's surface than to enter pores. And third, oTP being a larger molecule than salol is hindered from entering pores. However, within one week Vycor was filled up to  $f \approx 0.8$  and a Gelsil 5 nm sample took 3 weeks to gain  $f \approx 0.9$ . Gelsil 2.6 nm, although treated exactly the same way, did not take up a verifiable amount of oTP, even after 1 month. So for further measurement only Vycor 7.5 nm and Gelsil 5.0 nm were used.

Dynamic mechanical measurements were performed using both the DMA 7 and the Diamond DMA. A typical result is shown in Fig. 7.5. As done for toluene, Eqn. (4.7) was used with parameters of Tab. 7.4. Fig. 7.6 shows that the modeled relaxation time  $\tau(r, T_g)$  near the (untreated) pore wall is very similar for toluene (red line) and salol (black line). But only for salol a sudden change to an unmodified Vogel-Fulcher-Tammann behaviour without a radial dependence  $\tau(T_g)$  is found at  $r = R_c$  implying that salol molecules in the center behave *decoupled* from shell molecules (see chapter 4 and 5). Such a heterogeneous relaxation is also not found for oTP, showing a more shallow increase of  $\tau(r, T_g)$  approaching the pore walls (green line of Fig. 7.6).

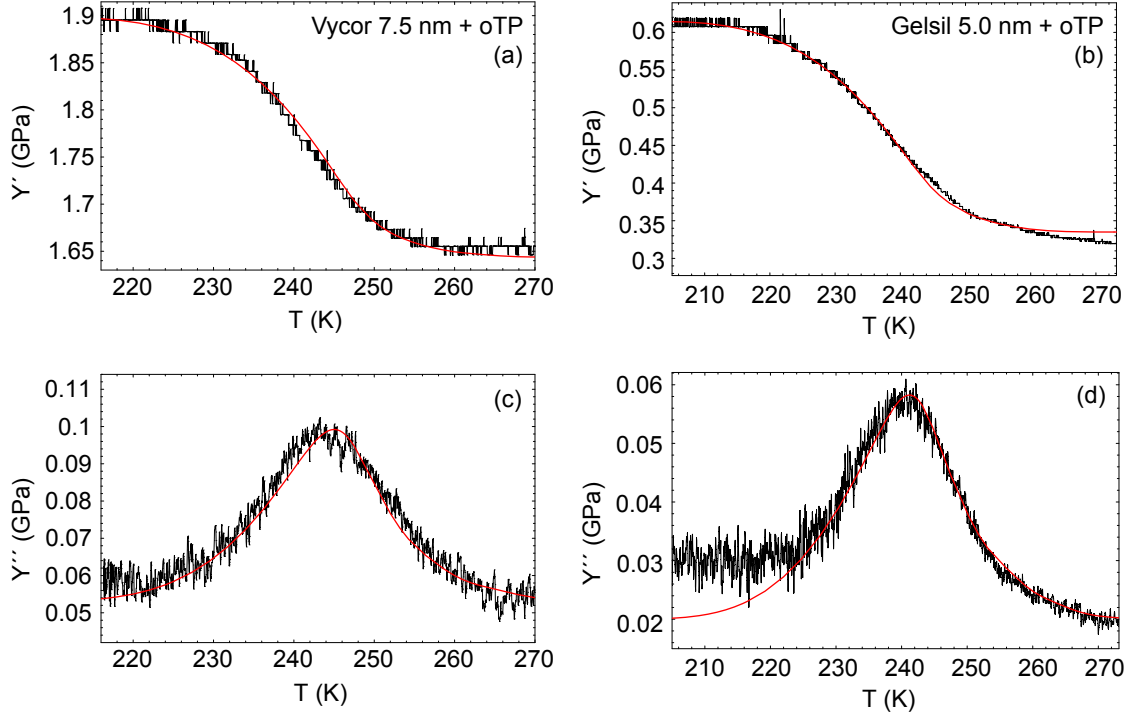


**Fig. 7.5:** Storage modulus  $Y'$  and loss modulus  $Y''$  of different porous samples filled with oTP. Shown are original DMA data, red lines are fits using Eqn. (4.7) with parameters of Tab. 7.4.

**Tab. 7.4:** Fit parameters of Fig. 7.5

	Gelsil 5	Vycor
$d$ (nm)	5.0	7.5
$E$ (K)	1500	1500
$k$ (nm $\cdot$ K)	5	5
$r_p$ (nm)	0	0
$\gamma$	0.19	0.16
$\tau_0$ (s)	$10^{-11}$	$10^{-11}$
$T_{00}(K)$	180.5	175.2

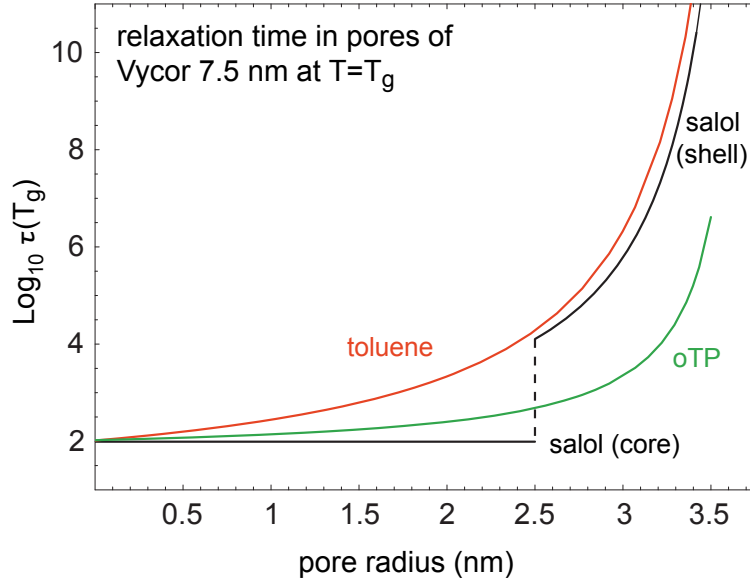


**Fig. 7.6:** Relaxation times  $\tau$  of toluene (red), salol (black) and oTP (green) in pores of Vycor 7.5 nm using Eqn. 4.6 and parameters of Tabs. 5.2, 7.3 and 7.4 at the individual glass transition temperatures  $T_g$ .

Resulting glass transition temperatures were derived following the procedure described in Ref. [38] Sec. III. A (Sec. 5.3.1). We find  $T_g$ s in very good agreement with literature data as shown in Fig. 7.7 and we cannot find an upshift in uncoated pores as reported in Ref. [143].

In contrast to salol [36, 38] (chapters 4 and 5), both toluene and oTP in 7.5 nm pores of Vycor do not show a heterogeneous relaxation behavior. Data can be described by a Vogel-Fulcher-Tammann equation modified by a Vogel temperature  $T_0(r)$  which increases as the pore wall is approached. Contrary to salol, in toluene and oTP there is no core volume where molecules would act decoupled and bulk-like. This discrepancy cannot be explained by molecule size or a fewer number of molecules within the pore, since the salol molecule is larger than the toluene molecule.

However, this point was left for further investigations due to the mentioned difficulties concerning sample preparation and since parallel investigations on salol in confinement needed to be finished first. For sure here is an interesting and important open problem waiting to be tackled by subsequent researchers.



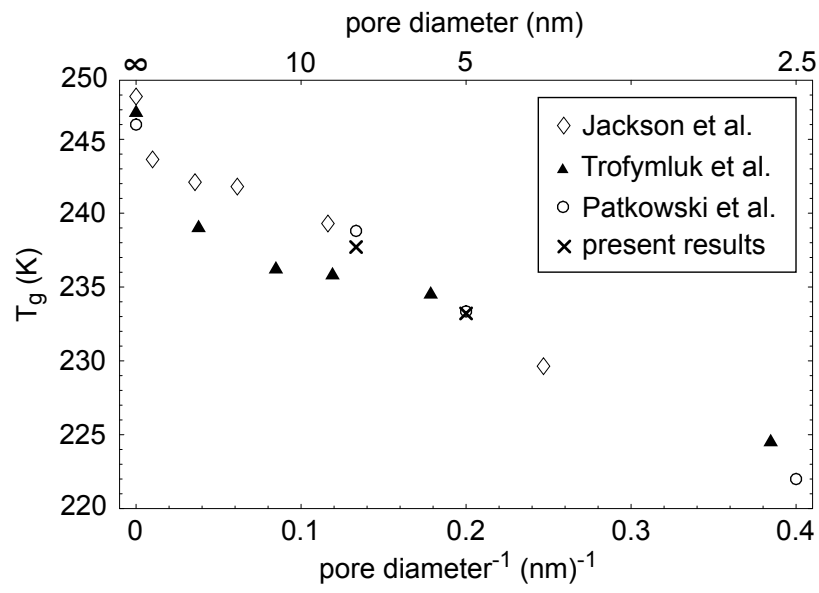


**Fig. 7.7:** Glass transition temperatures for oTP against inverse pore diameter. Open diamonds show results of Jackson et al. [26], filled triangles are data by Trofymuk et al. [28], whereas circles represent values of Patkowski et al. [32]. Crosses mark present results.



# Chapter 8

## RUS Results

This chapter will display results of resonant ultrasound spectroscopy (RUS) gathered at the University of Cambridge, Department of Earth sciences, achieved under supervision of Prof. Michael Carpenter. Results of room temperature scans (Sec. 8.2) were used in publications [38, 40] (see chapters 5 and 6) and Ref. [148]. Results of temperature scans (Sec. 8.3) are unpublished.

### 8.1 Method and Theory

Resonance ultrasound spectroscopy is a widespread and well known method of determining absolute elastic constants. For an extensive review see e.g. Ref. [149]. The natural mechanical resonances which every body regardless of outer shape and material performs, are used. This makes RUS a universal tool. Another advantage is the nondestructive character, the achieved accuracy and the quickness of a single test. In theory one spectrum collected within minutes is enough to determine the whole tensor of elastic constants of a single crystal sample.

Basic resonant eigenmodes of a body are for example torsion along a body axis, shear or a voluminal breathing mode. Each one of them is excited by transducers at a very specific frequency  $\nu_i$ , at which the transducers response shows a distinct peak. Scanning between 50 kHz and 1100 kHz then shows a landscape of peaks, each one corresponding to an eigenmode or its overtone.

A picture of the RUS apparatus used for RT scans is given in Fig. 8.1. The sample shape is rectangular, the lateral length of the parallelepipeds is about 3 mm. Each length should deviate slightly from 3 mm and none of them should coincide i.o. to split similar resonant modes and correspondent eigenfrequencies. The deviation of the rectangular shape has to be smaller than 3%. If else, eigenmodes are lost or not excited, and data analysis based on geometrical shapes becomes an impossible task. For that reason sample preparation is crucial and the more accurate the samples shape, the more easy it will be to deduce elastic moduli from resonance spectra.

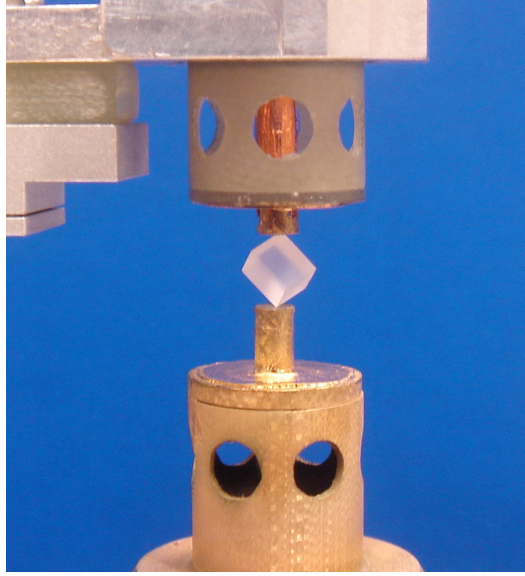


**Fig. 8.1:** Photo of RUS RT unit. Two opposing transducers covered with gold hold an empty Gelsil 2.6 nm sample. The upper transducer is vertically movable. All parts built by M.A. Carpenter and coworkers.

The theoretical description of eigenmodes and corresponding frequencies involves elastic constants. The potential energy of a system can be given in terms of the displacement field  $u_i$  as

$$E_{pot} = \frac{1}{2} \int_V C_{ijkl} \frac{\partial u_i}{\partial x_j} \frac{\partial u_k}{\partial x_l} dV, \quad (8.1)$$

with the body volume  $V$  and the tensor of elastic constants  $C_{ijkl}$ . The kinetic energy then can be written as

$$E_{kin} = \frac{\omega^2}{2} \int_V \rho u_i u_i dV \quad (8.2)$$

with angular frequency  $\omega = 2 \cdot \pi \cdot \nu$ . Resonance now calls for stationary points of the Lagrangian  $L = E_{pot} - E_{kin}$ , meaning  $\delta L = 0$  under  $\omega \rightarrow \omega + \delta\omega$  and  $\vec{u} \rightarrow \vec{u} + \delta\vec{u}$  [150]. In this case  $\{\omega, \vec{u}\}$  describe a resonant eigenmode of the body volume  $V$ . Finding pairs of displacement fields  $\vec{u}$  and correspondent eigenfrequencies  $\nu$  by the help of initial elastic constants now is a complex task and there is no analytical solution. But for simple shapes like cylinders, cubes or parallelepipeds and by the help of approximation methods (e.g. Rayleigh-Ritz approach [151]) and thanks to modern computer processors nowadays solutions can be found within seconds.

The software used herein has been developed by M. A. Carpenter and coworkers. It needs

peak positions (25 peaks were used), sample dimensions and weight and initial values for bulk modulus  $K$  and shear modulus  $G$ . Running the program leads to calculated peak positions. Initial values for  $K$  and  $G$  then are changed i.o. to minimize variations between calculated and experimental positions. Sometimes peaks can not be found, since the corresponding eigenmode has not been excited during the testing runs. For that reason scans are done in corner-to-corner (as in Fig. 8.1), edge-to-edge and face-to-face geometry i.o. to find as many resonances as possible. The goal is fitting 25 peak positions, each one within a frequency position variance  $< 3\%$ . The final calculation uses a root-mean-square deviation minimization to do a multiple fit and yields bulk and shear modulus with an astonishing accuracy.

The lowest modes correspond to shear motions. Higher modes include voluminal changes like a breathing mode and are therefore determined by the bulk modulus. That's why a large number (in our case 25) of modes and corresponding peaks is used, and why the shear modulus is always found with higher accuracy than bulk modulus. Uncertainties automatically given by the fitting routine are found by varying starting values and can be used as absolute uncertainties for the found moduli [152]. Concerning the present samples all uncertainties in determined elastic constants are  $\approx 1\%$ . Including errors made when determining sample size and weight via error propagation as done in Ref. [153] does not significantly increase this value.

## 8.2 Room temperature elastic constants of mesoporous silica

Bulk and shear moduli of Gelsil glasses were not published before. RUS is the ideal method to determine elastic constants since natural mechanical eigenmodes are found in samples of every composition, porosity and density. Although RUS measurements are performed in different frequency and strain ranges, one can compare the results with DMA data, at least at RT. Samples were cut and sanded to  $2.9 \times 3.0 \times 3.1 \text{ mm}^3$  orthogonal parallelepipeds and then cleaned and dried as described in Sec. 2.2. RT scans have been performed from 200 to 1100 kHz gathering 50.000 data points per run. Several runs with the sample mounted on corners, edges and faces have been performed. A typical result is shown in Fig. 8.2.

The absolute height of the response signal depends on the coupling of sample surface and transducer. The upper transducer contacts the sample just by its own weight. Nevertheless the pressure upon the contact point and the efficiency of excitation changes every time the sample is mounted. That's why e.g. peak heights in the inset of Fig. 8.2 are not equal.

The quality or Q-factor of a single resonance peak  $i$  is defined as [150]

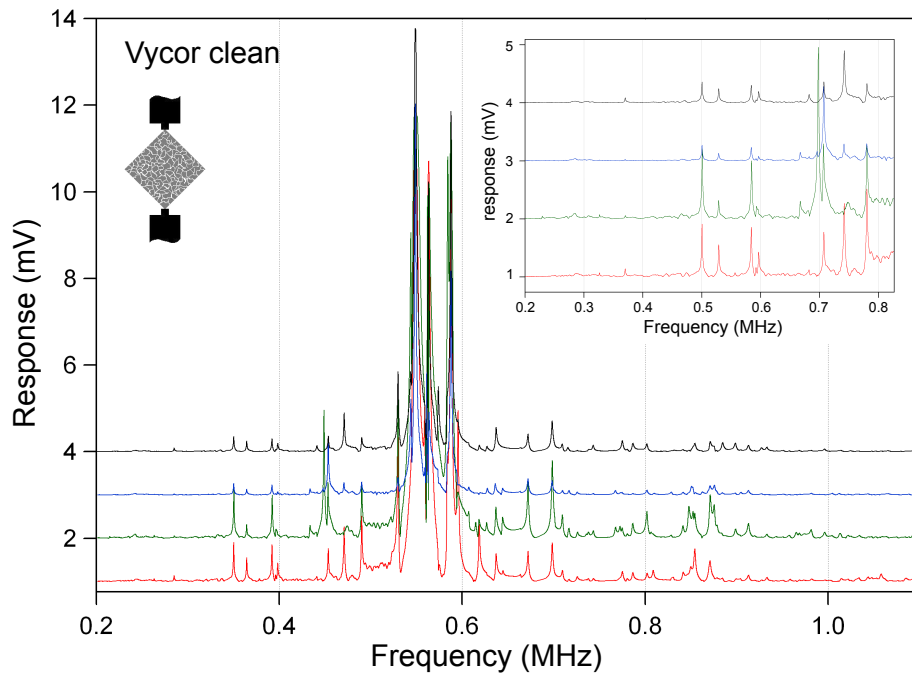


**Fig. 8.2:** RUS spectra of a clean Vycor sample at RT mounted in corners-to-corners geometry consecutively along the 4 body diagonals. Data are offset for sake of clarity. Inset displays a closer look at the lower modes.

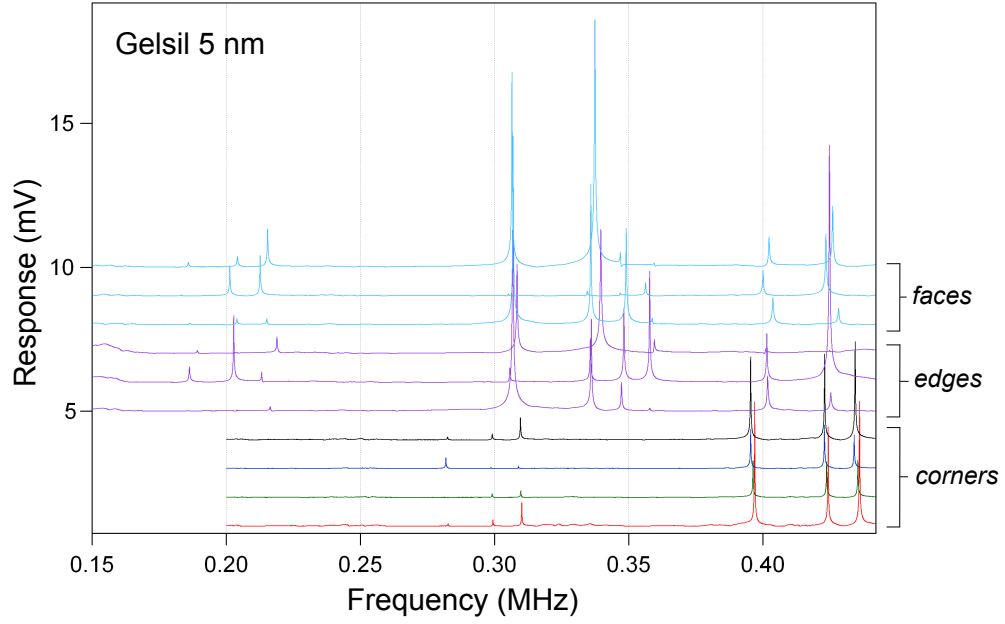


**Fig. 8.3:** RUS spectra showing the lower modes of a clean Gelsil 5.0 nm sample at RT mounted in different geometries.

$$Q_i = \frac{\nu_i}{\Delta\nu_i} \quad (8.3)$$

where  $\nu$  is the peak position within the spectrum and  $\Delta\nu$  is the FWHM of the corresponding peak. The higher  $Q$ , the more narrow and pronounced are the resonance peaks.  $Q$  describes ultrasonic attenuation and is connected to the phase lag  $\delta$  of a DMA experiment by

$$Q \propto (\tan \delta)^{-1} \quad (8.4)$$

$Q$  of Vycor at RT was found to be  $Q \approx 400$ . Comparable investigations yielded  $Q \approx 700$  in Ref. [154]. Gelsil samples showed sharper peaks and  $Q \approx 10^3$ . An analysis of fused silica reported  $Q = 2 \times 10^3$  in Ref. [155].

Gelsil 5.0 and 2.6 samples were treated equivalently and RUS spectra have been gathered at RT. An output of the Gelsil 5.0 nm spectra at low frequencies shown in Fig. 8.3 displays the difficulties arising when looking for the lowest excitations. As the sample was mounted on corners, the first shear eigenmode has not been excited. But as edges or faces were used, the lowest mode showed up as a small peak around 0.20 MHz. Fig. 8.4 shows the lowest modes of Gelsil 2.6 nm, the first one located at 0.23 MHz. The same procedure has also been used on silanated samples. All results of RT scans and subsequent analysis are given in Tab. 8.1.

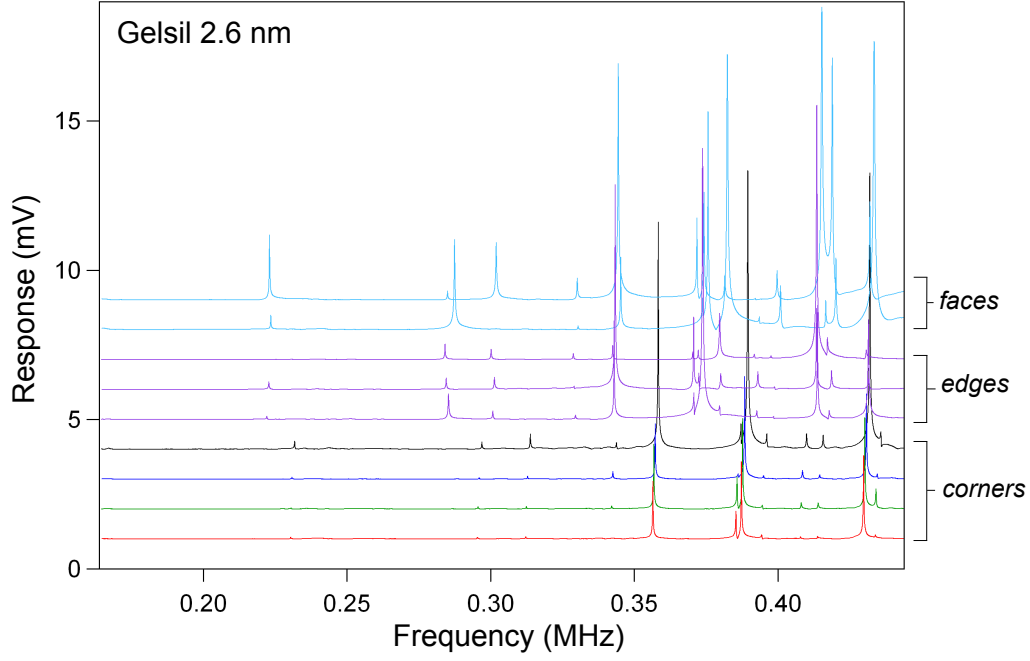


**Fig. 8.4:** RUS spectra showing the lower modes of a clean Gelsil 2.6 nm sample at RT mounted in different geometries.

**Tab. 8.1:** RUS results of porous silica host matrices

	Gelsil 2.6	Gelsil 5	Vycor
untreated			
porosity $\phi$	0.36	0.54	0.40
bulk mod. K (GPa)	9.6	3.9	8.1
shear mod. G (GPa)	7.7	3.3	6.7
Poisson's ratio $\nu$	0.18	0.17	0.18
Young's mod. Y (GPa)	18.2	7.7	15.8
silanated			
porosity $\phi$	0.30	0.49	0.33
bulk mod. K (GPa)	9.6	3.3	9.1
shear mod. G (GPa)	9.0	3.9	9.0
Poisson's ratio $\nu$	0.14	0.08	0.13
Young's mod. Y (GPa)	20.6	8.9	20.3

As seen from Tab. 8.1 silanation decreases porosity by  $\approx 15\%$  for all samples and clearly increases the shear modulus significantly. This may be explained by the following idea: The



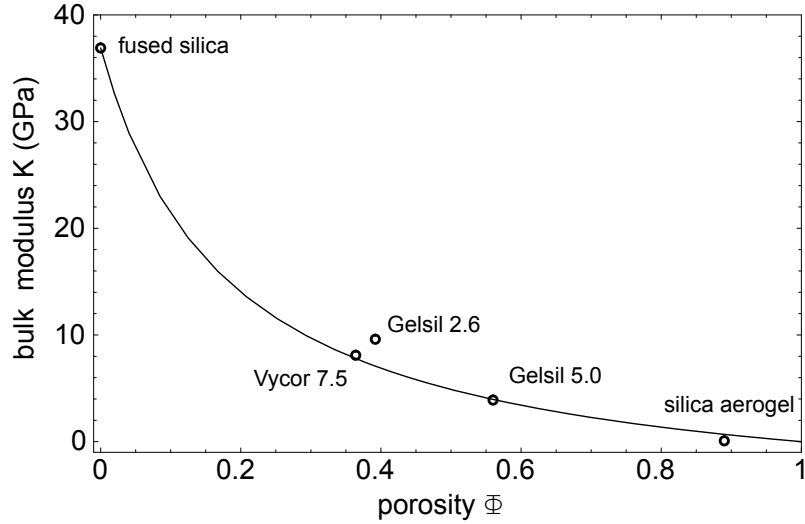


**Fig. 8.5:** Bulk moduli of porous samples measured within this work plus silica aerogel from Ref. [153] as used in Ref. [156]. The line shows a Hashin-Shtrikman upper bound.

applied HMDS layer within the sample creates additional contact points and nodes within a network, first of all effecting its resistance against shear [142]. At the same time bulk moduli are rather unchanged, only a slight decrease was found for Gelsil 5 and a slight increase for Vycor. Youngs modulus was calculated from  $Y = 9KG/(3K + G)$  and found to be increased by silanation for all samples. The gained values for  $Y$  were used to calibrate DMA data at RT, since a DMA measurement does not yield absolute values (see Ref. [40] or Sec. 6.2.3). Bulk moduli of clean empty samples are used for considerations on elasticity-porosity-relations and the elastic instability of porous silica in Ref. [156].

An increase of shear modulus leads to a decrease of Poisson's ratio  $\nu = \frac{E}{2G} - 1$  (see Tab. 8.1). Upon uniaxial load, silanated samples show less lateral expansion compared to untreated samples. Unfortunately in literature no theory is available which would describe the influence of inner pore coatings on elastic moduli of a mesoporous structure. But further work in this direction should be performed i.o. to explain the present data.

### 8.3 Low temperature scans

As done in DMA experiments, temperature scans were performed for both clean and filled samples. A cryostat using both liquid helium and liquid nitrogen was used to cool down the sample mounted into the RUS low temperature head. At predefined points, temperature was equilibrated for 30 min and the frequency scans were performed. Cooling then was continued

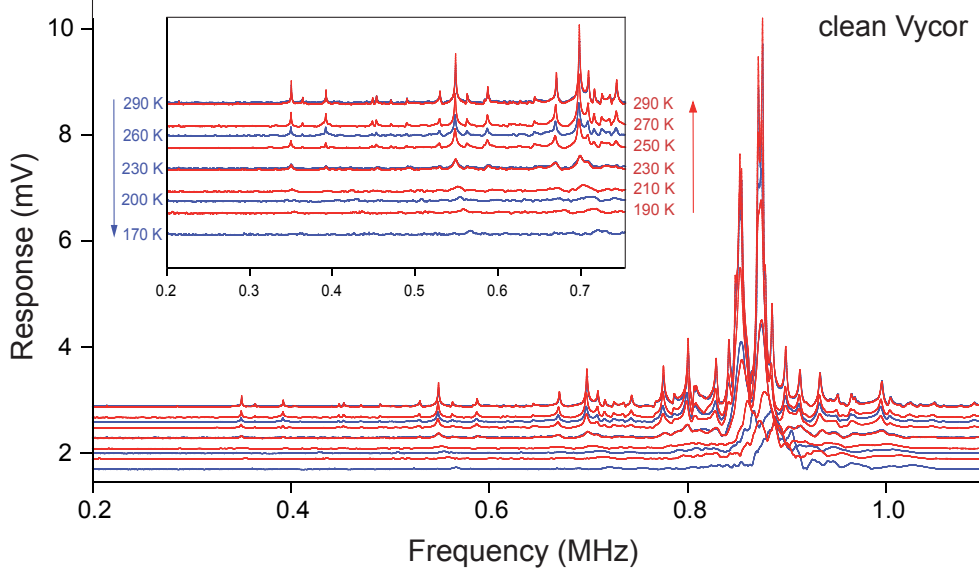


**Fig. 8.6:** RUS spectra of clean Vycor in the temperature range  $170 \text{ K} < T < 290 \text{ K}$ . Data collected upon cooling are denoted in blue, heating in red. Data are offset by factor  $0.01 \cdot T$ . Inset displays the lower modes.

to the next step following a preset program. The same procedure was used upon heating. During 24 hours 25 data sets, each one containing 50.000 data points, were collected. The most challenging part was mounting the sample into the low temperature head and lowering it into the cryostat without dropping the sample, which is mounted in the instable corner-to-corner geometry. During tests, the sample often tilted into the face-to-face position or even fall off the head. Furthermore, both Gelsil samples broke apart during the cooling section. That's why low-temperature runs can be presented for Vycor only.

### 8.3.1 Vycor clean

A clean Vycor sample prepared following Sec. 2.2 was mounted and lowered into the cryostat. The temperature program was set as follows:

cooling:	290 K $\rightarrow$ 170 K	in 30 K steps
heating:	170 K $\rightarrow$ 290 K	in 20 K steps

At previous RT scans the first peak was found at 218 kHz (see Fig. 8.2), so the scanning range was set to 200 – 1100 kHz and 50.000 data points were gathered at each step after 30 min of temperature equilibration. The resulting spectra are shown in Fig. 8.6.

As expected, absolute peak positions  $\nu_i$  did not change at lower temperature. Since

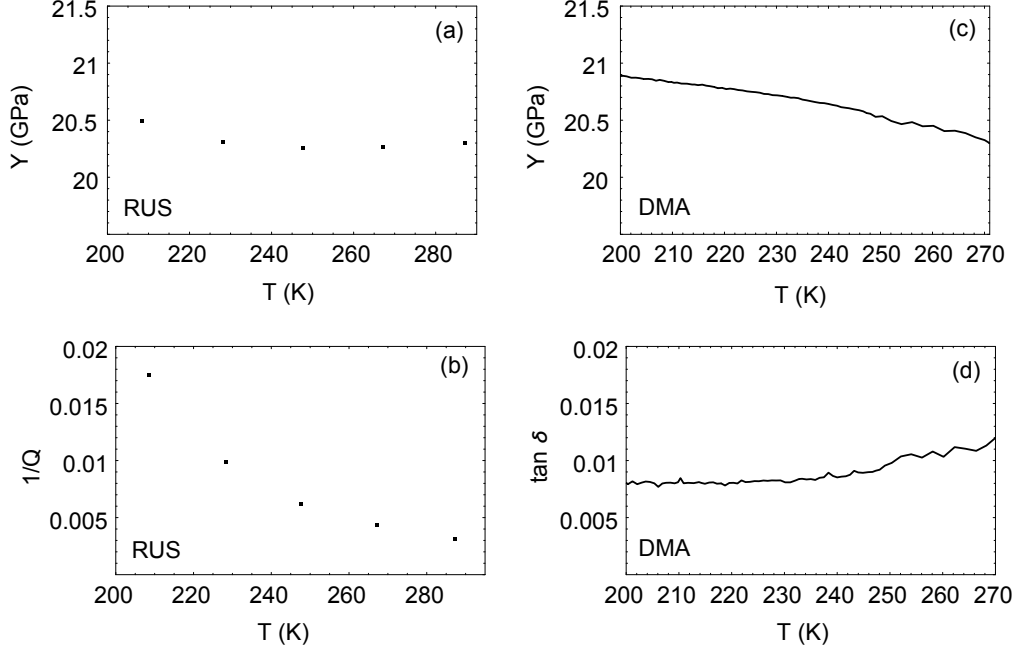


**Fig. 8.7:** Clean Vycor: Young's modulus  $Y$  and  $Q$  of RUS experiments (a and b) at 0.55 MHz in comparison to  $Y$  and  $\tan \delta$  obtained from DMA analysis (c and d) at 10 Hz.  $Y$  of DMA data in (c) was calibrated at RT according to RUS RT results.

$$(\nu_i)^2 \propto K \propto Y \quad (8.5)$$

this corresponds to a nearly constant bulk and Young's modulus (assuming a constant Poisson's ratio  $\nu$ ). Peaks found at RT broaden up with decreasing temperature and at 170 K can no longer be located. Peaks return to their initial shape as temperature approaches RT. For further analysis a single distinctive peak is chosen and at each temperature a Lorentzian function

$$g(\nu) = a_0 + a_4 \cdot x + \frac{a_2}{(\nu - a_1)^2 + a_3} \quad (8.6)$$

with frequency  $\nu$  and fit parameters  $a_0 - a_4$  is fitted and peak position  $\nu$  and FWHM  $\Delta\nu$  are calculated.  $Q$  is derived from Eqn. (8.3). Bulk and Young's modulus are calibrated via Eqn. (8.5). Both are plotted against temperature and compared to DMA results in Fig. 8.7.

DMA data in Fig. 8.7c show a linear increase of Young's modulus by 0.008 GPA/K upon cooling. RUS results (a) display an increase of 0.003 GPA/K. At a first glance this behavior seems reasonable, but things are more subtle in this case. Following Ref. [157], consolidated

Vycor (no pores, the skeleton material) against intuition shows an *decrease* of the bulk modulus upon cooling. On the other hand, Vycor 7930 (also used herein) contains pores which adsorb moisture. Upon cooling the freezing of capillary water leads to an *increase* of the bulk modulus and a  $\tan \delta$  peak around 190 K [157]. Peak height and broadness depend on the moisture content. So the increase of  $(1/Q)$  upon cooling in Fig. 8.7b could be interpreted as the onset of of capillary water, which was adsorbed during the previous RT tests.

In contrast to the behaviour described in Ref. [157], which was found in a DMA apparatus at 1 kHz, the present dynamic mechanical analysis (10 Hz) does not show a corresponding increase or peak of  $\tan \delta$  in Fig. 8.7d. Moreover, a lower moisture content during DMA tests would not explain the - compared to RUS results - larger increase of  $Y$ . After intense discussions and literature research, all further work in this direction was abandoned, since it would have led too far away from the central points of this thesis.

### 8.3.2 Vycor filled with glass forming liquids

The first aim of RUS analysis was measuring filled samples i.o. to compare results to DMA data and to explore the glass transition in confinement at different frequency ranges. In dynamic mechanical analysis a shift of the glass transition of about 10 K was observed in the range of 1 - 100 Hz.

The same samples as used for RT scans (see Sec. 8.2) were filled with salol as described in Sec. 2.5.  $\tan \delta$  peak positions in DMA experiments have been observed at  $\approx 220$  K, and an upshift of 5 K at 100 Hz was observed. Since the frequency-driven upshift in RUS is expected to be larger, and i.o. to scan it in more detail, the temperature program was set as follows:

cooling:	290 K $\rightarrow$ 170 K	in 30 K steps
heating:	170 K $\rightarrow$ 210 K	in 5 K steps
	210 K $\rightarrow$ 270 K	in 2 K steps
	270 K $\rightarrow$ 290 K	in 5 K steps

Again, temperature was held constant for 30 min at the individual steps to ensure isothermal conditions for the subsequent RUS scan. Single scans collected 50.000 data points from 200 to 1100 kHz. Overall  $2.1 \times 10^6$  data points were collected at 42 temperature levels during heating. Fig. 8.8 shows a cut-out of the overall peak landscape and the evolution of an exemplary single peak at about 0.77 MHz at 180 K due to temperature change. First of all, compared to the same unfilled piece of Vycor (Fig. 8.6), peaks are distinctive and more narrow also at lower temperatures. Peaks change position and broaden up around  $T = 245$  K, sharpening again and moving further to lower frequencies. At RT peaks are very broad again. The analysis as

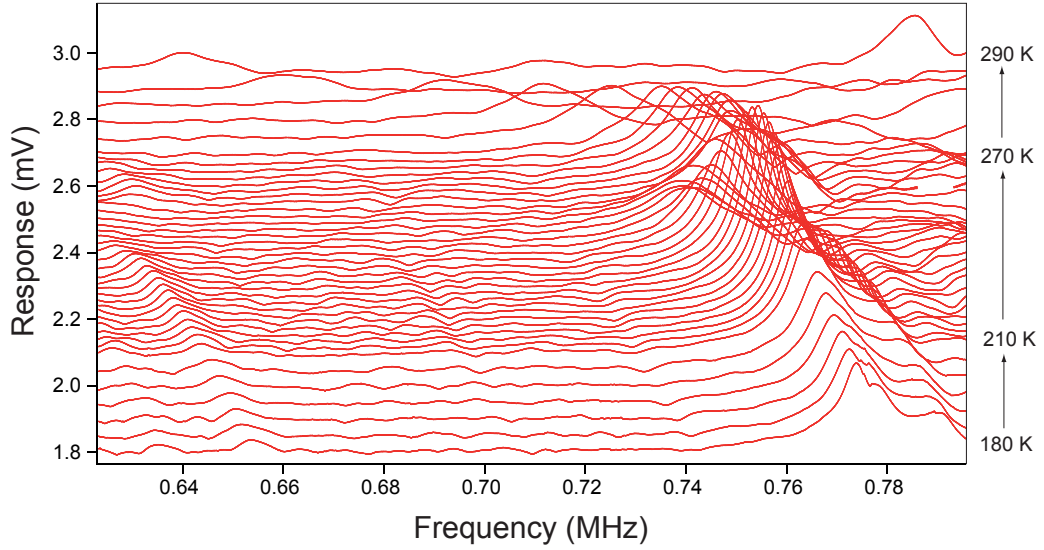


**Fig. 8.8:** Vycor filled with salol: development of an exemplary resonance peak upon heating. All signals are offset by  $0.01 \cdot T$ .

described above yields Young's modulus  $Y$  and  $Q$  as a function of temperature as shown in Fig. 8.9 again in comparison to DMA data.

Using the resonance peak displayed in Fig. 8.8 the lines in Figs. 8.9a and b are achieved, whereas the dotted line arises from tracing a different resonance peak at 1.0 MHz. The gray line represents results from the clean Vycor sample (Figs. 8.6 and 8.7). Both the DMA and the RUS method yield the same decrease in  $Y$  upon heating within the chosen temperature range (Fig. 8.9a and c) which is  $\Delta Y \approx 10$  GPa. RUS data show a decrease of  $Y$  being intercepted by an anomaly at 247 K and a continuing decrease with rising temperature and no constant value of lower  $Y_0$  at RT has been found. DMA data in Fig. 8.9c shows a two-level step in  $Y$  from a low temperature upper level before the transition to a high temperature lower level  $Y_0$  afterwards.

$(1/Q)$  and  $\tan \delta$  vary in nearly equivalent ranges from 0 to 0.04 (see Fig. 8.9b and d). But whereas DMA data at 20 Hz (d) showed a single peak  $\approx 220$  K and a distinctive shoulder at  $\approx 245$  K. RUS results are rather different. Both analyzed resonances show a clear attenuation maximum around 245 K, one even displays a second peak about 5 K higher (Fig. 8.9b). Approaching RT both  $(1/Q)$  lines show a second peak around 270 K and 290 K respectively.

A prediction of the attenuation peak position in the MHz region based on our model successfully used in the 1 - 100 Hz region can be tried. As done in Ref. [38] for Vycor, we use Eqns. (5.5)

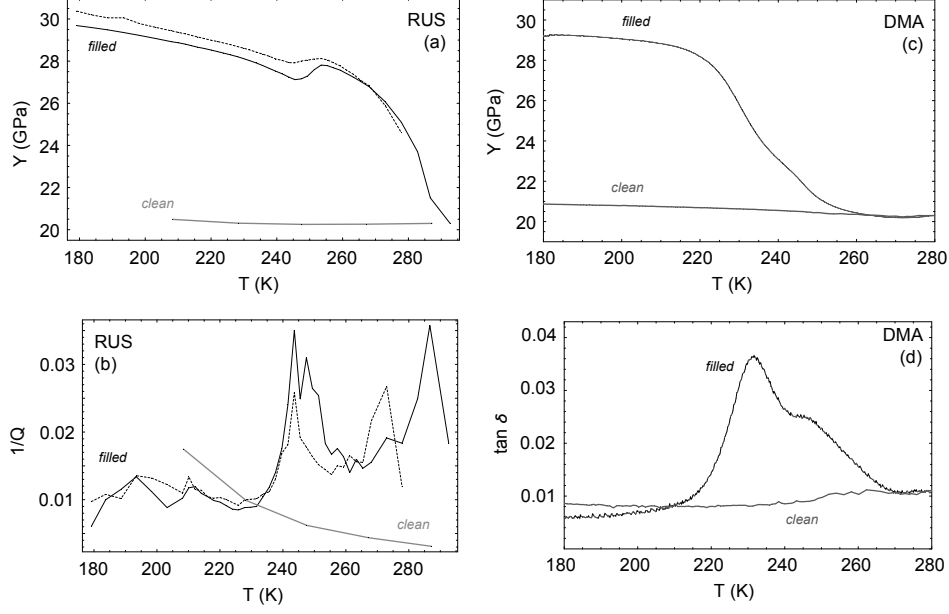


**Fig. 8.9:** Vycor filled with salol: RUS results of filled and clean sample (line derived from a peak at 0.75 MHz shown in Fig. 8.8, dotted line from a peak at 1.0 MHz) in comparison to an exemplary DMA measurement at 20 Hz.

with parameters of Tab. 5.2, and set  $\nu = 10^6$  Hz. The corresponding Young's modulus is shown in Fig. 8.10a and the peaks in  $\tan \delta$  corresponding to molecules in the pore center (core) and molecules interacting with the untreated rough pore wall (shell) are displayed in Fig. 8.10b. The core and shell contributions at  $\nu = 1$  MHz add up to one broad peak around 320 K. This is far above the peaks observed in Fig. 8.9b and leads to the assumption that a Cole-Davidson approach may no longer hold at high frequencies. However, further work has to be done to clarify the nature of these peaks.

For a meaningful and correct RUS analysis narrow peaks are needed. Ref. [152] states  $Q > 100$  to gain satisfying fits, corresponding to  $1/Q < 0.01$ . A look at Fig. 8.9b shows that in our case this is only true below 230 K. In rather soft porous glass matrices it is possible to determine elastic moduli with great accuracy (Sec. 8.2). But as a filling liquid comes into play, attenuation rises and resonance peaks get broad, and especially at higher temperature often cannot be localized and fitted any more. That's also why just a rough position of a  $(1/Q)$ -peak can be found, but no details as peak broadness or a shoulder (d).

Analog measurement runs have been performed on both Gelsil 5.0 and Gelsil 2.6 samples. Both samples broke during the cooling sections, and the spectra collected before showed noisy

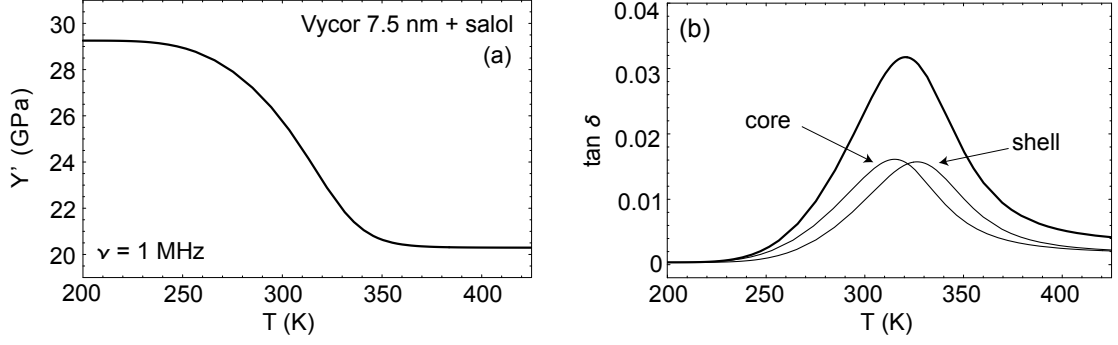


**Fig. 8.10:** Plot of Eqns. (5.5) with parameters of Tab. 5.2 at an exemplary frequency of  $\nu = 10^6$  Hz.

and broad peaks which could not be fitted. Liquid in pores is known to increase ultrasonic attenuation [158], which in Gelsil samples was too large to gain any meaningful information. For this reason all further analysis of the glass transition in confinement was continued using the DMA technique.

The collapse of Gelsil structures cannot be explained by mechanical stress since the RUS technique applies very small strain of  $\approx 10^{-7}$  whereas in 3PB dynamic elastic experiments strain is  $\approx 10^{-3}$  (see Fig. 7.2). Probably water in pores crystallizing at LT could be the reason for the observed destruction.





## Chapter 9

# Conclusions

### 9.1 Spatial Confinement and the Glass Transition

The glass transition of salol confined to porous host matrices of Vycor and Gelsil with pore sizes of 7.5, 5.0 and 2.6 nm has been measured for the first time by Dynamic Mechanical Analyzers (DMA 7 and Diamond DMA, Perkin Elmer). The complex dynamic elastic susceptibility data can be well fitted assuming two types of dynamic processes: A "bulk" relaxation in the core of the pores and a radially increasing "surface relaxation" of molecules near the pore surface. The calculated core relaxation time shows a typical Vogel-Fulcher temperature dependence and decreases with decreasing pore size  $d$ . This confinement induced acceleration of dynamics leads to a shift of the glass transition temperature  $T_g \propto 1/d$ , which is in perfect agreement with recent DSC results [32].

Measurements of the sample height with filling (adsorption swelling) and thermal expansion were used to calculate the magnitude of "negative pressure" which occurs at cooling due to thermal mismatch between the porous host matrix and the glass forming liquid. Such negative pressure could at least partly explain a shift of  $T_g$  in confined glass forming liquids [52, 39]. Some authors attribute even the whole downshift of  $T_g$  to the effect of negative pressure [32]. The present data show that for salol this effect of thermal mismatch can describe at most 30% of the observed downshift of  $T_g$ , which is in harmony with enthalpy recovery experiments [39].

In order to get rid of surface interactions slowing down the molecular motions, extensive dynamic mechanical measurements have also been performed on silanated samples. It turns out that silanation is able to reduce the liquid-surface interactions drastically. Simultaneously it turned out that the negative pressure contribution to the downshift of the glass transition temperature  $T_g$  remains the same as in uncoated pores. As a result the observed stronger (as compared to uncoated pores) downshift of  $T_g$  with decreasing pore size can be fully attributed

to the confinement induced acceleration of the dynamics, which occurs due to the hindering of cooperativity. In Ref. [129] it is shown that finite size effects are expected to set in when the pore size  $d \approx 7 r_0 - 10 r_0$  yielding 4.8 – 8 nm for salol with  $r_0 \approx 0.8$  nm. This is in excellent agreement with our observations.

Hunt et al. [129] calculated the finite size effect of the glass transition from percolation and effective medium models yielding

$$T_g(d) = T_g(\text{bulk}) - \frac{0.5 \cdot E}{\ln(t \cdot \nu_{ph})} \cdot \frac{r_0}{L} . \quad (9.1)$$

Inserting for the time scale of the "laboratory glass transition"  $t = 100$  s,  $\nu_{ph} = 1/\tau_0$ , and our fit parameters from Tab. 5.2, and assuming that the typical distance between molecules  $r_0$  is about the diameter of a salol molecule [120] ( $\approx 0.8$  nm), we obtain  $\Delta T_g^{Hunt}$  as 3.2, 4.8 and 9.1 K for 7.5, 5.0 and 2.6 nm pores, respectively. These calculated values agree surprisingly well with the measured confinement induced downshifts of  $T_g(d)$  (see Fig. 5.11 and  $\Delta T_g^{exp}$  in Tab. 5.4).

Moreover Eqn. (9.1) predicts [129] that the size dependence of  $\Delta T_g$  increases with increasing fragility [130]

$$m = \frac{E \cdot T_g}{\ln(10) (T_g - T_0)^2} , \quad (9.2)$$

since  $m \propto E$ . Indeed, this correlation between  $\Delta T_g(d) \sim m$  was verified experimentally for many systems, i.e. for glycerol [126] ( $m = 53$ )  $\Delta T_g(d = 2.5 \text{ nm}) \approx -4$  K, benzyl-alcohol [26] ( $m = 65$ )  $\Delta T_g(d = 2.5 \text{ nm}) \approx -9$  K, salol [32] ( $m = 73$ )  $\Delta T_g(d = 2.5 \text{ nm}) \approx -11$  K, o-terphenyl [32] ( $m = 81$ )  $\Delta T_g(d = 2.5 \text{ nm}) \approx -25$  K.

We think that these considerations, i.e. the good agreement to the downshift of  $T_g$  calculated via percolation theory with our experimental findings, as well as the clear correlation between the magnitude of the induced  $T_g$  shift and the fragility of a glass forming liquid, both confirm our other findings (see Fig. 5.11) that the main effect of the confinement on a glass forming liquid is to suppress cooperative motion. Negative pressure effects although always present contribute only little.

After we had revealed the pure confinement effect on the dynamics we analyzed the data in terms of a newly proposed theory [12] which relates the number of dynamically correlated molecules  $N_{corr,T}$  to the temperature derivative of a dynamical two-point correlation function, which in our case can be identified with the dynamic elastic susceptibility  $Y(\omega, T)$ . The results

clearly show an increase of  $N_{corr,T}$  with decreasing temperature approaching  $T_g$ .

In spite of the fact that the precise relation between  $N_{corr,T}$  and a corresponding length scale is hampered due to unknown prefactors and exponents [18], this implies that the size  $\xi$  of dynamically correlated regions increases when approaching  $T_g$ . This result clearly represents a highlight in the present research, since for the first time a dynamic correlation length is determined for dynamic elastic susceptibility data. Moreover it is also for the first time, that the temperature dependence of a dynamic correlation time is measured for a glass transition in confinement.

For smaller pore sizes  $\xi(T', d)$  at a given temperature  $T'$  shifts to smaller values which is concomitant to the systematic decrease of the relaxation time  $\tau(T', d)$  and the resulting downshift of  $T_g(d)$ . However at the glass transition temperature the dynamic correlation length is almost independent of the pore size with  $\xi(T_g, d) = 3.2$  nm, a value which was also found by calorimetric [92] and dielectric [139] measurements.

Very similar as very recently observed [18], we found a modest growth of  $N_{corr,T}$  from about 2 at  $T = 270$  K to 8 at  $T_g$ , whereas the relaxation time  $\tau$  increases dramatically by about 12 orders of magnitude in this temperature interval (see inset of Fig. 6.9). This characteristic behavior was observed for all measured pore sizes. It is very different from an ordinary structural phase transition, where the increase of the relaxation time and the correlation length occur simultaneously when approaching  $T_c$ .

Unfortunately at present there is no unique theory that relates the relevant parameters controlling the confinement effects in glass-forming materials to experimental data. The reason for this is that the microscopic mechanism behind the glass transition is still not completely understood and more theoretical (e.g. of the type presented in Ref. [140]) and experimental work is required to close the gap of knowledge and understand confinement effects in glass-forming liquids.

Summarizing, the present thesis demonstrates that Dynamic Mechanical Analysis provides a very sensitive method and is a very powerful tool to test the dynamic behaviour of glass-forming liquids in confined systems. The present approach models heterogeneous molecular relaxation dynamics within nanoscopic pores and allows to separate side effects as surface interaction and negative pressure from the pure confinement effect. Moreover, the number and size of dynamically correlated molecules can be quantitatively determined down to the glass transition temperature.

In this respect the method is even superior to e.g. NMR-methods [9, 10, 11] where the

dynamic heterogeneities can only be followed to temperatures about 10 K above  $T_g$ .

Since answering one question in science usually opens up a few other ones and the time for preparing a thesis is restricted, the following problems had to be left open:

- Different ways of sample filling: While filling pore space with liquid salol via capillary wetting was successful, different liquids (toluene, oTP) with different surface tension, and also due to their volatile nature, narrow the efficiency of this method. Filling from the vapor phase as done during silanation could be much more efficient.
- Silanation of inner pore walls in the frame of this work has not been rechecked. Especially for Vycor the silan layer does not seem as stable as in Gelsil. This could be tested e.g. via infrared spectroscopy.
- Silanation and oTP: Silanated samples should be filled with oTP and tested i.o. to find out the effect of surface interaction on  $T_g$ . The determination of negative pressure could be difficult due to the extended filling times (see first point).
- After gathering more experimental data on oTP and toluene, an explanation for Fig. 7.6 should be found, i.e. the reason why salol shows crucially different spatial behaviour of the relaxation dynamics in pores of 7.5 nm and 5.0 nm size as compared to toluene and oTP should be investigated.
- Concerning toluene in confinement, the efforts described herein should be extended to Gelsil 5 nm. A way has to be found to cool down the sample below the limit set by the original Diamond DMA cooling setup. A cryostat once built for the DMA 7 could be applied. Additionally, a way should be found to avoid the fast evaporation of toluene out of pores within the sample chamber.
- Different host matrices should be used. The random structure of both Vycor and Gelsil samples makes it difficult to think about a realistic pore geometry. For Vycor samples a cylindrical pore shape seems reasonable, but of course pores are interconnected and molecules may interact amongst each other in different pores. Gelsil samples, consisting of randomly placed, roughly identical spheres touching and penetrating each other, shows a much larger pore size distribution since pores are empty spaces between spheres, strongly interconnected in a more fractal manner. These pore-pore interactions cannot be treated straightforward, but could be avoided by the use of other mesoporous host matrices like electrochemically etched silicon wafers, showing tubular pores arranged parallel [159].

## 9.2 Resonant ultrasonic spectroscopy

The initial aim of testing the glass transition and covering a wider frequency range could not be achieved since the confinement material seems too soft and  $Q < 100$  for filled samples.  $(1/Q)$  variations were found not corresponding to the data on  $\tan \delta$  achieved via DMA. The poor resolution of attenuation data did not allow further investigation. In addition, the highly porous and brittle Gelsil samples collapsed when filled and cooled. Due to the intense effort and compared to the poor results, further investigations in this direction had to be abandoned.

Temperature scans of clean Vycor down to 180 K showed a slight increase of bulk modulus corresponding to DMA results and close to literature values. A strong increase of  $(1/Q)$  found by RUS is explained by literature as an onset of capillary moisture freezing within the pore system. A corresponding increase of  $\tan \delta$  in DMA could not be detected.

On the other hand RT tests were very successful and found their way into 2 reviewed articles: It turned out that especially for Gelsil samples no elastic moduli data were available in literature before. The moduli were determined with high accuracy and used to calibrate DMA results obtaining absolute values [38, 40]. They also were used to investigate the role of critical porosity and the stability of dry, porous minerals and sustained a selfconsistent effective medium theory (see Ref. [156]). Nevertheless the following points remain open:

- A considerable growth of sound attenuation in clean mesoporous silica samples upon cooling was found via RUS. A possible explanation is the onset of freezing of capillary water adsorbed from air moisture. However, up to now this could not be verified by DMA experiments. Test of as-prepared, clean samples (only exposed to dry  $N_2$  after the heat treatment in high vacuum) versus samples exposed to air could be done.
- Influence of inner pore coating on elastic moduli of mesoporous materials: To our best knowledge there is no theory explaining the enhancement of shear modulus due to silanation (see Tab. 2.1). A possible explanation based on the assumption of formation of additional nodes within a network of contact points, first of all having an impact on the shear modulus [142]. Besides RUS, the use of the recently installed Bohlin rheometer would be advisable to determine variations of  $G$ .
- Nonlinear elasticity of porous silica: An explanation for the enhanced nonlinear stress-strain-behavior of porous silica vs. the bulk material as seen in Fig. 7.2 and Tab. 7.2 is missing. A possible reason is the deformation (bending, shear, compression,...) of walls between pores, leading to less macroscopic strain upon increasing stress [142]. Again, the use of a rheometer i.o. to test the stress-strain relation upon torsion is recommended.



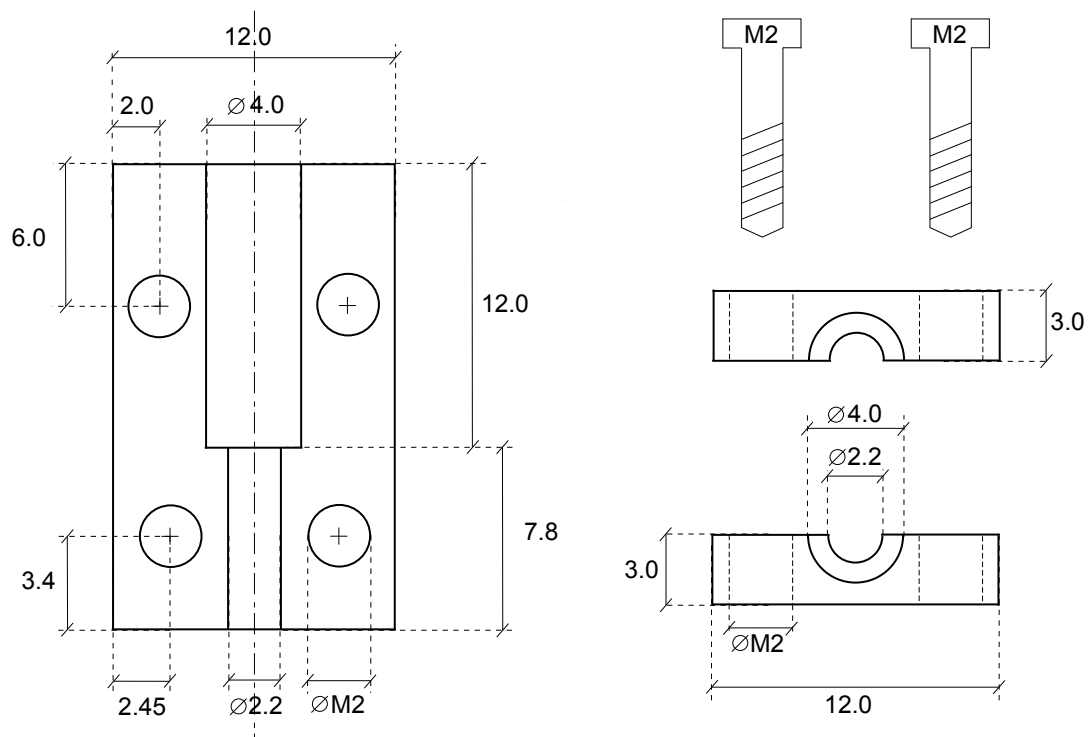
## Chapter 10

# Workshop drawings

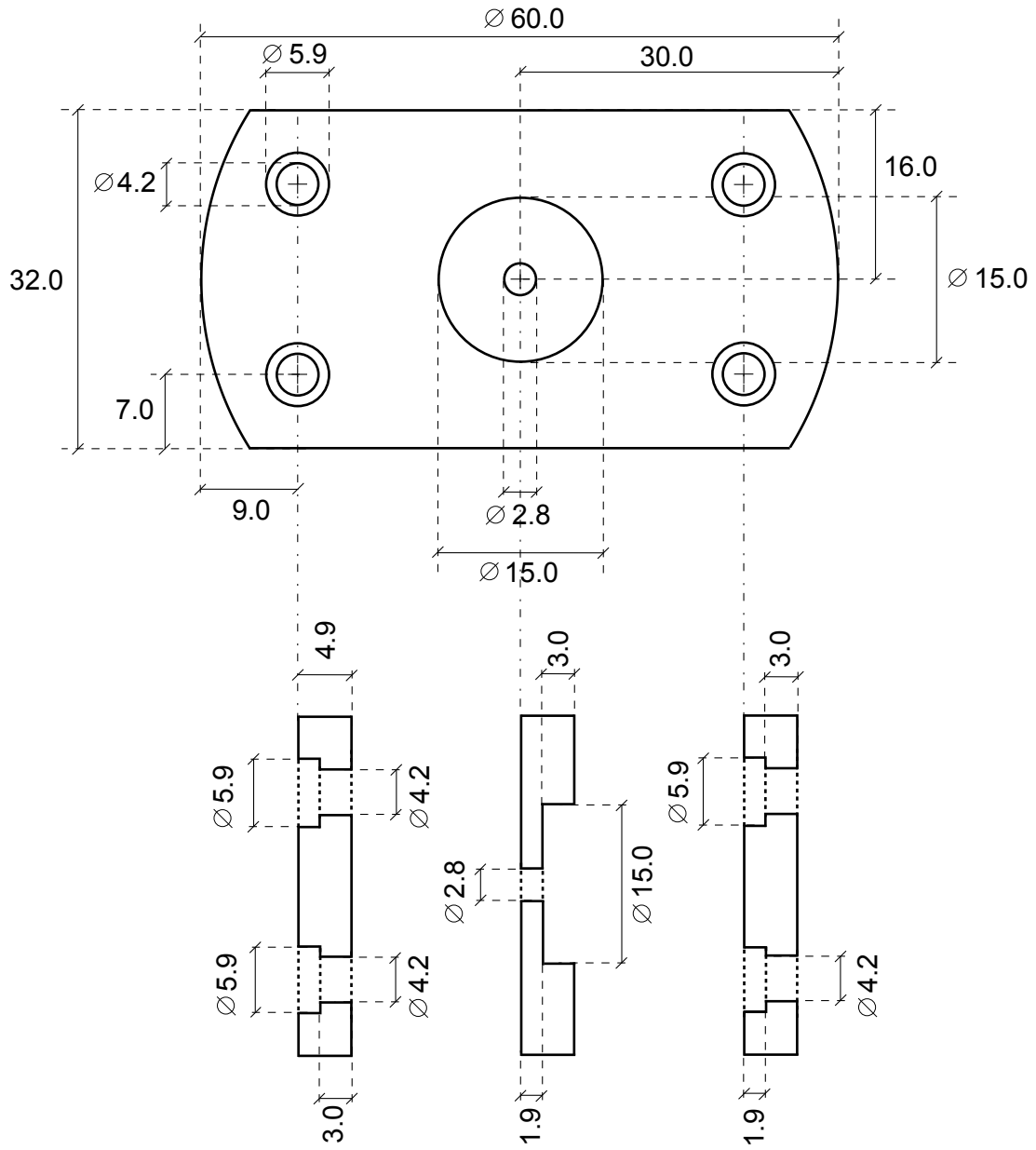
Section drawings of Diamond DMA extension for DMA 7 attachments

- parts designed by J. Koppensteiner
- parts built by the machine shop of the Faculty of Physics

(a) rod attachment (stainless steel)



(b) bottom support plate (stainless steel)





# Chapter 11

## List of Figures and Tables

### 11.1 List of Figures

2.1	schematic pore model of Vycor 7930 showing interconnected pores and pockets	9
2.2	Scheme of Gelsil structure: randomly placed spheres of $r = 4$ in a (100 x 100) square, $\Phi=0.25$ . . . . .	10
2.3	Picture of Gelsil 2.6 nm rods as produced by 4F International. The change in color indicates small amounts of contamination, mostly organic molecules adsorbed by the pores along with air moisture. After cleaning samples appear clear and transparent. . . . .	10
2.4	holders, clamps and sand paper used for sample preparation . . . . .	12
2.5	Adsorption/Desorption isotherms of porous silica measured by Marie-Alexandra Neouze and coworkers at the Institute of Materials Chemistry at the Vienna University of Technology. . . . .	13
2.6	Pore size distribution of untreated and silanated samples obtained by BJH/BET analysis of the individual desorption isotherms. Red lines show data of silanated samples (see Sec. 2.4). . . . .	14
2.7	Hexamethyldisilazane molecule replacing $\text{OH}^-$ on a silica surface. . . . .	16
2.8	Sketch of silanation process: Placed on a metal grid the cleaned samples are exposed to HMDS vapor in a closed glass vessel. . . . .	16
2.9	Sketch of adsorption swelling measurements. Crystalline salol is placed next to the samples bottom and the quartz rod is placed on top of the sample with $F = 0$ N. As temperature is raised to $T_m = 317$ K of salol, the sample adsorbs the melted liquid. . . . .	18

3.1	Sketch of a DMA analyzer (a) and measurement geometries parallel plate (b) and three point bending (c). . . . .	20
3.2	Position signal of the DMA7's rod placed on a cylindrical piece of indium upon heating. Inset shows the first derivative w. r. to temperature and melting at $T = 430.0$ K. . . . .	23
3.3	Photos of Perkin Elmer DMA 7 and Diamond DMA. . . . .	27
3.4	Diamond DMA calibration: a standard PMMA sample measured in bending and tension geometry at 1 Hz. . . . .	28
3.5	PP test of indium at 1 Hz showing a narrow $\tan \delta$ peak at 429.0 K. . . . .	29
3.6	Elastic measurement range of a Diamond DMA dependent on the sample's geometry factor $\alpha$ . Zone A and B denote a probable loss of accuracy at high frequency [83]. . . . .	31
3.7	Photo of Diamond DMA measurement cell designed for 3PB tests of small samples. A workshop drawing also is shown in chapter 10. The picture also shows the lowered furnace with the $N_2$ supply (black, in front). . . . .	33
4.1	Scheme of the pore structure of Vycor glass. On the right hand side the increase the relaxation time of confined salol molecules approaching the rough walls according to simulations of Ref. [37] is sketched. . . . .	39
4.2	Sample heights $h(T)$ measured for pure Vycor and Vycor filled with salol, normalized at 300 K. . . . .	40
4.3	Real (a) and imaginary (b) parts of the complex Young's modulus of salol confined to Vycor glass ( $d = 7$ nm) measured in parallel plate geometry. The curves are offset from the 1 Hz data for sake of clarity. The inset shows typical results from three point bending measurements. . . . .	43
4.4	Fit of the dynamic ( $f=1.6$ Hz) elastic response of salol confined to 7 nm pores with the inhomogeneous model – Eqn. (4.7) – described in the text. The inset shows calculations with different pore sizes. . . . .	45
5.1	Sketch of (a) parallel plate and (b) three point bending geometry. . . . .	52
5.2	Real (a) and imaginary parts (b) of the complex Young's modulus of Vycor 7.5 nm filled with salol (filling fraction $f \approx 0.79$ ) measured in three point bending geometry. The curves are offset from the 1 Hz data for sake of clarity. . . . .	54
5.3	Real (a) and imaginary (b) parts of the complex Young's modulus of Gelsil 5.0 nm filled with salol (filling fraction $f \approx 0.75$ ) measured in parallel plate geometry (Diamond DMA). 1Hz signal are original data, other signals are offset for sake of clarity. . . . .	55

5.4	Real (a) and imaginary (b) parts of the complex Young's modulus of Gelsil 2.6 nm filled with salol (filling fraction $f \approx 0.65$ ) measured in three point bending geometry (Diamond DMA). 1 Hz signal are original data, other signals are offset for sake of clarity. . . . .	56
5.5	Real (a) and imaginary (b) part of the complex Young's modulus of salol in Vycor or Gelsil for different pore sizes, all measured at 20 Hz. . . . .	57
5.6	Real part $Y'$ and imaginary part $Y''$ of different porous samples filled with salol. Lines are fits using Eqns. (8.5a,b) with parameters of Tab. 5.2. . . . .	59
5.7	Modeled relaxation time distributions in pores of diameter 7.5 nm to 2.6 nm from Eqn. (5.3) used in Eqns. (8.5a,b) for fits of Fig. 5.6. . . . .	60
5.8	Relaxation time in pore centers calculated from Eqns. (5.1) and (5.3) with corresponding parameters from Tab. 5.2. Horizontal line shows $\tau = 100$ s. . . .	61
5.9	Height of Vycor sample during the filling process against $\sqrt{t}$ . Inset shows sample height against time. . . . .	62
5.10	Linear thermal expansion of empty and salol filled samples with pore diameters of (a) 7.5 nm, (b) 5.0 nm and (c) 2.6 nm. . . . .	64
5.11	Shift of glass transition temperature against (pore diameter) $^{-1}$ . Boxes are $T_g$ s from Fig. 5.8, triangles show literature values from Ref. [32], open circles display the maximum negative pressure contribution (see section 5.4). . . . .	66
6.1	Real (a) and imaginary (b) parts of the complex Young's modulus of silanated Gelsil (4.8 nm) filled with salol (filling fraction $f = 0.87$ ) measured in three point bending geometry (Diamond DMA). 1Hz signal are original data, other signals are offset for sake of clarity since there is no frequency dependence of low and high temperature values aside the glass transition. . . . .	76
6.2	Comparison of DMA data: black lines represent untreated samples, green lines are new data for silanated pore surface. Since contact losses inhibit direct comparison, $Y'$ and $Y''$ signals of silanated samples were scaled i.o. to match $Y''$ peak heights. . . . .	77
6.3	Real part $Y'$ and imaginary part $Y''$ of different porous samples filled with salol, calibrated using RUS results at room temperature. Lines are fits using Eqns. (9.3a,b) and (6.1) with parameters of Tab. 6.2. . . . .	77
6.4	Modeled relaxation time in untreated and silanated pores of Gelsil 5 from Eqn. (6.1) used in Ref. [38] and in Eqns. (9.3a,b) for fits of data in Fig. 6.3b and e herein, at $T = 220$ K. . . . .	78

6.5	Relaxation time in pore centers calculated from Eqn. (6.1) with corresponding parameters from Tab. 6.2. Horizontal line shows $\tau = 100$ s. Gray lines are relaxation times in untreated pores from Ref. [38]. . . . .	78
6.6	Shift of glass transition temperature against inverse pore diameter. Open circles display the maximum negative pressure contribution (see Sec. III. C. of Ref. [38]), boxes are $\Delta T_g$ 's Ref. [38], filled triangles show literature values from Ref. [32]. Open triangles are the present results, and crosses mark corresponding literature data from Ref. [73]. . . . .	79
6.7	Linear thermal expansion of untreated (black) and silanated (red) Gelsil 5.0 nm, both empty and filled. Sample height is normalized at 280 K. . . . .	81
6.8	Shift of glass transition temperature $T_g$ and Vogel-Fulcher temperature $T_0$ against pore diameter $d$ . The points are determined from fitting the experimental data with Eqns. (9.3a,b) and (6.1), where $T_g(d)$ is obtained from $\tau(T, d) = 100$ s, as shown in Fig. 6.5. The lines are fits using Eqn. (6.6) yielding $c = 0.13$ and $T_g^{bulk} = 216$ K. For calculating $T_0(d)$ the relation $T_g - T_0 = \frac{E}{\ln(100/\tau_0)} = 50.6$ K was used, as indicated in the text. . . . .	82
6.9	Temperature dependence of $N_{corr,T}$ for various pore sizes. Lines are calculated from Eqn. (6.8) using the procedure described in the text. Symbols are calculated from DMA data using Eqn. (6.7). Inset shows $N_{corr,T}$ against relaxation time $\tau/\tau_0$ in the corresponding temperature range on logarithmic scales. . . . .	84
7.1	Modeling of strain in a 3PB experiment. Straight undeformed bar (a) and bar under stress (b). . . . .	88
7.2	Modeled strain due to stress of porous silica samples compared to fused silica. Points are calculated from raw data along Eqns. (7.5) and (7.4). Dotted lines are quadratical fits yielding parameters of Tab. 7.2. . . . .	90
7.3	Storage and loss modulus of Vycor (a,b) and Gelsil 2.6 nm (c,d) filled with toluene, both at 5 Hz. Both cooling runs performed at 10 K/min from RT $\rightarrow$ 225 K, and at 2 K/min 225 K $\rightarrow$ 120 K, the DMAs lower limit. Fits use Eqns. (4.7) with parameters of Tab. 7.3. . . . .	92
7.4	Non-monotonic variation of $T_g$ of nanoscopically confined toluene. Boxes stem from Ref. [94], open triangles indicate present data. Dotted line displays $T_g^{bulk} = 117$ K. The line is a guide to the eyes. . . . .	93
7.5	Storage modulus $Y'$ and loss modulus $Y''$ of different porous samples filled with oTP. Shown are original DMA data, red lines are fits using Eqn. (4.7) with parameters of Tab. 7.4. . . . .	95

7.6	Relaxation times $\tau$ of toluene (red), salol (black) and oTP (green) in pores of Vycor 7.5 nm using Eqn. 4.6 and parameters of Tabs. 5.2, 7.3 and 7.4 at the individual glass transition temperatures $T_g$ . . . . .	96
7.7	Glass transition temperatures for oTP against inverse pore diameter. Open diamonds show results of Jackson et al. [26], filled triangles are data by Trofymuk et al. [28], whereas circles represent values of Patkowski et al. [32]. Crosses mark present results. . . . .	97
8.1	Photo of RUS RT unit. Two opposing transducers covered with gold hold an empty Gelsil 2.6 nm sample. The upper transducer is vertically movable. All parts built by M.A. Carpenter and coworkers. . . . .	100
8.2	RUS spectra of a clean Vycor sample at RT mounted in corners-to-corners geometry consecutively along the 4 body diagonals. Data are offset for sake of clarity. Inset displays a closer look at the lower modes. . . . .	102
8.3	RUS spectra showing the lower modes of a clean Gelsil 5.0 nm sample at RT mounted in different geometries. . . . .	103
8.4	RUS spectra showing the lower modes of a clean Gelsil 2.6 nm sample at RT mounted in different geometries. . . . .	104
8.5	Bulk moduli of porous samples measured within this work plus silica aerogel from Ref. [153] as used in Ref. [156]. The line shows a Hashin-Shtrikman upper bound. . . . .	105
8.6	RUS spectra of clean Vycor in the temperature range $170\text{ K} < T < 290\text{ K}$ . Data collected upon cooling are denoted in blue, heating in red. Data are offset by factor $0.01 \cdot T$ . Inset displays the lower modes. . . . .	106
8.7	Clean Vycor: Young's modulus $Y$ and $Q$ of RUS experiments (a and b) at 0.55 MHz in comparison to $Y$ and $\tan \delta$ obtained from DMA analysis (c and d) at 10 Hz. $Y$ of DMA data in (c) was calibrated at RT according to RUS RT results. . . . .	107
8.8	Vycor filled with salol: development of an exemplary resonance peak upon heating. All signals are offset by $0.01 \cdot T$ . . . . .	109
8.9	Vycor filled with salol: RUS results of filled and clean sample (line derived from a peak at 0.75 MHz shown in Fig. 8.8, dotted line from a peak at 1.0 MHz) in comparison to an exemplary DMA measurement at 20 Hz. . . . .	110
8.10	Plot of Eqns. (5.5) with parameters of Tab. 5.2 at an exemplary frequency of $\nu = 10^6\text{ Hz}$ . . . . .	111



## 11.2 List of Tables

2.1	N <sub>2</sub> adsorption characteristics and porosities of untreated and silanated porous silica samples. . . . .	15
5.1	N <sub>2</sub> adsorption characteristics of porous silica samples. . . . .	51
5.2	Fit parameters used in Eqns. (8.5a,b) for fits of Fig. 5.6. . . . .	60
5.3	Variables of Eqn. (5.6). . . . .	63
5.4	Parameters of $\Delta T_g$ estimations, $\Delta T_g^{exp} = \Delta T_g^{np} + \Delta T_g^{conf}$ . . . . .	65
6.1	N <sub>2</sub> adsorption characteristics and elastic moduli of untreated and silanated porous silica samples. . . . .	74
6.2	Fit parameters used in Eqns. (9.3a,b) for fits of Fig. 6.3. . . . .	84
7.1	Comparison of fitted compliances and bulk moduli. . . . .	90
7.2	Parameters of Eqn. (7.6) used for fits of Fig. 7.2. . . . .	90
7.3	Fit parameters of Fig. 7.3 . . . . .	91
7.4	Fit parameters of Fig. 7.5 . . . . .	95
8.1	RUS results of porous silica host matrices . . . . .	104





# Chapter 12

## Literature

- [1] M. Cukiermann, J. W. Lane, and D. R. Uhlmann, J. Chem. Phys. **59**, 3639 (1973).
- [2] M. D. Ediger, C. A. Angell, and S. R. Nagel, J. Phys. Chem. **100**, 13200 (1996).
- [3] G. Adam and J. H. Gibbs, J. Chem. Phys. **43**, 139 (1965).
- [4] J. Jäckle and A. Krönig, J. Phys.:Cond. Matter **6**, 7633 (1994).
- [5] E. Hempel, G. Hempel, A. Hensel, C. Schick, and E. Donth, J. Phys. Chem. B **104**, 2460 (2000).
- [6] T. R. Kirkpatrick and P. G. Wolynes, Phys. Rev. A **35**, 3072 (1987).
- [7] V. Lubchenko and P. G. Wolynes, Phys. Rev. Lett. **87**, 195901 (2001).
- [8] E. Donth, H. Huth, and M. Beiner, J. Phys.: Condens. Mat. **13**, L451 (2001).
- [9] U. Tracht, M. Wilhelm, A. Heuer, H. Feng, K. Schmidt-Rohr and H.W. Spiess, Phys. Rev. Lett. **81**, 2727 (1998).
- [10] S. A. Reinsberg, A. Heuer, B. Doliwa, H. Zimmermann and H.W. Spiess, J. Non-Cryst. Sol. **307-310**, 208 (2002).
- [11] X. H. Qiu and M. D. Edinger, J. Phys. Chem. B **107**, 459 (2003).
- [12] L. Berthier, G. Biroli, J.-P. Bouchard, L. Cipelletti, D. El Masri, D. L'Hôte, F. Ladieu, and M. Pierno, Science **310**, 1797 (2005).
- [13] B. M. Erwin and R. H. Colby, J. Non-Cryst. Sol. **307-310**, 225 (2002).
- [14] C. Donati, J. F. Douglas, W. Kob, S. J. Plimpton, P. M. Poole, and S. C. Glotzer, Phys. Rev. Lett. **80**, 2338 (1998).

- [15] C. Bennemann, C. Donati, J. Baschnagel, and S. C. Glotzer, *Nature* **399**, 246 (1999).
- [16] P. Scheidler, W. Kob, K. Binder, and G. Parisi, *Phil. Mag. B* **82**, 283 (2002).
- [17] G. Biroli, J.-P. Bouchaud, K. Miyazaki, and D. R. Reichmann, *Phys. Rev. Lett.* **97**, 195701 (2006).
- [18] C. Dalle-Ferrier, C. Thibierge, C. Alba-Simionesco, L. Berthier, G. Biroli, J.P. Bouchaud, F. Ladieu, D. L'Hôte, and G. Tarjus, *Phys. Rev. E* **76**, 041510 (2007).
- [19] R. Bergman and J. Swenson, *Nature* **403**, 283 (2000).
- [20] J. C. Dore, M. Dunn, T. Hasebe, J. H. Strange, and M. C. Bellissent-Funel, *Springer Proc. in Physics* **37**, 144 (1989)
- [21] V. P. Soprunyuk, D. Wallacher, P. Huber, K. Knorr, and A. V. Kityk, *Phys. Rev. B* **67**, 144105 (2003).
- [22] P. Huber and K. Knorr, *Mater. Res. Soc. Symp. Proc.* **876E**, R3.1 (2005).
- [23] G. S. Iannacchione, G. P. Crawford, S. Qian, J. W. Doane, and D. Finotello, *Phys. Rev. E* **53**, 2402 (1996).
- [24] A. V. Kityk, T. Hofmann, and K. Knorr, *Phys. Rev. Lett* **100**, 036105 (2008).
- [25] B. Frick, M. Koza, and R. Zorn (Editors), *Eur. Phys. J. , Special Issue: Dynamics in Confinement*, Vol. **12**, 3 (2003).
- [26] C. L. Jackson and G. B. McKenna, *J. Non-Cryst. Sol.* **131-133**, 221 (1991).
- [27] C. L. Jackson and G. B. McKenna, *J. Chem. Phys.* **93**, 9002 (1990).
- [28] O. Trofymuk, A. A. Levchenko, and A. Navrotsky, *J. Chem. Phys.* **123**, 194509 (2005).
- [29] A. Schönhals, H. Göring, C. Schick, B. Frick, and R. Zorn, *Colloid. Polym. Sci.* **282**, 882 (2004).
- [30] R. Kremer, A. Huwe, A. Schönhals, and A. S. Rzanski, *Molecular Dynamics in Confining Space in Broadband Dielectric Spectroscopy*, Edts. F. Kremer and A. Schönhals, Springer Verlag, Berlin (2000) p. 171.
- [31] R. Zorn, L. Hartmann, B. Frick, D. Richter, and F. Kremer, *J. Non-Cryst. Sol.* **307**, 547 (2002).
- [32] A. Patkowski, T. Ruths, and E. W. Fischer, *Phys. Rev. E* **67**, 021501 (2003).

- [33] P. Scheidler, W. Kob, and K. Binder, Europhys. Lett. **52**, 277 (2000).
- [34] H. Sillescu, J. Noncryst. Sol. **243**, 81 (1999).
- [35] E. Donth, *The Glass Transition*, Springer Verlag Heidelberg (2001).
- [36] W. Schranz, M. R. Puica, J. Koppensteiner, H. Kabelka, and A. V. Kityk, Europhys. Lett. **79**, 36003 (2007).
- [37] P. Scheidler, W. Kob, and K. Binder, Europhys. Lett. **59**, 701 (2002).
- [38] J. Koppensteiner, W. Schranz, and M. R. Puica, Phys. Rev. B **78**, 054203 (2008).
- [39] S. L. Simon, J. -Y. Park, and G. B. McKenna, Eur. Phys. J. E **8**, 209 (2002).
- [40] J. Koppensteiner, W. Schranz, and M. A. Carpenter, accepted by Phys. Rev. B, in print (2009).
- [41] W. Schranz, Phase Transitions **64**, 103 (1997).
- [42] W. Schranz and D. Havlik, Phys. Rev. Lett. **73**, 2575 (1994).
- [43] W. Schranz, A. Fuith, P. Dolinar, H. Warhanek, M. Haluska, and H. Kuzmany, Phys. Rev. Lett. **71**, 1561 (1993).
- [44] W. Schranz, A. Tröster, A. V. Kityk, P. Sondergeld, and E. K. H. Salje, Europhys. Lett. **62**, 512 (2003).
- [45] W. Schranz, P. Sondergeld, A. V. Kityk, and E. K. H. Salje, Phys. Rev. B **80**, 094110 (2009).
- [46] M. Y. Lin, B. Abeles, J. S. Huang, H. E. Stasiewski, and Q. Zhang, Phys. Rev. B **46**, 10701 (1992).
- [47] Y. Guo, K. H. Langley, and F. E. Karasz, Phys. Rev. B **50**, 3400 (1994).
- [48] A. Vyalikh, T. Emmler, B. Grünberg, Y. Xu, I. Shenderovich, G. H. Findenegg, H.-H. Limbach, and G. Buntkowsky, Z. Phys. Chem. **221**, 1500 (2007).
- [49] M. Ma, B. I. Halperin, and P. A. Lee, Phys. Rev. B **34**, 3136 (1986).
- [50] D. Wallacher, T. Hofmann, and K. Knorr, and A. V. Kityk, Phys. Rev. B **71**, 224202 (2005).
- [51] H. K. Christenson, J. Phys.: Cond. Mater. **13**, R95 (2001).
- [52] M. Alcoutlabi and G. B. McKenna, J. Phys. : Cond. Matter **17**, R461-R524 (2005).

- [53] M. Adinolfi, G. Barone, L. De Napoli, A. Iadonisi, and G. Piccialli, *Tetrahedron Lett.* **39**, 1953 (1998).
- [54] R. Schnabel and P. Langer, *J. Chromatography A* **544**, 137 (1998).
- [55] J. Y. Park and G. B. McKenna, *Phys. Rev. B* **61**, 6667 (2000).
- [56] A. Vyalikh, Th. Emmler, B. Grünberg, Y. Xu, I. Shenderovich, G. H. Findenegg, H.-H. Limbach, and G. Buntkowsky, *Z. Phys. Chem.* **221**, 105 (2007).
- [57] P. Levitz, G. Ehret, S. K. Sinha, and J. M. Drake, *J. Chem. Phys.* **95**, 6151 (1991).
- [58] G. Dosseh, Y. Xia, and C. Alba-Simionesco, *J. Phys. Chem. B* **107**, 6445 (2003).
- [59] D. Brandhuber, N. Huesing and C. K. Raab, V. Torma, and H. Peterlik, *J. Mater. Chem.* **15**, 1801 (2005).
- [60] S. Hartmann, D. Brandhuber, and N. Hüsing, *Acc. Chem. Res.* **40**, 885 (2007).
- [61] T. H. Elmer, *Engineered Materials Handbook* **4**, 427 (1992).
- [62] N. Eschricht, E. Hoinkis, F. Mädler, and P. Schubert-Bischoff, *Stud. Surf. Sci. Catalysis.* **144**, 355 (2002).
- [63] P. Pissis, A. Kyritsis, D. Daoukaki, G. Barnt, R. Pelster, and G. Nimtz, *J. Phys.: Cond Matt.* **10**, 6205 (1998).
- [64] A. G. Kalampounias and S. N. Yannopoulos, *J. Chem. Phys.* **118**, 8340 (2003).
- [65] W. Zheng and S. L. Simon, *J. Chem. Phys.* **127**, 194501 (2007).
- [66] V. Crupi, D. Majolino, P. Migliardo, and V. Venuti, *J. Mol. Structure* **790**, 135 (2006).
- [67] private communication with Dr. Marie-Alexandra Neouze, Department of Materials Chemistry, University of Technology, Vienna.
- [68] K. S. W. Sing, D. H. Everett, R. A. W. Haul, L. Moscou, R. A. Pieretti, J. Rouquerol, and T. Siemieniewska, *Pure and Appl. Chem.* **57**, 603 (1985).
- [69] M. Thommes, R. Köhn, and M. Fröba, *Appl. Surf. Sci.* **196**, 239 (2002).
- [70] S. Brunauer, P. H. Emmett, and E. Teller, *J. Am. Chem. Soc.* **60**, 309 (1938).
- [71] E. P. Barrett, L. G. Joyner, and P. H. Halenda, *J. Am. Chem. Soc.* **73**, 373 (1951).
- [72] F. Rouguerol, J. Rouguerol, and K. Sing, *Adsorption by Powders and Porous solids: Principles, Methodology and Applications*, Academic Press, NY (1999).

- [73] M. Arndt, R. Stannarius, H. Groothues, E. Hempel, and F. Kremer, Phys. Rev. Lett. **79**, 2077 (1997).
- [74] L. D. Landau and E. M. Lifshitz, *Course of theoretical physics*, Vol. VI., Edt. G. Heber, Akademie-Verlag Berlin (1996).
- [75] R. Lucas, Kolloid Z. **23**, 15 (1918).
- [76] E. W. Washburn, Phys. Rev. **17**, 273 (1921).
- [77] P. Huber, S. Grüner, C. Schäfer, K. Knorr, and A. V. Kityk, Europ. Phys. J. -Special Topics **141**, 101 (2007).
- [78] G. Rogl, L. Zhang, P. Rogl, A. Grytsiv, D. Rajs, H. Müller, E. Bauer, J. Koppensteiner, W. Schranz, and M. Zehetbauer, accepted by J. Appl. Phys. , in print (2009).
- [79] L. Zhang, G. Rogl, A. Grytsiv, S. Puchegger, J. Koppensteiner, H. Kabelka, M. Reinecker, P. Rogl, W. Schranz, M. Zehetbauer, and M. A. Carpenter, submitted to Mater. Sci. Eng. B, in review process (2009).
- [80] E. K. H. Salje, J. Koppensteiner, M. Reinecker, W. Schranz, and A. Planes, Appl. Phys. Lett. **95**, 1 (2009).
- [81] D. Havlik, doctoral thesis, University of Vienna (1999)
- [82] Handbook of Perkin Elmer series 7 DMA, by Perkin Elmer Corp. (1991).
- [83] Handbook of Perkin Elmer Diamond DMA, by SII Nano Technology Inc. (2003).
- [84] K. Wondraczek, J. Adams, and J. Fuhrmann, Macromolec. Chem. Phys. **205**, 1858 (2004).
- [85] J. E. Mark (Edt.), *Polymer Data Handbook*, Oxford University Press, USA (1999).
- [86] G. S. Iannacchione, G. P. Crawford, S. Qian, J. W. Doane, D. Finotello, and S. Zumer, Phys. Rev. E **53**, 2402 (1996).
- [87] C. L. Jackson and G. B. McKenna, Chem. Mater. **8**, 2128 (1996).
- [88] D. Wallacher and K. Knorr, Phys. Rev. B **63**, 104202 (2001).
- [89] D. Wallacher, V. P. Sopronyuk, K. Knorr, and A. V. Kityk, Phys. Rev. B **69**, 134207 (2004).
- [90] B. Frick, H. Büttner and R. Zorn (Editors), J. Phys. IV (Proceedings), **10** Pr7 (2000).

- [91] A. Schönhals, H. Goering, C. H. Schick, B. Frick, and R. Zorn, Eur. Phys. J. E **12**, 173 (2003).
- [92] E. Donth, E. Hempel, and C. Schick, J. Phys.:Cond. Mat. **12**, L281 (2000).
- [93] B. Frick, C. Alba-Simionesco, G. Dosseh, C. Le Quellec, A. J. Moreno, J. Colmenero, A. Schönhals, R. Zorn, K. Chrissopoulou, S. H. Anastasiadis, and K. Dalnoki-Veress, J. Non-Cryst. Solids **351**, 2657 (2005).
- [94] C. Alba-Simionesco, G. Dosseh, E. Dumont, B. Frick, B. Geil, D. Morineau, V. Teboul, and Y. Xia, Eur. Phys. J. E **12**, 19 (2003).
- [95] P. Scheidler, W. Kob, and K. Binder, Eur. Phys. J. E **12**, 5 (2003).
- [96] H. Huth, M. Beiner, and E. Donth, Phys. Rev. B **61**, 15092 (2000).
- [97] A. Faivre, L. David, and J. Perez, J. Phys. II France **7**, 1635 (1997).
- [98] F. Kremer, A. Huwe, A. Schönhals, and A. S. Rózanski, *Molecular Dynamics in Confining Space in Broadband Dielectric Spectroscopy*, edited by F. Kremer and A. Schönhals (Springer Verlag, Berlin) 2000, p.171.
- [99] J. C. Dore, M. Dunn, T. Hasebe, J. H. Strange and M. C. Bellissent-Funel, *Dynamics of Disordered Materials*, Edt. D. Richter, Springer-Verlag, Berlin (1989).
- [100] G. Liu, Y. Li and J. Jonas, J. Chem. Phys. **95**, 6892 (1991).
- [101] C. Alba-Simionesco, B. Coasne, G. Dosseh, G. Dudziak, K. E. Gubbins, R. Radhakrishnan, and M. Sliwiska-Bartkowiak, J. Phys. : Cond. Matter **18**, R15-R68 (2006).
- [102] T. Scopigno, G. Ruocco, F. Sette, and G. Monaco, Science **302**, 849 (2003).
- [103] H. Wagner and R. Richert J. Chem. Phys. **110**, 11660 (1999).
- [104] H. Kamioka, Jpn. J. Appl. Phys. **32**, 2216 (1993).
- [105] K. Niss, B. Jakobsen, and N.B. Olsen, J. Chem. Phys. **123**, 234510 (2005).
- [106] P. A. O'Connell and G. B. McKenna, J. Chem. Phys. **110**, 11054 (1999).
- [107] M. Tabellout, P.Y. Baillif, H. Randriananantoandro, F. Litzinger, J. R. Emery, T. Nicolai, and D. Durand, Phys. Rev. B **51**, 12295 (1995).
- [108] O. Ishai and L.J. Cohen, Int. J. Mech. Sci. **9**, 539 (1967).
- [109] E. M. Schulson, JOM **51**, 21 (1999).

- [110] E. J. Sellevold and F. Radjy, J. Mat. Sci. **11**, 1976 (1972).
- [111] M. Arndt, R. Stannarius, W. Gorbatschow, and F. Kremer, Phys. Rev. E **54**, 5377 (1996).
- [112] K. P. Dixon, Phys. Rev. B **42**, 8179 (1990).
- [113] W. Kauzmann, Chem. Rev. **9**, 219 (1948).
- [114] K. Kim and R. Yamamoto, Phys. Rev. E **61**, R41 (2000).
- [115] S. Karmakar, C. Dasgupta, and S. Sastry, arXiv:0805.3104v1 (2008).
- [116] K. P. Menard, Encyclopedia of Chemical Processing, 799 (2006).
- [117] W. Gorbatschow, M. Arndt, R. Stannarius, and F. Kremer, Europhys. Lett. **35**, 719 (1996).
- [118] D. A. Sappelt and J. Jäckle, J. Phys. A: Math. Gen. **26**, 7325 (1993).
- [119] F. Kremer and R. Stannarius, Lect. Notes Phys. **634**, 275 (2004).
- [120] E. Eckstein, J. Qian, R. Hentschke, T. Thurn-Albrecht, W. Steffen, and E. W. Fischer, J. Chem. Phys. **113**, 4751 (2000).
- [121] R. Richert, C. A. Angell, J. Chem. Phys. **108**, 9016 (1998).
- [122] G. Diezemann and K. Nelson, J. Phys. Chem. B **103**, 4089 (1999).
- [123] D. I. Dimitrov, A. Milchev, and K. Binder, Phys. Rev. Lett. **99**, 054501 (2007).
- [124] F. T. Meethan, Roy. Soc. Proc. A **15**, 223 (1927).
- [125] D. P. Bentz, E. J. Garboczi, and D. A. Quenard, Modell. Simul. Mater. Sci. Eng. **6**, 211 (1998).
- [126] J. Zhang, G. Liu, and J. Jonas, J. Phys. Chem. **96**, 3478 (1992).
- [127] R. Casalini, M. Paluch, and C. M. Roland, J. Phys. Chem. A **107**, 2369 (2003).
- [128] D. Morineau, Y. D. Xia, and C. Alba-Simionesco, J. Chem. Phys. **117**, 8966 (2002).
- [129] A. Hunt, Sol. Stat. Comm. **90**(8), 527 (1994).
- [130] R. Boehmer, K. L. Ngai, C. A. Angell, and D. J. Plazek, J. Chem. Phys. **99**, 4201 (1993).
- [131] M. Arndt, R. Stannarius, W. Gorbatschow, and F. Kremer, Phys. Rev. E **54**, 5377 (1996).

- [132] F. Rittig, A. Huwe, G. Fleischer, J. Kärger, and F. Kremer, *Phys. Chem. Chem. Phys.* **1**, 519 (1999).
- [133] J.-L. R. Nogues and W. Moreshead, *J. Non-Cryst. Sol.* **121**, 136 (1990).
- [134] A. Migliori and J. D. Maynard, *Rev. Sci. Instrum.* **76**, 1 (2005).
- [135] G. Dosseh, C. Le Quellec, N. Brodie-Lindner, C. Alba-Simionesco, W. Haeussler, and P. Levitz, *J. Non.-Cryst. Sol.* **352**, 4964 (2006).
- [136] F. Varnik, J. Baschnagel, and K. Binder, *Eur. Phys. J. E* **8**, 175 (2002).
- [137] S. Capaccioli, G. Ruocco, and F. Zamponi, *J. Phys. Chem. B* **112**, 10652 (2008).
- [138] G. Biroli and J. P. Bouchaud, *Europhys. Lett.* **67**, 21 (2004).
- [139] F. Strichel, doctoral thesis, Mainz University, Germany (1995).
- [140] V. Krakoviack, *Phys. Rev. Lett.* **94**, 065703 (2005).
- [141] D. Gross, W. Hager, J. Schröder, and W. A. Wall, *Technische Mechanik, Teil II: Elastostatik*, Springer Verlag, Berlin (2007).
- [142] private communication with Prof. E. K. H. Salje.
- [143] C. L. Quellec, G. Dosseh, F. Audonnet, N. Brodie-Linder, C. Alba-Simionesco, W. Häussler, and B. Frick, *Eur. Phys. J. Special Topics* **141**, 11 (2007).
- [144] Q. Qin and G. B. McKenna, *J. Noncryst. Sol.* **352**, 2977 (2006).
- [145] A. Tölle, *Rep. Prog. Phys.* **64**, 1473 (2001).
- [146] A. Barbieri, G. Giorini, and D. Leporini, *Phys. Rev. E* **69**, 061509 (2004).
- [147] G. Baranovic, L. Bistric, V. Volovs, and D. Kirin, *Mol. Phys.* **99**, 33 (2001).
- [148] E. K. H. Salje, J. Koppensteiner, W. Schranz, and E. Fritsch, work in progress (2009).
- [149] R. G. Leisure and F. A. Willis, *J. Phys. : Condens. Matter* **9**, 6001 (1997).
- [150] A. Migliori and J. L. Sarrao, *Resonant Ultrasound Spectroscopy*, John Wiley and Sons Inc., New York, USA (1997).
- [151] A. W. Leissa, *J. Sound Vibr.* **287**, 961 (2005).
- [152] A. Migliori and J. D. Maynard, *Rev. Sci. Instrum.* **76**, 121301 (2005).



- [153] S. Puchegger, D. Brandhuber, N. Hüsing and H. Peterlik, J. Noncryst. Solids **352**, 5251 (2006).
- [154] S.K. Watson and R.O. Pohl, Phys. Rev. B **68**, 104203 (2003).
- [155] H. Zhang, R. S. Sorbello, C. Hucho, J. Herro, J. R. Feller, D. E. Beck, M. Levy, D. Isaak, J. D. Carnes, and O. Anderson, J. Acoust. Soc. Am. **1030**, 2385 (1998).
- [156] E. K. H. Salje, J. Koppensteiner, W. Schranz and E. Fritsch, work in progress (2009).
- [157] E. J. Sellevold and F. Radjy, J. Mat. Sci. **10**, 1927 (1976).
- [158] W. F. Murphy, J. Acoustic Soc. Am. **71**, 1458 (1982).
- [159] P. Kumar and P. Huber, J. Nanomat. **2007**, 89718 (2007).



# Ad Persona

## 10.1 Curriculum Vitae

### PARTICULARS

---

name:	Mag. Johannes Koppensteiner
born:	19 <sup>th</sup> of June 1980 in Krems, Austria
parents:	Hubert and Renate Koppensteiner
domiciled:	Scheibenhof 8, 3500 Krems
marital status:	unwedded
military service:	Oct. 1998 - May 1999

### EDUCATION

---

1990 – 1998:	BG/BRG Krems, Piaristengasse 2, humanistic branch
1999 – 2000:	Vienna University, studies in meteorology and geophysics
2000 – 2005:	Vienna University, studies in physics
01 – 09/2005:	diploma thesis at the Institute of Experimental Physics: "Birch-coefficients and axial equations of state at extreme pressure"
03/2006:	degree examination
10/2006 – 09/2009:	participant of the PhD program "Experimental materials science - nano- structured materials" (Initiative College I022-N)
12/2006 – 11/2009:	coworker within FWF-project "Dynamic elasticity of complex materials" (P19284-N20)

## 10.2 Publications

*related to diploma thesis:*

J. Koppensteiner, A. Tröster and W. Schranz, *Efficient parametrization of high pressure elasticity*, Phys. Rev. B **74**, 014111 (2006).

W. Schranz, A. Tröster, J. Koppensteiner, and R. Miletich, *Finite strain Landau theory of high pressure phase transformations*, J. Phys.: Cond. Matter **19**, 275202 (2007).

*related to the present thesis:*

W. Schranz, M.R. Puica, J. Koppensteiner, H. Kabelka and A. V. Kityk, *Heterogeneous relaxation dynamics of nano-confined salol probed by DMA*, Europhys. Lett. **79**, 36003 (2007).

J. Koppensteiner, W. Schranz and M.R. Puica, *Confinement effects on glass forming liquids probed by dynamic mechanical analysis*, Phys. Rev. B **78**, 054203 (2008).

J. Koppensteiner, W. Schranz and M.A. Carpenter, *Revealing the pure confinement effect on glass forming liquids by dynamic mechanical analysis*, accepted by Phys. Rev. B, in print (2009).

*others:*

E.K.H. Salje, J. Koppensteiner, M. Reinecker, W. Schranz and A. Planes, *Jerky elasticity: Avalanches and the martensitic transition in  $\text{Cu}_{74.08}\text{Al}_{23.13}\text{Be}_{2.79}$  shape-memory alloy*, Appl. Phys. Lett. **95**, 1 (2009).

G. Rogl, L. Zhang, P. Rogl, A. Grytsiv, D. Rajs, H. Müller, E. Bauer, J. Koppensteiner, W. Schranz and M. Zehetbauer, *Thermal Expansion of Skutterudites*, accepted by J. Appl. Phys., in print (2009).

L. Zhang, G. Rogl, A. Grytsiv, S. Puchegger, J. Koppensteiner, H. Kabelka, M. Reinecker, P. Rogl, W. Schranz, M. Zehetbauer and M.A. Carpenter, *Mechanical properties of filled antimonide skutterudites*, submitted to Mater. Sci. Eng. B, in review process (2009)

### 10.3 Conference contributions

*The glass transition in nano-confined geometry probed by DMA*, talk given at the "11th European Meeting on Ferroelectricity" (EMF-2007) in Bled, Slovenia on 3<sup>rd</sup> of September 2007.

*The Hindered Glass Transition in nanoscaled confinement probed by DMA*, poster presentation at the "33rd Conference of the Middle European Cooperation (MECO-33) in Statistical Physics" in Wels, Austria on 15<sup>th</sup> of April 2008.

*Confinement effects on a glass forming liquid probed by mechanical spectroscopy*, talk given at the Conference "Dynamical Properties of Solids" (DyProSo 2009) in Antwerp, Belgium on 17<sup>th</sup> of September 2009.

### 10.4 Honouring

Participation at the "58<sup>th</sup> Meeting of Nobel Laureates" dedicated to Physics in Lindau, Lake Constance, Germany, in Juli 2008 after being suggested by the BMWF and selected by the organization committee out of 20.000 applications as one out of five Austrian attendants.

### 10.5 Cooperations within IK "Nanostructured Materials"

Prof. Dr. Peter Franz Rogl, M.Sc. Long Zhang and Gerda Rogl: Dynamic elastic response, absolute elastic moduli and thermal expansion of skutterudites (bulk and nanostructured),

Prof. Dr. Gerhard Krexner, Prof. Dr. Wolfgang Pichl, MSc. Abdul Ghaffar: confinement effects on Na and Li in mesoporous silica, transfer of samples, knowhow, technology and contacts.

Mag. Daria Setman: DSC measurements of clean and salol filled mesoporous silica, dynamic mechanic analysis of bulk and HPT-nanostructured Ni samples.

Mag. Florian Spieckermann: Dynamic tension tests on rubber suspended with carbon black and carbon nanotubes.

## 10.6 National and international cooperations

Prof. Dr. Michael Carpenter, Department of Earth Sciences, University of Cambridge, UK: resonance ultrasonic measurements of mesoporous silica, both clean and filled with salol.

Prof. Dr. Ekhard Salje, Head of Department of Earth Sciences, University of Cambridge, UK: investigations on porosity - elasticity relations and critical porosity of silica samples tested via RUS. DMA experiments showing avalanche characteristics of the martensitic phase transition in CuAlBe.

Prof. Dr. Irena Drevenšek-Olenik and Miha Devetak, Institut Jožef-Stefan, University of Ljubljana, Slovenia: Silanation process for mesoporous silica.

Dr. Zhiying Zhang, Department of Earth Sciences, University of Cambridge, UK: dynamic mechanical analysis of structural and spin-transitions in various perovskites, single and mixed crystals.

Dr. Marie-Alexandra Neouze, Institute of Materials Chemistry, Vienna University of Technology: N<sub>2</sub>-sorption analysis and characterization of mesoporous silica host matrices.

Dipl. Ing. Martin Kriegisch, Institute of Materials Physics, Vienna University of Technology: Dynamic elastic response of magnetostrictive Fe<sub>53</sub>Mn<sub>47</sub>.

Dr. Vytautas Samulionis, Faculty of Physics, Vilnius University, Lithuania: Dynamic mechanical analysis of the nanoscopically lamellar thiophosphate CuInP<sub>2</sub>S<sub>6</sub>.

Dr. Martin Lederer, Faculty of Physics, Vienna University: thermomechanical analysis of Al layered Si-wafers for a possible application within the automobile industry by Infineon Technologies Austria.

## 10.7 Acknowledgements

First of all I would like to thank my supervisor, Prof. Dr. Wilfried Schranz, whose enthusiasm for physics always was and still is a great inspiration to me. Looking back on - including diploma thesis - 4 years of fruitful cooperation, he not only gave me the opportunity to work on the intriguing fields of high pressure elasticity and glass physics, but also guided me to exactness in theory, experiment and scientific writing. All of that he managed in his warm-hearted and world-open manner. Within the university I also would like to thank the IK initiators, most of all Prof. Dr. Hans-Peter Karnthaler and Prof. Dr. Michael Zehetbauer for giving me the chance for three years of intense, but rich work on the field of nanostructured materials. I also would like to mention Dr. Erhard Schaffler for technical support and the crew of the technical workshop, who did a great job when building the DMA 's replacement and new parts.

According to the University of Cambridge I especially would like to thank Prof. Dr. Michael Carpenter, who always gave me a warm welcome and introduced me to resonance ultrasound spectroscopy with great patience and friendly advice, at the same time encouraging me to self-sustained working. Also Prof. Ekhard Salje's broad knowledge and intuition for physics has been a huge motivation. It was a great honor to work with him and I am very pleased with the results of this very productive cooperation. At Jožef Stefan Institute in Ljubljana I was received with great warmth and lead by Prof. Irena Drevenšek-Olenik and supported by Miha Devetak, both generously spending their time on my samples.

A large debt of gratitude I owe to my parents, Hubert and Renate Koppensteiner and my brother Roland for always building my stable and down-to-earth background. Without their regardless support and help I would not have come to the point of finishing a PhD thesis. In equal measure I thank my closest friends. Their authentic and reliable loyalty and solidarity escorted me all the way and their company was my necessary distraction and recreation.

Finally, financial support by the Austrian FWF (P19284-N20) as well as the University of Vienna (IC "Experimental Materials Science - Bulk Nanostructured Materials", I022-N) is gratefully acknowledged.